Quantum Theory of Electronic and Thermal Transport through Nano-scale and Single-Molecule Devices

Mohsin Kadhim Abed Al-Khaykanee

B.Sc., M.Sc.

Department of Physics, Lancaster University, UK

Ph.D. Thesis

This Thesis is submitted in partial fulfilment of the requirements for degree of Doctor of Philosophy

January 2018

Declaration

Except where stated otherwise, this thesis is a result of the author's original work and has not been submitted in substantially the same form for the award of a higher degree elsewhere. Other sources of information have been used, they have been acknowledged. This thesis documents work carried out between October 2014 and November 2017 at Lancaster University, UK, under the supervision of Prof. Colin J. Lambert and funded by Higher Committee for Education Development (HCED) in partnership with University of Babylon, IRAQ.

Mohsin Kadhim Al-Khaykanee

January 2018

I would like to dedicate my thesis to

Al-Imam Mahdi and the

memory of my late beloved father

and mother

Abstract

This thesis presents a series of studies into the electronic, thermal and thermoelectric properties of molecular junctions containing single organic molecules. The exploration and understanding the electronic and phononic characteristics of molecules connected to metallic leads is a vital part of nanoscience if molecular electronics is to have a future. This thesis documents a study for various families of organic and organometallic molecules, studied using a combination of density functional theory (DFT), which is implemented in the SIESTA code, and the Green's function formalism of transport theory. The main results of this thesis are as follows:

To elucidate the nature of the high and low conductance groups observed in break-junction measurements of single 4,4-bipyridine molecules, I present a combined experimental and theoretical study of the electrical conductance of a family of 4,4-bipyridine molecules, with a series of sterically-induced twist angles α between the two pyridyl rings. I show that their conductances are proportional to cos2(α), confirming that pi-pi overlap between adjacent rings plays a dominant role. Since both peaks exhibit a $\cos^2(\alpha)$ dependence of conductance on torsion angle, this is evidence that the high and low conductances correspond to molecular orientations within the junctions, in which the electrical current passes through the C-C bond linking the pi systems of the two rings. Furthermore, this result demonstrates that the Fermi energy is located within the HOMO-LUMO gap and not close to a transmission resonance.

A theoretical investigation into the Seebeck coefficient in pi-stacked molecular junctions is performed using a first principles quantum transport method. Using oligo (phenyleneethynylene) (OPE)-type molecules as a model system, I show that quantum

interference produces anti-resonances in the gap between the HOMO and LUMO resonances and the stacking geometry can control the position of this quantum interference feature. The shifting of this resonance enhances the thermopower S is expected when the junction is tuned through a node in the transmission function. We found supramolecular π-π interactions between two molecules changed the sign of thermopower.

I have investigated a family molecules with various side branched atoms to study the electron and phonon transport through nanoscale molecular junctions, with a view to understanding the performance thermoelectric materials. My calculations focus on the effect of heteroatoms formed from C, Si, Ge, and Sn on the thermal phonon conductance, electrical conductance, and Seebeck Coefficient. I also examine how the thermoelectric figure of merit is affected by side branched atoms, as the bond length and mass play an important role in determining the thermal phonon conductance of molecular wires. Due to the rigid nature of C-side branching, the thermal phonon conductance decreases monotonically with the bond length and mass, whereas thermal phonon conductance with Si-side branches increases with the length of the bond and mass. The low thermal conductance k_{el} with S-bridging, combined with their higher thermopower and higher electrical conductance leads to a maximum thermoelectric figure of merit of ZT = 1.76, which is several orders of magnitude higher than that of bridges.

Acknowledgment

First and foremost, I would like to thank ALLAH for blessing me much more than I deserve. Also, I would like to express my deep gratitude and appreciation to my beloved parents, to whom I owe my life for their constant love, encouragement, support and blessings. This thesis would never have completed without the excellent supervision, continuous guidance, utmost efforts, and interest throughout the work that contributed to its completion I received from **Professor Colin J. Lambert.**

I would like also to express my grateful admiration to Dr. Iain Grace for providing the help, discussion and suggestion through my study, Dr. Steve , Dr Hatef for their continues support, Dr. Sara, and Dr. Ali. I would like also to thank my sponsor, Higher Committee for Education Development (HCED) in Iraq, University of Babylon funding my PhD study. I would like to thank the collaborating experimental groups, Prof. Richard Nichols, Prof. Simon Higgins, Dr Andrea Vezzoli from Liverpool University for their successful experiments. I would like to thank all my friends and colleagues in Colin's group, especially Dr. Oday, Dr. Zain, Dr. Qusiy, Dr. Mohammed, Dr. Alaa, Dr. Nasser, Michel, Abdalghani, Abdelkareem, Afaf, Asma, Norah, Qinqqing and Songjun. Many gratitude and unlimited thanks to my family, you have done a lot to me, I hope you are proud and satisfied of me and I wish one day I will be able to serve you. My dear wife, many thanks for your support during my study. You were really very kind and without your support, I would not be able to complete the PhD study. My children Ali, Buttol, Sajeed, Manther, and Baqer, you are my hope in life; I hope to be a good father to you and support you with a good life. Finally, a big thanks to my brothers and sisters for the support and encouragement I received from them.

Above all, my great thanks to **ALLAH** for his mercy and blessing.

Mohsin

List of Publications

During my PhD studies I published the following journal articles:

1. Ali Khalid Ismael, Kun Wang, Andrea Vezzoli, **Mohsin K. Al-Khaykanee**, Harry E. Gallagher, Iain M. Grace, Colin J. Lambert, Bingqian Xu, Richard J. Nichols, and Simon J. Higgins. Angew. Chem. Int. Ed. 2017, 56, 1 – 6.

Contents

Chapter 1

Introduction

1.1 Molecular electronics

Controlling individual molecules and their utilization is one of the scientific ambitions of our age. The realization of this ambition can open up broad prospects to a miniaturisation revolution in electronic devices. In recent decades, developments in nanofabrication techniques have made achievable the dream of contacting individual molecules to nano-electrodes and measuring their electronic transport characteristics [1]. Moreover, molecules are highly desirable as functional elements in nano-scale devices because of their ability to be chemically modified to tune their properties. Nowadays, these achievements have given rise to the field of *Molecular Electronics*.

In the mid-1960s, Gordon Moore developed what was to become known as 'Moore's law,' which stated that the number of transistors per unit area in practical applications would double approximately every two-years [2]. While it was expected that this trend might go on for just a 10 year period, the exponential growth continues over half a century later. The fact that it has proven to be much longer, is in part because the law has become self-fulfilling and became a directive for developments. Also, it was observed that the size of current silicon based transistors is approaching the tens of

nanometres length scale which is approaching the limit of this technology. Therefore, molecular electronics gives a method to extending Moore's law as it offers the required minimization in size, flexibility in design and the probability of realistic single-molecule electronics on the atomic scale. This is the ultimate aim for reducing the size of electronic circuits. The idea of using single molecules as molecular devices is not new, and the first theoretical work was carried out by Aviram and Ratner who proposed the first molecular rectifier in 1970s [3].

This thesis will focus on single molecule electronics which has become a rapidly expanding and popular field for understanding quantum transport at the nanoscale level both from the theoretical and experimental viewpoint. In these studies, I will apply theory in understanding the properties of different types of molecules with the aim of designing new types of materials, which could offer a route to increasing computing power and also optimize thermoelectric materials. To do this, I will utilize cutting edge theoretical tools such as density functional theory (DFT), and molecular dynamics (MD) [4]. The field of molecular electronic sits on the boundary between physics and chemistry and the role that theory can play in advancing the knowledge of this area is twofold. First, theory has the ability to make predictions and survey the properties of a wide range of molecules, thereby identifying target molecules for chemical synthesis. Secondly, by modelling the experimental measurements of these structures helps to interpret, for example, break junction and STM measurements, which can show a wide distribution of measured values due to variations in the unknown geometry of the electrodes and contacting of the molecule. Here an understanding of the measurements will be obtained by a first principles quantum transport approach using a DFT method.

Also, in the molecular electronics field, one of the most important roles is in the synthesis of new molecules and materials to study which so far has focused on typical

carbon based low-dimensional materials, for example fullerenes [5], carbon nanotubes [6-7], oligoynes [8] and graphene [9-11]. The main idea behind these efforts is to understand and control the electrical characteristics of a single-molecule, which can be incorporated into electronic devices. This has so far seen the following types of devices realized: molecular rectifiers [12], switches [13-14] and sensors [15].

A likely future contribution of molecular electronics will be to solve the major challenge of waste heat, by developing new materials and device concepts by investigating nanoscale thermoelectricity, and contributing to design of new environmentally organic thermoelectric materials [16,17]. These materials will allow highly-efficient heat-to-electrical-energy conversion from otherwise wasted low-level heat sources and could have enormous impact on global energy consumption. These developments have been accelerated by recent measurements of single-molecule thermoelectricity, which have confirmed some underpinning strategies for enhancing their thermoelectric performance [18], which could lead to more efficient thermoelectric devices and materials [19, 20].

Nanoscale systems and especially nanoscale structures are very promising in this respect, due to the fact that transport takes place through discrete energy levels. The ability to measure thermopower in nanoscale junctions opens the way to developing fundamentally new strategies for enhancing the conversion of heat into electric energy [21]. The thermoelectric properties of such materials will be discussed in this thesis.

In this thesis, I will strive to understand single-molecule devices by calculating the probability of an electron passing through a single molecule via two theoretical techniques [22]. The first is density functional theory (DFT), which is implemented in the SIESTA code [23], and the second is a non-equilibrium Green's function formalism of transport theory, which is implemented in the GOLLUM code [22]. On the

experimental side, scanning tunnelling microscopy break junction (STM-BJ) [24-26], which have been used to study the transport properties of the single-molecules that are the subject of investigation. In the course of this thesis, theoretical calculations will be compared with experimental studies of my collaborators on a range of organic and organometallic single-molecules.

Beyond the molecules themselves, one might also consider the effect of varying the electrode material. Recently graphene has been suggested as a viable electrode material [27-33], but defects such as 5-7fold rings [34] lead to fluctuations in the density of states near the graphene edges, which hamper unequivocal identification of signatures of single-molecule transport. Platinum, palladium and iron [35,36] and even silicene [37,38] have been considered, but at the moment, gold remains the metal of choice, mainly because it is relatively free of contaminants and does not oxidise in air. For this reason, I shall use gold electrodes throughout this thesis

1.2 Thesis Outline

In this thesis, I will introduce a brief discussion of the electrical and thermoelectrical properties of families of single molecules. The second chapter describes density functional theory (DFT) and the SIESTA code, which will be used to calculate the electronic and thermal properties of single-molecule junctions. The third chapter contains the theory of quantum transport, which includes the Green's functions method that used for the quantum transport calculations.

In the fourth, I will present a combined experimental and theoretical study of the electrical conductance of a family of 4,4-bipyridine molecules, with a series of sterically-induced twist angles α between the two pyridyl rings. In the fifth chapter, I will present a theoretical investigation into the Seebeck coefficient S in π-stacked oligo

(phenyleneethynylene) (OPE)-type molecular junctions, performed using a first principles quantum transport method to control quantum interference and sign of the thermopower.

The sixth chapter will investigate a family of thiophene molecules that have various side branched atoms (C, Si, Ge, and Sn) to study electron and phonon transport through nanoscale molecular junctions, with a view to increasing the performance of thermoelectric materials. And finally, the seventh chapter presents conclusions and future works.

Bibliography

[1] Kiguchi, Manabu, ed. Single-Molecule Electronics: An Introduction to Synthesis, Measurement and Theory. Springer, 2016.

[2] Moore, G. "Cramming more components onto integrated circuits', Electronics, vol. 38, no. 8." (1965).
[3] A. Aviram and M. A. Ratner, Chem. Phys. Lett 29 (1974).

[4] Musa, Sarhan M., ed. Computational Nanotechnology: Modeling and Applications with MATLAB®. CRC Press, 2011.

[5] H. W. Kroto, J. R. Heath, S. C. O'Brien, R. F. Curl, and R. E. Smalley, Nature 318, 162 (1985).

[6] Iijima, Sumio. "Helical microtubules of graphitic carbon." nature 354, no. 6348 (1991): 56-58.

[7] S. Iijima and T. Ichimashi, Nature 363, 603 (1993).

[8] Wang, Changsheng, Andrei S. Batsanov, Martin R. Bryce, Santiago Martin, Richard J. Nichols, Simon J. Higgins, Victor M. Garcia-Suarez, and Colin J. Lambert. "Oligoyne single molecule wires." Journal of the American Chemical Society 131, no. 43 (2009): 15647-15654.

[9] K. S. Novoselov, A. K. Geim, S. V. Morozov, D. Jiang, Y. Zhang, S. V. Dubonos, I. V. Grigorieva, and A. A. Firsov, Science 306, 666 (2004).

[10] K. S. Novoselov, A. K. Geim, S. V. Morozov, D. Jiang, M. I. Katsnelson, I. V. Grigorieva, S. V. Dubonos, and A. A. Firsov, Nature 438, 197 (2005).

[11] Sparks, Rachel Elizabeth. "Mechanical and electrical control of transport through single molecules." PhD diss., Lancaster University, 2012.

[12] Ashwell, Geoffrey J., Barbara Urasinska, and Wayne D. Tyrrell. "Molecules that mimic Schottky diodes." Physical Chemistry Chemical Physics 8, no. 28 (2006): 3314-3319.

[13] Collier, Charles P., Gunter Mattersteig, Eric W. Wong, Yi Luo, Kristen Beverly, José Sampaio, Francisco M. Raymo, J. Fraser Stoddart, and James R. Heath. "A [2] catenane-based solid state electronically reconfigurable switch." Science 289, no. 5482 (2000): 1172-1175.

[14] Li, Yonghai, Masoud Baghernejad, Q. Al-Galiby, D. Manrique, Guanxin Zhang, Joseph Hamill, Yongchun Fu et al. "A Three State NDI Switch: Integration of Pendant Redox Unit for Conductance Tuning." arXiv preprint arXiv:1611.02725 (2016).

[15] Leary, Edmund, H. Höbenreich, Simon J. Higgins, H. Van Zalinge, Wolfgang Haiss, Richard J. Nichols, C. M. Finch et al. "Single-molecule solvation-shell sensing." Physical review letters 102, no. 8 (2009): 086801.

[16] Rincón-García, L. et al. Molecular design and control of fullerene-based bi-thermoelectric materials. NATURE MATERIALS, 2016, 15, pp. 289- 294.

[17] Zhang, Q.; Sun, Y.; Xu, W.; and Zhu, D. Organic thermoelectric materials: Emerging green energy materials converting heat to electricity directly and efficiently. Adv. Mater. 2014, 26, pp. 6829–6851.

[18] Lambert, Colin J., Hatef Sadeghi, and Qusiy H. Al-Galiby. "Quantum-interference-enhanced thermoelectricity in single molecules and molecular films." Comptes Rendus Physique 17, no. 10 (2016): 1084-1095.

[19] Sadeghi, Hatef, Sara Sangtarash, and Colin J. Lambert. "Oligoyne molecular junctions for efficient room temperature thermoelectric power generation." Nano letters 15, no. 11 (2015): 7467-7472.

[20] Al-Galiby, Qusiy H., Hatef Sadeghi, Laith A. Algharagholy, Iain Grace, and Colin Lambert. "Tuning the thermoelectric properties of metallo-porphyrins." Nanoscale 8, no. 4 (2016): 2428-2433.

[21] Algharagholy, Laith A., Qusiy Al-Galiby, Haider A. Marhoon, Hatef Sadeghi, Hayder M. Abduljalil, and Colin J. Lambert. "Tuning thermoelectric properties of graphene/boron nitride heterostructures." Nanotechnology 26, no. 47 (2015): 475401.

[22] Ratner, Mark. "A brief history of molecular electronics." Nature nanotechnology 8, no. 6 (2013): 378-381.

[23] Soler, José M., Emilio Artacho, Julian D. Gale, Alberto García, Javier Junquera, Pablo Ordejón, and Daniel Sánchez-Portal. "The SIESTA method for ab initio order-N materials simulation." Journal of Physics: Condensed Matter 14, no. 11 (2002): 2745.

[24] Ferrer, Jaime, Colin J. Lambert, Víctor Manuel García-Suárez, D. Zs Manrique, D. Visontai, L. Oroszlany, Rubén Rodríguez-Ferradás et al. "GOLLUM: a next-generation simulation tool for electron, thermal and spin transport." New Journal of Physics 16, no. 9 (2014): 093029.

[25] Manrique, David Zsolt, Cancan Huang, Masoud Baghernejad, Xiaotao Zhao, Oday A. Al-Owaedi, Hatef Sadeghi, Veerabhadrarao Kaliginedi et al. "A quantum circuit rule for interference effects in single-molecule electrical junctions." arXiv preprint arXiv:1509.00990 (2015).

[26] Ismael, Ali Khalid, Kun Wang, Andrea Vezzoli, Mohsin K. Al-Khaykanee, Harry E. Gallagher, Iain M. Grace, Colin J. Lambert, Bingqian Xu, Richard J. Nichols, and Simon J. Higgins. "Side Group-Mediated Mechanical Conductance Switching in Molecular Junctions." Angewandte Chemie (2017).

[27] H Sadeghi, S Sangtarash, C Lambert, “Robust molecular anchoring to graphene electrodes.” Nano letters 17 (8), (2017): 4611-4618

[28] Pascal Gehring, Jakub K Sowa, Jonathan Cremers, Qingqing Wu, Hatef Sadeghi, Yuewen Sheng, Jamie H Warner, Colin J Lambert, G Andrew D Briggs, Jan A Mol, “Distinguishing lead and molecule states in graphene-based single-electron transistors.” ACS Nano 11 (3) (2017): 3404 -3412

[29] Pascal Gehring, Hatef Sadeghi, Sara Sangtarash, Chit S. Lau, Junjie Liu, Arzhang Ardavan, Jamie H. Warner, Colin J. Lambert, G. Andrew. D. Briggs, Jan A. Mol, "Quantum interference in graphene nanoconstrictions," Nano Letters 16 (7), (2016): 4210–4216

[30] Haoxue Han, Yong Zhang, Zainelabideen Y Mijbil, Hatef Sadeghi, Yuxiang Ni, Shiyun Xiong, Kimmo Saaskilahti, Steven Bailey, Yuriy A Kosevich, Johan Liu, Colin J Lambert, Sebastian Volz, "Functionalization mediates heat transport in graphene nanoflakes," Nature Communications 7 (2016): 11281

[31] Chit Siong Lau, Hatef Sadeghi, Gregory Rogers, Sara Sangtarash, Panagiotis Dallas, Kyriakos Porfyrakis, Jamie H Warner, Colin J Lambert, G Andrew D Briggs, Jan Mol, "Redox-dependent Franck-Condon blockade and avalanche transport in a graphene-fullerene single-molecule transistor," Nano Letters 16, (2016): 170-176

[32] H Sadeghi, S Sangtarash, CJ Lambert, "Enhancing the thermoelectric figure of merit in engineered graphene nanoribbons," Beilstein Journal of Nanotechnology 6 (1), (2015): 1176-1182 4

[33] H Sadeghi, JA Mol, CS Lau, GAD Briggs, J Warner, CJ Lambert," Conductance enlargement in picoscale electroburnt graphene nanojunctions." Proceedings of the National Academy of Sciences 112 (9), (2015): 2658-2663

[34] CJ Lambert, DL Weaire, "Theory of the arrangement of cells in a network." Metallography 14 (4), (1981): 307-318

[35] VM García-Suárez, AR Rocha, SW Bailey, CJ Lambert, S Sanvito, J Ferrer, "Single-channel conductance of H 2 molecules attached to platinum or palladium electrodes." Physical Review B 72 (4), (2005): 045437

[36] VM García-Suárez, CM Newman, CJ Lambert, JM Pruneda, J Ferrer, "Optimized basis sets for the collinear and non-collinear phases of iron." Journal of Physics: Condensed Matter 16 (30), (2004): 5453

[37], H Sadeghi, S Bailey, CJ Lambert, "Silicene-based DNA nucleobase sensing" Applied Physics Letters 104 (10), (2014): 103104

[38] Sadeghi, H.; S. Sangtarash, S.; Lambert, C. J., "Enhanced Thermoelectric Efficiency of Porous Silicene Nanoribbons," Scientific Reports 5, (2015): 9514

Chapter 2

Density Functional Theory

2.1. Introduction

In an attempt to understand the behaviour of molecular electronics devices, it is desirable to have a reliable technique to determine the structural and electronic behaviour of organic molecules, which density function theory (DFT) provides. Also, it is important in understanding the electronic properties of the transport of electrons across molecular structures which are suspended between the metallic electrodes. In this chapter, I will give a brief overview of DFT and the SIESTA code (Spanish Initiative for Electronic Simulations with Thousands of Atoms) [1], which I have used extensively during my PhD studies as a theoretical tool to study the structures of molecules as well as calculating charge densities, band structures, and binding enerigies. SIESTA is an implementation of DFT which is used to perform calculations on molecular systems, and one of its main advantages is that it can perform calculations of large scale systems (thousands of atoms).

The physical theories that underpin the fundamental assertion of DFT were introduced by Hohenberg and Kohn [2] and then expanded by Kohan and Sham [3] to solve the intractable many-body problem of interacting electrons in a static external potential to a tractable problem of non-interacting electrons in an effective potential. This has led to DFT becoming one of the main tools in theoretical physics, molecular chemistry and biology [4]. In this chapter I present a short summary of the foundations and numerical applications of (DFT), however a much more detailed treatment of the theory can be found in the literature [5-6].

2.2. The many-body problem

A long term goal in theoretical physics is to find a method to solve the many-body problem in quantum statistical mechanics [7]. To find the eigenvalues and eigenstates of the full Hamiltonian operator of a general system via solving the Schrodinger equation:

$$H\psi = E\psi \qquad (2.1.1)$$

where E is the energy eigenvalue, ψ is the total wave function and H is the Hamiltonian described the system. The many-body Hamiltonian can be written as:

$$H = -\sum_i \frac{\hbar^2}{2m_e}\nabla_i^2 + \frac{1}{8\pi\varepsilon_0}\sum_{i\neq j}\frac{e^2}{|r_i - r_j|}$$

$$-\sum_I \frac{\hbar^2}{2m_n}\nabla_I^2 + \frac{1}{8\pi\varepsilon_0}\sum_{I\neq J}\frac{Z_I Z_J e^2}{|R_I - R_J|} - \frac{1}{4\pi\varepsilon_0}\sum_{iI}\frac{Z_I e^2}{|r_i - R_I|} \qquad (2.1.2)$$

where m_I, Z_I and R_I are the mass, atomic number and position of the *I-th* nucleon in the solid respectively. The position of *i-th* electron is indicated by r_i and m_e is the mass of a single electron. The Hamiltonian of the many-body problem is divided into five parts; the first part is the electron kinetic energy, the second part is electron-electron

interactions, the third part is the nucleon kinetic energy, the forth part is nucleon-nucleon interactions and the last part is electron-nucleon interactions.

Finding the exact solution to the Schrödinger equation, apart from the hydrogen atom or a small number of electrons, is impossible due to the fact the interaction terms in the Hamiltonian cannot be directly uncoupled and independently solved. So an approximations is needed. Since the mass of nucleons is a few orders of magnitude higher than that of electrons, one can employ the Born-Oppenheimer approximation [8] to dissociate the wave-function of the electrons and the motion of the nuclei. Here, the Schrodinger equation is solved for the electron degrees of freedom only. Therefore, if we know the electronic structure of a molecular system, we can calculate forces on the nuclei and in addition minimize these forces to find the ground state geometry. With the Born-Oppenheimer approximation the assumption that the nucleon wave-function is independent of the electron the equation (2.1.2) can be rewritten:

$$H = T_e + U_{e-e} + V_{e-nuc} \tag{2.1.3}$$

Here T_e is defined the kinetic of all electrons which is written by;

$$T_e = \sum_i \frac{\hbar^2}{2m_e} \nabla_i^2 \tag{2.1.4}$$

The second part of equation (2.1.3) $U_{e\text{-}e}$ is defined as the electron-electron interaction and sum of all potentials acting on a given electron position r_i by all other electrons at position r_j, which can be written by;

$$U_{e-e} = \sum_{i,j,i\neq j} \frac{e^2}{4\pi\varepsilon_0} \frac{1}{|r_i - r_j|} \tag{2.1.5}$$

And the last part of the equation (2.1.3) V_{e-nuc} describes the interaction between electrons and nuclei, and it depends on the positions of electrons r_i , nuclei R_I, the nuclear potential υ_{nuc}, which is given by;

$$V_{e-nuc} = \sum_I \sum_i v_{nuc}(r_i - R_I) \tag{2.1.6}$$

Therefore, the corresponding time independent Schrödinger equation is given by:

$$H\Psi(r_1, r_2, ...r_i...) = E\Psi(r_1, r_2, ...r_i...) \tag{2.1.7}$$

Despite the Born-Oppenheimer approximation minimizing the size of the system, it is still difficult to solve equation (2.1.7), even on a modern supercomputer. Therefore, Density functional theory solves this problem by expressing the physical quantities in terms of the ground-state density.

2.3. The Hohenberg-Kohen theorems

The essential building blocks of Density Functional Theory began with two important theories by the pioneering work of Hohenberg and Kohn in 1964 [2]. From the first theorem, the external potential $V_{ext}(r)$ is uniquely defined via the ground state particle density $n_0(r)$, except for a constant. To have a better understanding for the first theorem, it can be considered there are two Hamiltonians H_1 and H_2, which have the same ground-state density $\rho_{0\,(r)}$, but different external potentials $V_{ext}^{(1)}$ and $V_{ext}^{(2)}$. The wavefunctions of them could be obtained through solving the Schrodinger equation, and

for a non-degenerate system there is one solution of the Schrodinger equation that presents the ground state wave-functions $\Psi^{(1)}$ and $\Psi^{(2)}$. Since $\Psi^{(2)}$is not a ground state of Hamiltonian $H^{(1)}$, we have:

$$E^{(1)} = \langle \Psi^{(1)} \big| H^{(1)} \big| \Psi^{(1)} \rangle < \langle \Psi^{(2)} \big| H^{(1)} \big| \Psi^{(2)} \rangle \tag{2.1.9}$$

Also,

$$E^{(2)} = \langle \Psi^{(2)} \big| H^{(2)} \big| \Psi^{(2)} \rangle < \langle \Psi^{(1)} \big| H^{(2)} \big| \Psi^{(1)} \rangle \tag{2.1.10}$$

As assuming that, the ground states are not-degenerate [9-10], one can rewrite the equation (2.1.9) as below:

$$\langle \Psi^{(2)} \big| H^{(1)} \big| \Psi^{(2)} \rangle = \langle \Psi^{(2)} \big| H^{(2)} \big| \Psi^{(2)} \rangle + \langle \Psi^{(2)} \big| H^{(1)} - H^{(2)} \big| \Psi^{(2)} \rangle$$

$$= E^{(2)} + \int dr \left(V_{ext}^{(1)}(r) - V_{ext}^{(2)}(r) \right) \rho_0(r) \tag{2.1.11}$$

And eqn. (2.1.10):

$$< \langle \Psi^{(1)} \big| H^{(2)} \big| \Psi^{(1)} \rangle = E^{(2)} + \int dr \left(V_{ext}^{(2)}(r) - V_{ext}^{(1)}(r) \right) \rho_0(r) \tag{2.1.12}$$

Adding together the two expressions (2.1.11) and (2.1.12) to obtain the equation as follows:

$$E^{(1)} + E^{(2)} < E^{(1)} + E^{(2)} \tag{2.1.13}$$

This expression gives us a contradicting inequality, showing that there cannot be two external potentials differing by more than a constant which lead to the same non-degenerate ground state density. The second theorem of the Hohenberg-Kohen states that a universal functional for the energy E[ρ] is defined in terms of the density. The ground state is exactly the global minimum value of this functional. Moreover, the external potential is uniquely determined by the density, and the potential in contrast uniquely determines the ground-state wave function, as well as all the other observables of the system (such as kinetic energy (T) of electrons) are uniquely determined. One could write the total energy E[ρ] of the system as a functional of the density as shown:

$$E[\rho] = T[\rho] + E_{int}[\rho] + \int drV_{ext}(r)\rho(r) \qquad (2.1.14)$$

where the first terms are defined as the kinetic and internal interaction of the electrons which are usually added together as one functional $F_{HK}[\rho]=T[\rho]+E_{int}[\rho]$ because these are universal and depending on the charge density without influence of the environment. From the first theorem, the Hamiltonian of the system is determined by the ground-state density (ρ_0) for that system with external potential (V_{ext}) and wavefunction (Ψ_o). Therefore, for any density (ρ), wavefunction (Ψ), and other than the ground-state, we can find:

$$E_0 = \langle \Psi_0 | H | \Psi_0 \rangle < \langle \Psi | H | \Psi \rangle = E \qquad (2.1.15)$$

So, the ground state density (ρ_0) minimizes the functional (eqn (2.1.14)). Consequently, in the case that if we know the functional $F_{HK}[\rho]$, by minimizing equation (2.1.14), and we can obtain the ground-state of the system and can calculate all ground-state characteristics.

2.4. The Kohn-Sham Approach

The Kohn–Sham equation [3] is the Schrödinger equation of a fictitious system of non-interacting particles, which generate the same density as any given system of interacting particles [11]. As mentioned before, by obtaining the ground-state density, one could in principle calculate the ground-state energy. However, the exact form that is shown in equation (2.1.14) is not known. So, the first terms in the equation (2.1.14) T[ρ] and $E_{int}[\rho]$ cannot generally be presented as functionals of the density. In 1965 there was a solution introduced by Kohn and Sham [3] to replace the original Hamiltonian of the system by an effective Hamiltonian of non-interacting particles in an effective external potential that has the same ground-state density as the original system [12-13].

So, the energy functional is written:

$$E_{KS}[\rho] = T_{KS}[\rho] + \int drV_{ext}(r)\rho(r) + E_H[\rho] + E_{xc}[\rho] \qquad (2.1.16)$$

Hence, T_{KS} is the kinetic energy of the non-interacting system, where the kinetic energy (T) in the equation (2.1.14) has been used for the interacting system. This difference is due to the exchange correlation functional E_{xc}, which will be explained later in the equation (2.1.18). Also, E_H presents the Hartree function, and describes the electron-electron interaction using the Hartree- Fock method [14-17] as given by:

$$E_H[\rho] = \frac{1}{2}\iint \frac{\rho(r)\rho(r')}{|r-r'|}drdr' \qquad (2.1.17)$$

The above equation represents an approximate version of internal interactions of the electrons E_{int}. So, the exchange correlation functional E_{xc} describes the differences between the exact and approximated solutions to the kinetic energy and the electron-electron interaction terms that defined as:

$$E_{xc}[\rho] = (E_{int}[\rho] - E_H[\rho]) + (T[\rho] - T_{KS}[\rho]) \qquad (2.1.18)$$

The Kohn-Sham theorem reduces the problem of a complicated many-body system to a set of simple non-interacting equations exactly, if the exchange correlation functional is known. Only ground-state quantities are correctly calculated due to the formulation of the theory, such as the ground-state energy, ground-state density, the fictitious Kohn-Sham eigenvalues and the ground-state electron geometry. In other words, DFT cannot be used to calculate higher energetic states correctly such as the lowest unoccupied orbital of a molecule, and consequently underestimates band gaps in semiconductors. It is worth mentioning that DFT remains an approximate technique of finding these ground state properties, as the exchange-correlation functional is not known precisely, therefore approximations have to be made.

2.5. Functional of exchange and correlation

Density functional theory reduces the quantum mechanical ground-state many-electron problem to self-consistent one-electron form, by the Kohn-Sham equations [18]. This method is formally precise, while for practical calculations, the exchange-correlation energy, E_{xc}, as a functional of the density has to be approximated. To do that, the local density approximation (LDA) has long been the standard choice [19]. Despite its simple nature, the predictions made using LDA gives realistic descriptions of the atomic structure, elastic, and vibrational characteristics for a wide range of systems. Yet, LDA is generally not accurate enough to describe the energetics of chemical reactions (heats of reaction and activation energy barriers), which lead to an overestimate of the binding energies of molecules and solids. As well, there are numerous examples where the LDA puts molecular conformations or crystal bulk phases in an even qualitatively wrong energetic order [20,21]. Recently, generalized gradient approximations (GGA's) have overcome such deficiencies to a considerable extent [18,22], giving for example a more

realistic description of energy barriers in the dissociative adsorption of hydrogen on metal and semiconductor surfaces [23]. Gradient corrected (GGA) functionals depend on the local density and on the spatial variation of the density. So, the two most commonly functionals used approximations are LDA and GGA to the exchange and correlation energies in density functional theory. To give more information about the Local Density Approximation and the Generalized Gradient Approximation, the following section will briefly describe it.

2.5.1. Local Density Approximation

The LDA approximation assumes that the exchange-correlation functional depends only on the local density which was introduced by Kohn and Sham [3] and it therefore can be expected to give good predictions for systems where the density is relatively smooth locally. The functional of the approximation is

$$E_{xc}^{LDA}[\rho] = \int dr\rho(r)\left(\in_x^{hom}\left(\rho(r)\right) + \in_c^{hom}\left(\rho(r)\right)\right) \qquad (2.1.19)$$

where the exchange and correlation for the homogeneous electron gas can be defined by terms $\in_x^{hom}$ and $\in_c^{hom}$, respectively. Moreover, the analytical formula [5] of exchange energy $\in_x^{hom}$ can be given by:

$$\in_x^{hom} = -\frac{3}{4\pi}\sqrt[3]{3\pi^2\rho} \qquad (2.1.20)$$

On the other hand, the numerical calculation of the correlation energy $\in_c^{hom}$ that has been performed by Ceperley and Alder [24] using the quantum Monte-Carlo method. And then, Perdew and Zunger [25] fitted this numerical data to analytical expressions, as follows:

$$\in_c^{hom}$$

$$= \begin{cases} -0.048 + 0.031 lnr_{(s)} - 0.0116 r_s + 0.002 r_s \ln(r_s) & r_s < 1 \\ -\dfrac{0.1423}{\left(1 + 1.9529\sqrt{r_s} + 0.3334 r_s\right)} & r_s > 1 \end{cases} \quad (2.1.21)$$

Hence, the term $r_s = \left(\frac{3}{4\pi\rho}\right)^{1/3}$ represents the average electron radius of the homogeneous electron gas. Also, alternative parametrizations for the correlation energy exist. The functional suggested by Hedin and Lundquist [26], or the functional by Vosko, Wilk and Nusair [27], preceded the parameterization of Perdew and Zunger [28]. The resulting exchange correlation potential produces relatively precise findings for systems with well-behaved densities.

However, LDA is in some sense the simplest form one can imagine for the exchange and correlation energies. It is a simple yet powerful functional and it is known to be accurate for graphene and carbon nanotubes or where the electron density is slowly changing. For instance, a large error is predicted for atoms that have d- and f-type orbitals, and it provides a very poor description for hydrogen bonding [29,30]. Also, difficulties emerge where it is not clear whether the LDA is applicable. For instance, despite the LDA performs well in bulk group-IV semiconductors it is not exactly clear how well it performs at surfaces of these materials [26-27].

2.5.2. Generalized gradient approximation

As the LDA approximates the energy of the true density by the energy of a local constant density, it fails in situations where the density is subjected to rapid changes such as in molecules. Therefore, an improvement to this can be made by considering the

gradient of the electron density, the so-called Generalized Gradient Approximation (GGA). So, the GGA approximation extends the LDA by involving the derivatives of the density into the functional form of the exchange and correlation energies. In the GGA approximation, there is no closed form for the exchange term of the function, but it has been calculated along with the correlation contribution by using numerical methods. In other words, there are different parameterizations are used with the GGA approximation for the exchange and correlation energy [31-33]. Hence, we discuss in this section the functional form that was proposed by Perdew, Burke and Ernzherhof [23], the correlation energy is given by:

$$E_{xc}^{GGA} = E_x^{GGA}[\rho] + E_c^{GGA}[\rho] \qquad (2.1.22)$$

And the the exchange part is

$$E_x^{GGA}[\rho] = \int \in_x \left(\rho(r)\right) V_x\big(\rho(r)\, \nabla\rho(r)\big)\rho(r)dr \qquad (2.1.23)$$

where,

$$V_x(\rho, \nabla\rho) = 1 + k - \frac{k}{1 + \frac{\mu s^2}{k}}$$

The values of k and μ parameters are 0.804 and 0.21951, respectively. The dimensionless density gradient is $s = \frac{|\nabla\rho|}{2k_F\rho}$ where k_F is the Fermi wavelength, and $V_x(\rho, \nabla\rho)$ is the enhancement factor. Note that the correlation energy form is expressed as

$$E_c^{GGA}[\rho] = \int \rho(r)[\in_c (\rho(r)) + F(\rho(r), \nabla\rho(\mathrm{r}))]\, dr \qquad (2.1.24)$$

where,

$$F(\rho, \nabla\rho) = \frac{\gamma e^2}{a_0} ln\left[1 + \frac{\beta t^2}{\gamma}\left(\frac{1+At^2}{1+At^2+A^2t^4}\right)\right], \qquad A = \frac{\beta}{\gamma}\frac{1}{\left(e^{-\in c(\rho)/\gamma}-1\right)}$$

Here, the parameters in the last equation are β = 0.066725, $\gamma = \frac{(1-ln2)}{\pi^2}$γ, $a_0 = \frac{\hbar}{m^2}$, and $s = \frac{|\nabla\rho|}{2k_{TF}\rho}$ is the dimensionless density gradient, where $K_{TF} = \sqrt[3]{12/\pi}/\sqrt{r_s}$ is representing the Thomas-Fermi screening wavelength and r_s can be defined as the local Seitz radius. In general, the performance of GGA functional is a better approximation than LDA, and it has considerably influential in both performing actual calculations and as the basis for functionals including higher derivatives and exact exchange [34]. In this thesis, the GGA will be used in all the presented calculations.

2.6. SIESTA

The DFT electronic structure calculations have been performed using the SIESTA code [1]. One of the main features of SIESTA is that it is designed to perform efficient calculations on huge systems consisting of thousands of atoms, and it uses the standard Kohn-Sham self-consistent density function method. In addition, the functionals that are used in SIESTA are the Local Density Approximation (LDA) and the Generalized Gradient Approximation (GGA). In this section, we will explain briefly the important methods and how they are used to perform all DFT calculations.

2.6.1. The Pseudopotential Approximation

In a system that has a large number of atoms containing complex potentials there is large computational expense for time and memory. One method to solve the computational problem is to reduce the number of electrons by introducing the pseudopotential approximation which was proposed by Fermi in 1934 [35-36]. This method, has developed from creating non-relativistic empirical pseudopotentials [37, 38] to more realistic ab-initio pseudopotentials [39-41]. The idea of this concept that the electrons in an atom are split into two parts, the first is core and the second is valence, where core electrons lie within filled atomic shells as well as they are spatially localized around the nucleus. Whereas, the valence electrons are arranged in partially filled shells, and they are the ones contributing to the formation of molecular orbitals. Therefore, this reduces the number of the electrons in a system considerably. Moreover, in the SIESTA code a special kind of ab-initio pseudopotential which called the norm-conserving pseudopotential [39] is carried out.

2.6.2. SIESTA Basis Sets

One of the most important features of the SIESTA code is the kind of basis set used in the calculations. In order to find the ground state energy, the Hamiltonian of the system should be diagonalised. This step includes the inversion of a large matrix [1] whose computation time scales with the number of non-zero elements. To minimize the size of the Hamiltonian, SIESTA uses a linear combination of atomic orbital (LCAO) basis set which are constrained to be zero outside of a certain radius (cut-off radius). Furthermore, this generates the required sparse form for the Hamiltonian, and that reduces the overlap between basis functions. Therefore, a minimal size basis set can

produce characteristics which model that of the studied system. In addition, the simplest basis set for an atom is called a single-ζ basis which corresponds to a single basis function $\Psi_{nlm}(r)$ per electron orbital (i.e. 1 for an *s*-orbital, 3 for a *p*-orbital, etc...). In this case, each basis function consists of a product of one radial wavefunction ϕ_{nl}^{1}, and one spherical harmonic Y_{lm}:

$$\Psi_{nlm}(r) = \phi_{nl}^{1}(r)Y_{lm}(\varphi, \vartheta) \qquad (2.1.25)$$

The radial part (Eq. (2.1.25)) of the wavefunction is found by using the Sankey method [42], and by solving the Schrodinger equation for the atom placed inside a spherical box, as well as the radial wavefunction equals zero at the cut-off radius, r_c . Therefore, this restriction generates an energy shift δE within the Schrödinger equation such that eigenfunction has a node at the cut-off radius, r_c , as shown by:

$$\left[-\frac{d^2}{dr^2} + \frac{l(l+1)}{2r^2} + V_{nl}^{ion}(r)\right]\phi_{nl}^{1}(r) = (\in_{nl} + \delta E)\phi_{nl}^{1}(r) \qquad (2.1.26)$$

Here, the radial wavefunction follows the previous constraint to disappear at a cut-off radius r_{cut}. So, the energy shift δE is produced by this constraint within the Schrodinger equation for example the, the eigenfunction's first node appears at r_{cut}. Therefore, for higher accuracy basis sets (multiple-ζ), additional radial wavefunctions could be involved for each electron orbital. By using a split-valence method to calculate the additional radial wavefunctions ϕ_{nl}^{i}, for $i > 1$. This includes the defining a split-valence cut-off for each addition wavefunction r_s^i. Therefore, from the function above r_s^i represents a single- ζ function and below r_s^i represents a polynomial that has parameters calculated at r_s^i. The wavefunction and its derivative are assumed continuous, and can be expressed in this formula:

$$\phi_{nl}^{i}(r) = \begin{cases} r^{l}(a_{nl} - b_{nl}r^{2}) & r > r_{s}^{i} \\ \phi_{nl}^{i-1} & r_{s}^{i} < r < r_{s}^{i-1} \end{cases} \qquad (2.1.27)$$

Further accuracy (multiple- ζ polarised) can be obtained by including wavefunctions with different angular momenta corresponding to orbitals which are unoccupied in the atom. This is done by solving (2.1.26) in an electric fieldeld such that the orbital is polarised or deformed due to the field so a different radial function is obtained. This is now combined with the appropriate angular dependent spherical harmonic which increases the size of the basis. Table (2.1) shows the number of basis orbitals for a selected number of atoms for single-ζ (SZ), double-ζ (DZ), Single-ζ Polarised (SZP) and double-ζ polarized (DZP)

Table 2.1*: Example of the radial basis functions per atom as used within the SIESTA for different degrees of precisions.*

Atom/Valence configuration	**Single-ζ (SZ)**	**Double-ζ (DZ)**	**Single-ζ Polarised (SZP)**	**Double-ζ Polarised (DZP)**
$H^{1}/(1s)$	1	2	4	5
$C^{6}/(2s^{2}\ 2P^{2})$	4	8	9	13
$N^{7}/(2s^{2}\ 2P^{3})$	4	8	9	13
$S^{16}/(3s^{2}\ 2P^{4})$	4	8	9	13
$Au^{79}/(6s^{1}\ 5d^{10})$	6	12	9	15

2.6.3 Calculating binding energy using the counter poise method

To calculate the binding energy, I shall use the counter poise method. Calculations using DFT to compute the ground state energy of different molecules allows the calculation of binding energies as well as optimum geometries. However, these calculations are subject to errors, due to the use of localized basis sets that are focused on the nuclei. When atoms are close to each other, their basis functions will overlap which leads to strengthening of atomic interactions and this could affect the total energy of the system. In general, to solve this type of error, the Basis Set Superposition Error correction (BSSE) [43] or the counterpoise correction [44] must be performed in calculations when utilizing the linear combination of atomic orbitals. The energy of interaction of two systems *a* and *b* can be donated as:

$$\Delta E(ab) = E_{ab}^{ab} - \left(E_a^a + E_b^b\right) \qquad (2.1.28)$$

Here, E_{ab}^{ab} is the total energy for the dimer system *a* and *b*, and the E_a^a and E_b^b are the total energy of the two isolated systems. So, to perform these correction inside SIESTA, I use ghost states to assess the total energy of segregated systems *a* or *b* in the dimer basis.

$$\Delta E(ab) = E_{ab}^{ab} - \left(E_a^{ab} + E_b^{ab}\right)$$

Where E_a^{ab} (E_b^{ab}) is the energy of system a (b) evaluated in the basis of the dimer. This method is used in calculations in chapter 4 and 5, which provides the most accurate approach for these systems [45-47]. To implement these corrections within SIESTA, we

use 'ghost' states to evaluate the total energy of isolated systems a or b in the dimer basis. Ghost states mean keeping the basis of one part of a dimer on atomic centres and ignore its electrons and nuclear charge while keeping the other part of dimer without neglecting anything. This method provides accurate results for different systems [48-50].

2.6.4. The Electron Hamiltonian

The electron Hamiltonian that is generated by SIESTA follows the Kohn-Sham formalism and involves the local and non-local parts of pseudopotential:

$$H = \hat{T} + \sum_i V_i^{KB}(r) + \sum_i V_i^{loc}(r) + V_H(r) + V_{xc}(r) \qquad (2.1.29)$$

Hence, $\hat{T}$ denotes to the kinetic operator, V_i^{loc} and V_i^{KB} represent the local and non-local parts of the pseudopotential for atom *i*, as well as V_H and V_{xc} are the Hartree and exchange-correlation potentials. Moreover, to calculate the first two parts of (Eq. (2.1.29)) by using two centre integrals in *k-space*, which are defined as follows:

$$\langle \Psi_1 | \hat{O} | \Psi_2 \rangle = \int \Psi_1^*(k)\, \hat{O} \Psi_1(k) e^{-ik.R} dk \qquad (2.1.30)$$

From last equation, by taking a Fourier transforms in *k-space* with Ψ_α corresponding to either the basis orbitals (for $\hat{O} = \hat{T}$) or the Kleinmann-Bylander pseudopotential projects (for $\hat{O} = V_i^{KB}$). The final three parts in (Eq. 2.1.29) that are calculated on a three-dimensional real space grid with a fineness Δx controlled a grid cut-off energy $\in_c$,

which is equivalent to a plane-wave cut-off $\epsilon_c = \frac{\pi^2}{2\Delta x}$. Within of all calculations a cut-off energy of 250 Ry has been used to provide adequate accuracy.

2.7. Calculations in Practice

To begin calculations, we have to start the computation. The first step is to build the atomic configuration of the system, and then the appropriate pseudopotentials are required for each component, which is distinctive for each exchange-correlation functional. Computationally, the main reason to choose an appropriate basis set for every element present in the calculation is in terms of time and memory. Therefore, as known that more accurate calculations need to more computationally expensive, thus it takes a longer time and uses a larger memory.

The fineness and density of the k-points that are another input parameters which leads to move precise calculations, on which the wavefunctions are evaluated or energy convergence tolerance, as well as the periodic system, the Brillouin zone sampling for the k-space integral.

The next step is to generate the initial charge density, assuming there is no interaction between atoms. If the pseudopotentials are known, then this step is simple, and the total charge density could be the sum of the atomic densities. The self-consistent calculation begins by calculating the Hartree potential and exchange-correlation potential, as shown that in figure 2.1.

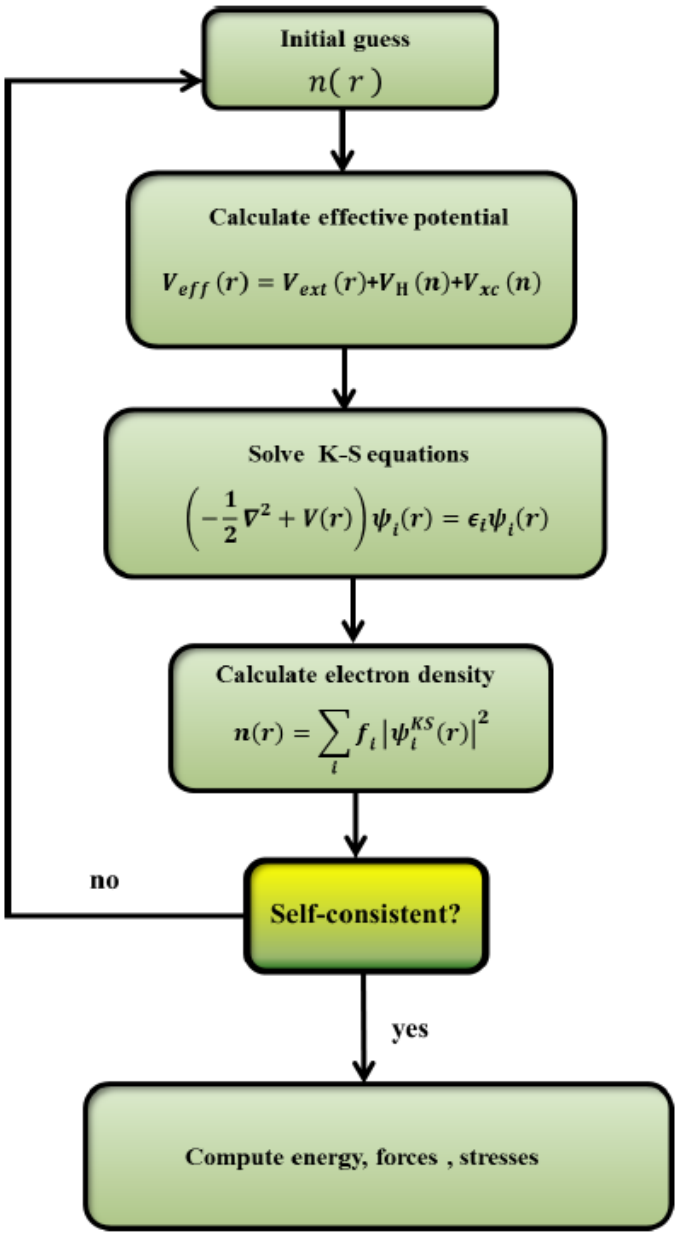

Figure 2.7.1*: Schematic of the self-consistency process within SIESTA.*

Therefore, the density is represented in real space, the Hartree potential has been obtained by solving the Poisson equation with the multi-grid [51] or fast Fourier transform [51-52].

By solving the Kohn-Sham equations and obtaining a new density $\rho(r)$, the next iteration is started, as shown in figure 2.1, on which the end of iteration when the

necessary convergence criteria are reached. Thus, we get the ground state Kohn-Sham orbitals as well as the ground state energy for a given atomic configuration that are achieved. For geometric optimization, the step that mentioned above described is in another loop, which is controlled via conjugate gradient method [53-54] to obtain the minimal ground state and the corresponding atomic configuration. Finally, when the self-consistency is implemented, the Hamiltonian and overlap matrices could be extracted so that they can be used within a scattering calculation.

Bibliography

[1] Soler, José M., Emilio Artacho, Julian D. Gale, Alberto García, Javier Junquera, Pablo Ordejón, and Daniel Sánchez-Portal. "The SIESTA method for ab initio order-N materials simulation." Journal of Physics: Condensed Matter 14, no. 11 (2002): 2745.

[2] Hohenberg, Pierre, and Walter Kohn. "Inhomogeneous electron gas." Physical review 136, no. 3B (1964): B864.

[3] Kohn, Walter, and Lu Jeu Sham. "Self-consistent equations including exchange and correlation effects." Physical review 140, no. 4A (1965): A1133.

[4] van Mourik, Tanja, Michael Bühl, and Marie-Pierre Gaigeot. "Density functional theory across chemistry, physics and biology." (2014): 20120488.

[5] Martin, Richard M. Electronic structure: basic theory and practical methods. Cambridge university press, 2004.

[6] Koch, Wolfram, Max C. Holthausen, and M. Kaupp. "BUCHER-A Chemist's Guide to Density Functional Theory." Angewandte Chemie-German Edition 113, no. 5 (2001): 989-989.

[7] Lee, Tsung Dao, and Chen Ning Yang. "Many-body problem in quantum statistical mechanics. I. General formulation." Physical Review 113, no. 5 (1959): 1165.

[8] Born, M. and Oppenheimer, R. On the quantum theory of molecules. Annalen der Physik, 1927. 84(20): p. 457–484.

[9] Levy, Mel. "Universal variational functionals of electron densities, first-order density matrices, and natural spin-orbitals and solution of the v-representability problem." Proceedings of the National Academy of Sciences 76, no. 12 (1979): 6062-6065.

[10] Dreizler, R., and J. da Providência. "NATOSA Division, eds., in “Density functional methods in physics,”, NATO ASI B Series." (1985).

[11] Parr, R. G., and W. Yang. "Density Functional Methods of Atoms and Molecules." (1989).

[12] Levy, Mel. "Electron densities in search of Hamiltonians." Physical Review A 26, no. 3 (1982): 1200.

[13] Lieb, Elliott H. "Thomas-Fermi and related theories of atoms and molecules." Reviews of Modern Physics 53, no. 4 (1981): 603.

[14] Hartree, Douglas R. "The wave mechanics of an atom with a non-Coulomb central field. Part I. Theory and methods." In Mathematical Proceedings of the Cambridge Philosophical Society, vol. 24, no. 1, pp. 89-110. Cambridge University Press, 1928.

[15] Hartree, Douglas R. "The wave mechanics of an atom with a non-Coulomb central field. Part I. Theory and methods." In Mathematical Proceedings of the Cambridge Philosophical Society, vol. 24, no. 1, pp. 89-110. Cambridge University Press, 1928.

[16] Fock, Vladimir. "Näherungsmethode zur Lösung des quantenmechanischen Mehrkörperproblems." Zeitschrift für Physik A Hadrons and Nuclei 61, no. 1 (1930): 126-148.

[17] Hartree, D. R. the Calculation of Atomic Structures; Structure of Matter Series; John Wiley & Sons Ltd.: London, 1957.

[18] Kohn, Walter, Axel D. Becke, and Robert G. Parr. "Density functional theory of electronic structure." The Journal of Physical Chemistry 100, no. 31 (1996): 12974-12980.

[19] Jones, R. O and Gunnarsson, O. The density functional formalism, its applications and prospects. Reviews of Modern Physics, 1989.61(3): p. 689-746.

[20] Grossman, Jeffrey C., Lubos Mitas, and Krishnan Raghavachari. "Structure and stability of molecular carbon: importance of electron correlation." Physical review letters 75, no. 21 (1995): 3870.

[21Zupan, Aleš, Peter Blaha, Karlheinz Schwarz, and John P. Perdew. "Pressure-induced phase transitions in solid Si, SiO 2, and Fe: Performance of local-spin-density and generalized-gradient-approximation density functionals." Physical Review B 58, no. 17 (1998): 11266.

[22] Perdew, John P., Kieron Burke, and Matthias Ernzerhof. "Generalized gradient approximation made simple." Physical review letters 77, no. 18 (1996): 3865.

[23] Penev, Evgeni, Peter Kratzer, and Matthias Scheffler. "Effect of the cluster size in modeling the H 2 desorption and dissociative adsorption on Si (001)." The Journal of chemical physics 110, no. 8 (1999): 3986-3994.

[24] Ceperley, David M., and B. J. Alder. "Ground state of the electron gas by a stochastic method." Physical Review Letters 45, no. 7 (1980): 566.

[25] Langreth, David C., and John P. Perdew. "Exchange-correlation energy of a metallic surface: Wave-vector analysis." Physical Review B 15, no. 6 (1977): 2884.

[26] Hedin, Lars, and Stig Lundqvist. "Effects of electron-electron and electron-phonon interactions on the one-electron states of solids." Solid state physics 23 (1970): 1-181.

[27] Vosko, Seymour H., Leslie Wilk, and Marwan Nusair. "Accurate spin-dependent electron liquid correlation energies for local spin density calculations: a critical analysis." Canadian Journal of physics 58, no. 8 (1980): 1200-1211.

[28] Perdew, John P., and Alex Zunger. "Self-interaction correction to density-functional approximations for many-electron systems." Physical Review B 23, no. 10 (1981): 5048.

[29] Fulde, P. Electron Correlations in Molecules and Solids. 1995. Springer.

[30] Car, Roberto. "Introduction to Density-Functional Theory and ab-Initio Molecular Dynamics." Molecular Informatics 21, no. 2 (2002): 97-104.

[31] Becke, Axel D. "Density-functional exchange-energy approximation with correct asymptotic behavior." Physical review A 38, no. 6 (1988): 3098.

[32] Perdew, John P., and Yue Wang. "Accurate and simple analytic representation of the electron-gas correlation energy." Physical Review B 45, no. 23 (1992): 13244.

[33Hammer, B. H. L. B., Lars Bruno Hansen, and Jens Kehlet Nørskov. "Improved adsorption energetics within density-functional theory using revised Perdew-Burke-Ernzerhof functionals." Physical Review B 59, no. 11 (1999): 7413.

[34] Perdew, John P., Adrienn Ruzsinszky, Jianmin Tao, Viktor N. Staroverov, Gustavo E. Scuseria, and Gábor I. Csonka. "Prescription for the design and selection of density functional approximations: More constraint satisfaction with fewer fits." The Journal of chemical physics 123, no. 6 (2005): 062201.

[35] Fermi, Enrico. "Sopra lo spostamento per pressione delle righe elevate delle serie spettrali." Il Nuovo Cimento (1924-1942) 11, no. 3 (1934): 157-166.

[36] Fermi, Enrico. "Motion of neutrons in hydrogenous substances." Ricerca sci 7 (1936): 13-52.

[37] Animalu, A. O. E., and V. Heine. "The screened model potential for 25 elements." Philosophical Magazine 12, no. 120 (1965): 1249-1270.

[38] Ashcroft, N. W. "Electron-ion pseudopotentials in metals." Physics Letters 23, no. 1 (1966): 48-50.

[39] Zunger, Alex, and Marvin L. Cohen. "First-principles nonlocal-pseudopotential approach in the density-functional formalism: Development and application to atoms." Physical Review B 18, no. 10 (1978): 5449.

[40] Hamann, D. R., M. Schlüter, and C. Chiang. "Norm-conserving pseudopotentials." Physical Review Letters 43, no. 20 (1979): 1494.

[41] Bachelet, Giovanni B., and M. Schlüter. "Relativistic norm-conserving pseudopotentials." Physical Review B 25, no. 4 (1982): 2103.

[42] Sankey, Otto F., and David J. Niklewski. "Ab initio multicenter tight-binding model for molecular-dynamics simulations and other applications in covalent systems." Physical Review B 40, no. 6 (1989): 3979.

[43] Jansen, H. B., and P. Ros. "Non-empirical molecular orbital calculations on the protonation of carbon monoxide." Chemical Physics Letters 3, no. 3 (1969): 140-143.

[44] Boys, S. F_, and Fiorenza de Bernardi. "The calculation of small molecular interactions by the differences of separate total energies. Some procedures with reduced errors." Molecular Physics 19, no. 4 (1970): 553-566.

[45] Haynes, P. D., C-K. Skylaris, A. A. Mostofi, and M. C. Payne. "Elimination of basis set superposition error in linear-scaling density-functional calculations with local orbitals optimised in situ." Chemical physics letters 422, no. 4 (2006): 345-349.

[46] Daza, Martha C., J. A. Dobado, José Molina Molina, Pedro Salvador, Miquel Duran, and José Luis Villaveces. "Basis set superposition error-counterpoise corrected potential energy surfaces. Application to hydrogen peroxide··· X (X= F−, Cl−, Br−, Li+, Na+) complexes." The Journal of chemical physics 110, no. 24 (1999): 11806-11813.

[47] Boese, A. Daniel, Georg Jansen, Martin Torheyden, Sebastian Höfener, and Wim Klopper. "Effects of counterpoise correction and basis set extrapolation on the MP2 geometries of hydrogen bonded dimers of ammonia, water, and hydrogen fluoride." Physical Chemistry Chemical Physics 13, no. 3 (2011): 1230-1238.

[48] Haynes, P. D., C-K. Skylaris, A. A. Mostofi, and M. C. Payne. "Elimination of basis set superposition error in linear-scaling density-functional calculations with local orbitals optimised in situ." *Chemical physics letters* 422, no. 4 (2006): 345-349.

[49] Daza, Martha C., J. A. Dobado, José Molina Molina, Pedro Salvador, Miquel Duran, and José Luis Villaveces. "Basis set superposition error-counterpoise corrected potential energy surfaces. Application to hydrogen peroxide··· X (X= F−, Cl−, Br−, Li+, Na+) complexes." *The Journal of chemical physics*110, no. 24 (1999): 11806-11813.

[50] Boese, A. Daniel, Georg Jansen, Martin Torheyden, Sebastian Höfener, and Wim Klopper. "Effects of counterpoise correction and basis set extrapolation on the MP2 geometries of hydrogen bonded dimers of ammonia, water, and hydrogen fluoride." *Physical Chemistry Chemical Physics* 13, no. 3 (2011): 1230-1238.

[51] Press, W. H. Numerical Recipes in C 2^{sd} Edition: The Art of Scientific Computing. Cambridge University Press, 1992.

[52] Cooley, James W., and John W. Tukey. "An algorithm for the machine calculation of complex Fourier series." Mathematics of computation 19, no. 90 (1965): 297-301.

[53] Press, W. H. Numerical recipes 3rd edition: The art of scientific com-putting. Cambridge university press, 2007.

[54] Payne, Mike C., Michael P. Teter, Douglas C. Allan, T. A. Arias, and J. D. Joannopoulos. "Iterative minimization techniques for ab initio total-energy calculations: molecular dynamics and conjugate gradients." Reviews of modern physics 64, no. 4 (1992): 1045.

Chapter 3

Theory of Quantum Transport

3.1. Introduction

The goal of molecular electronics is to understand the electrical behaviour and characteristics of molecular junctions. One of the challenges is how to connect the molecular structures to bulk electrodes to investigate electronic properties. The contact strength between the molecule and the metallic electrodes is generally a significant part in determining the transport properties, due to scattering processes within a lead|*molecule*|lead framework. The main theoretical method to study scattering in these systems is through the Green's function formalism.

The aim of this chapter is to briefly introduce the Landauer formalism with a simple derivation. To introduce of the concept of Green's functions, starting with a simple one-dimensional chain before expanding to systems of arbitrarily complex geometry.

3.2. The Landauer Formula

The standard theoretical model to describe transport phenomena in ballistic mesoscopic systems is the Landauer formula [1-2], which is an applicable method for phase coherent systems. To begin with, we assume that the system connects two large reservoirs with a scattering regain, as shown in figure 3.1.1, and in this case all inelastic relaxation processes are restricted to the reservoirs [3]. Therefore, the electron transport passing through the system is formed as a quantum mechanical scattering problem. The second important assumption is that this system is connected to external reservoirs by ideal quantum wires, which behave as waveguides for the electron waves.

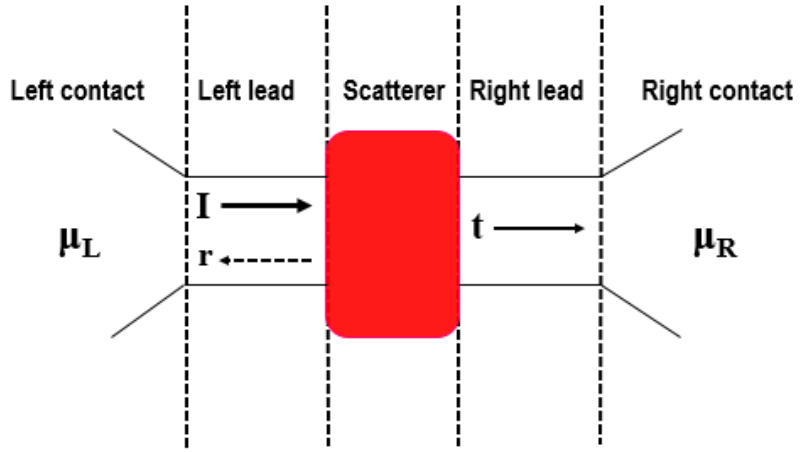

Figure 3.2.1: A mesoscopic scatterer connected to contacts by ballistic leads. The chemical potential in the contacts is μ_L and μ_R respectively. If an incident wave packet hits the scatterer from the left, it will be transmitted with probability $T = tt^*$ and reflected with probability $R = rr^*$. Charge conservation requires $T + R = 1$.

The mesoscopic scatter as shown in figure 3.2.1, is connected to two electron reservoirs, and these reservoirs have slightly different chemical potential $\mu_L - \mu_R = \delta E > 0$, and that leads to the movement of electrons from the left to the right reservoir. We will discuss the solution of one open channel for one electron: the incident electrical current δI that is generated by the chemical potential gradient, as given by:

$$\delta I = ev_g \frac{\partial n}{\partial E}\delta E = ev_g \frac{\partial n}{\partial E}(\mu_L - \mu_R) \tag{3.2.1}$$

the electron charge is *e*, the group velocity is v_g, and $\frac{\partial n}{\partial E}$ is density of states per unit length in the lead in the energy window that can be defined by the chemical potentials of the contacts:

$$\frac{\partial n}{\partial E} = \frac{\partial n}{\partial k}\frac{\partial k}{\partial E} = \frac{\partial n}{\partial k}\frac{1}{v_g \hbar} \tag{3.2.2}$$

As in one-dimension, after involving a factor of 2 for spin dependency $\frac{\partial n}{\partial k} = \frac{1}{\pi}$. When we substitute into Eq. 3.2.2, we will find that $\frac{\partial n}{\partial E} = \frac{1}{v_g h}$, which simplifies Eq. 3.2.1 to:

$$\delta I = \frac{2e}{h}(\mu_L - \mu_R) = \frac{2e^2}{h}\delta V \tag{3.2.3}$$

where δV represents the voltage generated by the potential mismatch. According to Eq. 3.2.3, the absence of a scattering region, the conductance of a quantum wire with one open channel is $\frac{e^2}{h}$ which is around 77.5 μS, or the resistance is 12.9 kΩ. In other words, if we consider a scattering region, the current passing through the scatterer to the right lead will be:

$$\delta I = \frac{2e^2}{h}\mathcal{T}\delta V \Rightarrow \frac{\delta I}{\delta V} = G = \frac{2e^2}{h}\mathcal{T} \tag{3.2.4}$$

This equation is the Landauer formula, relating the conductance *G* of a mesoscopic scatter to the transmission probability $\mathcal{T}$ for electrons passing through it. Also, it describes the linear response conductance, here it only holds for small bias voltages ie. $\delta V \approx 0$.

In the case where there is more than one open channel, the Landauer formula has been generalised by Büttiker [2], where the sum of all the transmission amplitudes leads, the formula to become:

$$\frac{\delta I}{\delta V} = G = \frac{2e^2}{h}\sum_{i,j}\left|t_{i,j}\right|^2 = \frac{2e^2}{h}Tr(tt^{\dagger}) \qquad (3.2.5)$$

Here, $t_{i,j}$ represents the amplitude of transmission describing scattering from the j^{th} channel of the left lead to i^{th} channel of the right lead and G is the electrical conductance. According to the definition of transmission amplitudes, the reflection amplitudes $r_{i,j}$ could be introduced to describe scattering processes where the particle is scattered back to the same lead as it came from it, here $r_{i,j}$ characterizes the probability of a particle arriving in channel j is reflected to channel i of the same lead. By combination the amplitudes of transmission and reflection, we can produce the scattering matrix which we call the S matrix, which connects states coming from the left lead to the right and vice versa, as follows:

$$S = \begin{pmatrix} r & t' \\ t & r' \end{pmatrix} \qquad (3.2.6)$$

In this equation, r and t represent the electrons transferring from the left, also r' and t' describe electrons coming from the right. When we go back to the equation (3.2.5), which suggests that r, t, r' and t' are matrices for more than one open channel, and in the presence of a magnetic field which can be complex. The S matrix is an important item in the scattering theory. In other words, it is useful not only in describing linear transport, but also in other problems such as adiabatic pumping [4].

3.3. One Dimension

To calculate the scattering matrix for a simple one-dimensional system, it is necessary to give an outline of the generalised methodology. In what follows, a Green's function approach is used in the derivation of a simple one-dimension lattice (section 3.3.1), and following this a calculation of the scattering matrix of a one-dimension scatter (section 3.3.2).

3.3.1. Perfect One-Dimensional Lattice

The form of the Green's function for a simple one-dimensional lattice will be discussed with on-site energies ε_0 and real hopping parameters -γ as shown in figure (3.3.1).

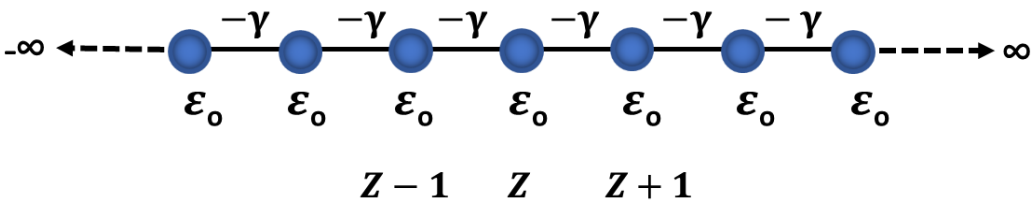

Figure 3.3.1*: One-dimensional periodic lattice tight-binding approximation with on-site energies ε_0 and hopping parameters γ.*

The Schrödinger equation describes the system's wavefunction with the Hamiltonian H,

$$\hat{H}|\psi\rangle = E|\psi\rangle \qquad (3.3.1)$$

The wavefunction Ψ_z is expanded in a one-dimensional orthogonal localized basis set $|z'\rangle$:

$$|\psi\rangle = \sum \psi_{z'} |z'\rangle \qquad (3.3.2)$$

Substituting (Eq. 3.3.2) in (Eq. 3.3.1) and multiplying the result by $|z\rangle$ yields:

$$\sum H_{z,z'}\psi_{z'} = E\psi_z \tag{3.3.3}$$

Hence,

$$H_{z,z'} = \langle z|\hat{\mathrm{H}}|z'\rangle$$

The Hamiltonian matrix has the form,

$$H = \begin{bmatrix} \ddots & -\gamma & 0 & 0 \\ -\gamma & \varepsilon_0 & -\gamma & 0 \\ 0 & -\gamma & \varepsilon_0 & -\gamma \\ 0 & 0 & -\gamma & \ddots \end{bmatrix} \tag{3.3.4}$$

The Schrödinger equation at a lattice site z in terms of the energy and wavefunction Ψ_z is given by (Eq. 3.3.6):

$$(E - H)\Psi = 0 \tag{3.3.5}$$

$$\varepsilon_0\Psi_z - \gamma\Psi_{z+1} - \gamma\Psi_{z-1} = E\Psi_z \tag{3.3.6}$$

By using the wavefunction as given by Block's theorem for the perfect lattice chain which has the form $\Psi_z = \frac{1}{\sqrt{v_g}}e^{ikz}$, where $-\pi \leq k < \pi$. The Schrödinger equation (3.3.6) can be solved to give the dispersion relation:

$$E = \varepsilon_0 - 2\gamma cosk \tag{3.3.7}$$

The group velocity can be normalized by

$$v_g = \frac{\partial E}{\partial k} = 2\gamma \sin(k) \tag{3.3.8}$$

Hence, *k* is the wavenumber. It is clear that for a given energy we can see there are two wavefunctions that satisfy (Eq. 3.3.1), and their *k* and *v* have opposite signs.

To calculate the retarded Green's function $g(z, z')$, which is closely related to the wavefunction, the following equation is solved:

$$(E - H)g(z, z') = \delta_{z,\, z'} \qquad (3.3.9)$$

In general, the retarded Green's function $g(z, z')$ explains the response of a system at a point z because of an excitation (a source) at point z'. In reality, the excitation give rise to two waves, which travel outwards with amplitudes A and B in the directions shown in figure (3.3.2).

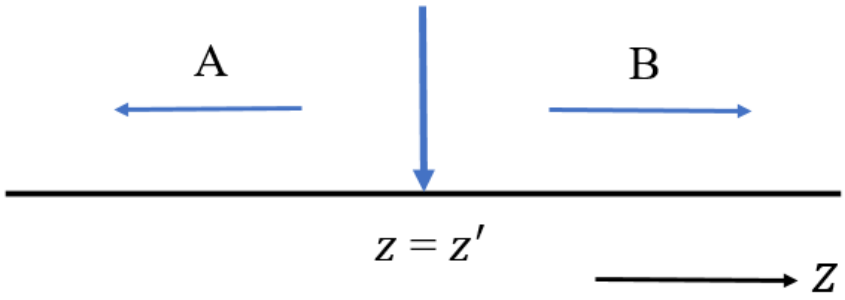

Figure 3.3.2: Retarded Green's function of an infinite one-dimensional lattice. The excitation at $z = z'$ causes waves to propagate left and right with amplitudes A and B respectively.

The resulting waves can be presented as:

$$g(z', z) = Be^{ikZ} \qquad z > z'$$
$$g(z', z) = Ae^{-ikZ} \qquad z < z' \qquad (3.3.10)$$

In this equation, the solution satisfies (Eq. 3.3.9) at every point except $z = z'$. To overcome this, the Green's function must be continuous (Eq. 3.3.11), and therefore the two are equated at $z = z'$:

$$[g(z, z')]_{z=z'\ left} = [g(z, z')]_{z=z'\ right} \qquad (3.3.11)$$

$$Be^{ikz'} = Ae^{-ikz'} \implies A = Be^{2ikz'} \qquad (3.3.12)$$

By substituting (Eq. 3.3.12) into the Green's function equation (3.3.10), we will find as shown:

$$g(z', z) = Be^{ikz} \qquad = Be^{ikz'}e^{ik(z-z')} \qquad z \geq z'$$

$$g(z', z) = Be^{2ikz'}e^{-ikz} \qquad = Be^{ikz'}e^{ik(z'-z)} \qquad z \leq z' \tag{3.3.13}$$

We can rewrite the equation (3.3.13) as:

$$g(z, z') = Be^{ikz'}e^{ik|z-z'|} \tag{3.3.14}$$

To find the value of the constant B, we use equation (3.3.9) we use Eq. (3.3.6) which for $z = z'$ given:

$$(\varepsilon_o - E)B - \gamma B\, e^{ik} - \gamma B e^{ik} = 1 \tag{3.3.15}$$

$$\gamma B\left(2cosk - 2e^{ik}\right) = 1$$

$$B = \frac{1}{2i\gamma sink} = \frac{1}{i\hbar v_g}$$

where the group velocity, found from the dispersion relation equation (3.3.7), is:

$$v_g = \frac{1}{\hbar}\frac{\partial E(k)}{\partial k} = \frac{2i\gamma sink}{\hbar} \tag{3.3.16}$$

We can rewrite the retarded Green's function as shown:

$$g^R(z - z') = \frac{1}{i\hbar v_g}e^{ik|z-z'|} \tag{3.3.17}$$

The literature [5,6,7] shows a more thorough derivation. The next step is to introduce a defect into the lattice to create a scattering region and then a transmission coefficient can be calculated.

3.3.2. One-Dimensional (1-D) Scattering

In this section, I will obtain the Green's function of a system that has two one-dimensional tight binding semi-infinite leads, connected by a coupling element α. The

two leads have equal on-site potentials ε_0 and coupling elements $-\gamma$, as shown in figure 3.3.3.

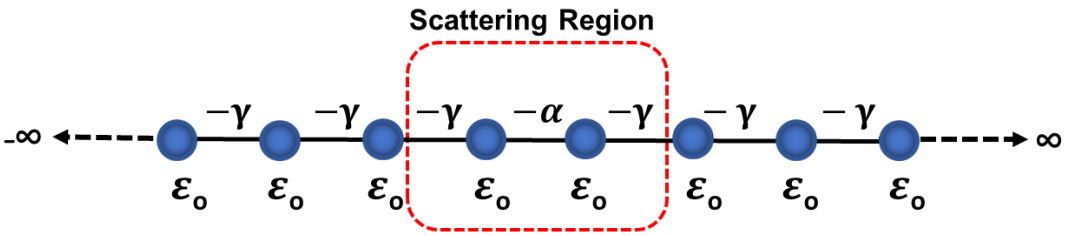

Figure 3.3.3: *Simple tight-binding model of a one-dimensional scatterer attached to one-dimensional leads.*

To solve this problem, I will derive the transmission and reflection equations for a particle moving from the left lead to right lead through the scattering region. First, the Hamiltonian that takes the form of an infinite matrix, is given by:

$$H = \begin{pmatrix} \ddots & -\gamma & 0 & 0 & 0 & 0 \\ -\gamma & \varepsilon_0 & -\gamma & 0 & 0 & 0 \\ 0 & -\gamma & \varepsilon_0 & \alpha & 0 & 0 \\ 0 & 0 & \alpha & \varepsilon_0 & -\gamma & 0 \\ 0 & 0 & 0 & -\gamma & \varepsilon_0 & -\gamma \\ 0 & 0 & 0 & 0 & -\gamma & \ddots \end{pmatrix} = \begin{pmatrix} H_L & V_c \\ V_c^{\dagger} & H_R \end{pmatrix} \tag{3.3.18}$$

Here, H_L and H_R are the Hamiltonians of the left lead and right lead, respectively. These leads are the semi-infinite equivalent of the Hamiltonian that is shown in (Eq. 3.3.4), and V_c is the coupling parameter connecting them. If γ is real, then the dispersion relation corresponding to the leads which is introduced above in (Eq. 3.3.7), and also the group velocity was written in (Eq. 3.3.16). By calculating the Green's function of this problem, we can obtain the scattering amplitudes. So, the form for the solution of equation (3.3.9), which is given as:

$$G = (E - H)^{-1} \tag{3.3.19}$$

This equation can be singular if the energy E is equal to eigenvalues of the Hamiltonian *H*, to deal with this it is practical to consider the limit:

$$G_{\mp} = \lim_{\eta \to 0}(E - H \pm i\eta)^{-1} \qquad (3.3.20)$$

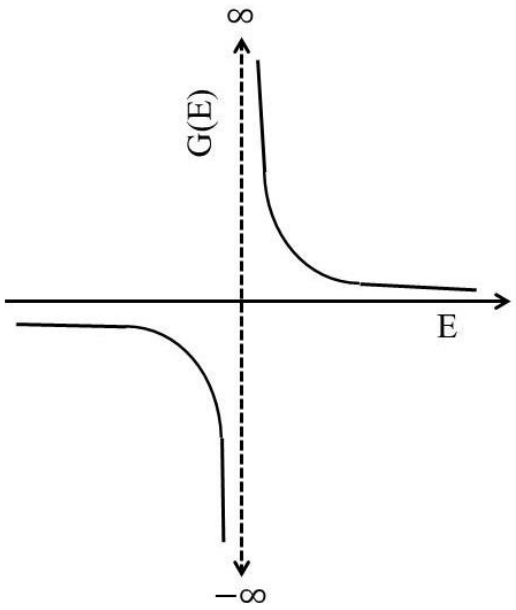

Figure 3.3.4*: shows the singularity behaviour of function (Eq 3.3.21).*

Hence, η denotes a positive number and $G_{\mp}$ represents the retarded (advanced) Green's function. In what follows, the retarded Green's function that has been used in, and the positive sign only has been chosen. For the infinite one- dimensional chain, the retarded Green's function can be defined in (Eq. 3.3.17), which is given as:

$$g^{\infty}_{zz'} = \frac{1}{i\hbar v_g} e^{ik|z-z'|} \qquad (3.3.21)$$

Hence, *z* and *z'* denote the labels of the sites in the chain and sufficient boundary conditions, which are needed to give the Green's function of a semi-infinite lead. The lattice is semi-infinite; therefore, the chain should be terminated at a given point z_0. The boundary condition is achieved via adding a wavefunction to the Green's function

equation to represent the mathematical part of this condition. So, the wavefunction for this case is given as:

$$\Psi_{z,z'}^{z_0} = -\frac{e^{ik(z+z'-2z_0)}}{i\hbar v_g} \tag{3.3.22}$$

Here, the labels of the sites of molecular chain at boundary conduction are $z = z' = z_0 - 1$. Therefore, to obtain the Green's function $g_{zz'} = g_{zz'}^{\infty} + \Psi_{z,z'}^{z_0}$ will have the simple form:

$$g_{z_0-1,z_0-1} = -\frac{e^{ik}}{\gamma} \tag{3.3.23}$$

In the case where there is no coupling between the molecule and the leads, α = 0, the Green's function can be given as:

$$g = \begin{pmatrix} -\frac{e^{ik}}{\gamma} & 0 \\ 0 & -\frac{e^{ik}}{\gamma} \end{pmatrix} = \begin{pmatrix} g_L & 0 \\ 0 & g_R \end{pmatrix} \tag{3.3.24}$$

If we consider a switch on of the interaction, then to obtain the Green's function of the coupled leads of this system, Dyson's equation is written:

$$G^{-1} = (g^{-1} - V) \tag{3.3.25}$$

where *V* is the operator that describes the interaction connecting the leads, which has the form:

$$V = \begin{pmatrix} 0 & V_c \\ V_c^{\dagger} & 0 \end{pmatrix} = \begin{pmatrix} 0 & -\alpha \\ -\alpha & 0 \end{pmatrix} \qquad (3.3.26)$$

By solving the Dyson's equation (3.3.25), we will obtain:

$$G = \frac{1}{\alpha^2 - \gamma^2 e^{-2ik}} \begin{pmatrix} \gamma e^{-ik} & -\alpha \\ -\alpha & \gamma e^{-ik} \end{pmatrix} \qquad (3.3.27)$$

Here, we can calculate the transmission (t) and the reflection (r) amplitudes from the Green's function equation (3.3.27). This is obtained by using the Fisher-Lee relation [3, 7], which relates the scattering amplitudes of a scattering problem to the Green's function of the problem. The Fisher-Lee relations for our case is given:

$$G_{1,1} = \frac{1}{i\hbar v_g}(1 + r)$$

$$G_{1,2} = \frac{1}{i\hbar v_g} t e^{ik} \qquad (3.3.28)$$

$$r = i\hbar v_g G_{1,1} \text{ -1} \qquad (3.3.29)$$

and

$$t = i\hbar v_g G_{1,2} e^{ik} \qquad (3.3.30)$$

Therefore, these amplitudes will be corresponded to particles incident from the left. On the other hand, particles are travelling from the right side, which means these expressions could be used for transmission t' and reflection r' amplitudes.

According to these coefficients above, the probability can be defined: $\mathcal{T} = tt^*$, R = rr^*. Thus, the transmission probability for this case can be given as:

$$T = \frac{\sigma^2}{(\gamma^2-\alpha^2)^2+\sigma^2} \qquad (3.3.31)$$

The parameters in this equation are $\sigma = 2\gamma\alpha sink$, and if α = γ that means the transmission T=1. In the case when α is greater or smaller than γ, which leads to create scattering region, and could be resulted to the transmission T ≤ 1.

Furthermore, we are now in the possession of the full scattering matrix, and the Landauer formula here can be used (Eqn. 3.2.4) to calculate the zero bias conductance. The procedures that are used in this analytical solution for the conductance G of a one-dimensional scatterer could be generalized for more complex geometries.

3.4. Generalization of the Scattering Formalism

Following the Lambert's derivation [8,9], I will show a generalized approach to transport calculations in this section. This approach has three parts; firstly, the surface Green's function of crystalline leads is computed. Secondly, the technique of decimation is indicated to reduce the dimensionality of the scattering region. Finally, calculating the scattering amplitudes by using a generalization of the Fisher-Lee relation.

3.4.1 Hamiltonian and Green's Function of the Leads

To study the general semi-infinite crystalline lead of arbitrary complexity then the structure of the Hamiltonian is a generalization of the one-dimensional (1-D) lead Hamiltonian in (Eq. 3.3.4), as shown in figure 3.4.1.

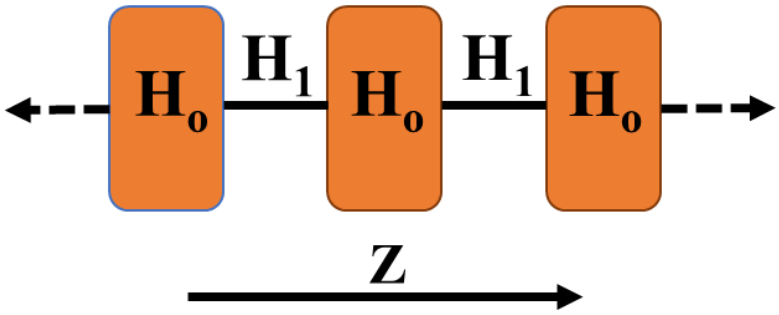

Figure 3.4.1*: Schematic representation of a semi-infinite generalized lead. It shows that H0 and H1 are the Hamiltonians and hopping energies, respectively. The direction Z is defined to be parallel to the axis of the chain.*

As shown in figure 3.4.1, the general system topology, the total Hamiltonian whose structure can be written as an infinite block tridiagonal matrix form:

$$H = \begin{pmatrix} \ddots & H_1 & 0 & 0 \\ H_1^{\dagger} & H_0 & H_1 & 0 \\ 0 & H_1^{\dagger} & H_0 & H_1 \\ 0 & 0 & H_1^{\dagger} & \ddots \end{pmatrix} \tag{3.4.1}$$

Hence, H_0 is the on-site energies of orbitals, and orbitals interactions between each other in the plane perpendicular through the direction of transport z-axis, and H_1 is the coupling between the orbitals belonging to nearest neighbour slices. In addition, H_0 and H_1 can be general complex matrices. By solving the Schrödinger equation, the spectrum of the Hamiltonian H has been calculated, and then the Schrödinger equation of this system can be taken the form:

$$E\Psi_Z = H_0\Psi_Z + H_1\Psi_{Z+1} + H_1^{\dagger}\Psi_{Z-1} \quad (3.4.2)$$

Hence, the Here, Ψ_z presents the column vector whose elements identify the amplitude of the wavefunction on each degree of freedom within a slice located at point z along the Z-direction, and the main idea from equation (3.4.2) is satisfied for all values Z, and the assumption that the system is infinity periodic in the Z-axis only. Therefore, the on-site wavefunction Ψ_z could be represented in the Block form, which consists of a product of a propagating plane wave and a wavefunction ϕ_k that is perpendicular to the transport Z-direction. If the dimensions of intra- Hamiltonian, H_0, $M \times M$ (or consists of M site energies and their respective hopping elements), the perpendicular wavefunction ϕ_k, can have M degrees of freedom and take the form of a $1\times M$ dimensional vector. Thus, the wavefunction Ψ_Z:

$$\Psi_Z = \sqrt{n_k}\, e^{ikZ}\phi_k \quad (3.4.3)$$

Here, n_k presents an arbitrary normalization parameter, when we substitute this equation into the Schrödinger equation (3.4.2), it will be given:

$$\left(H_0 + e^{ikZ}H_1 + e^{-ikZ}H_1^{\dagger} - E\right)\phi_k = 0 \quad (3.4.4)$$

Generally, to calculate the band structure for such a problem, one can select values of k and then calculate the eigenvalues at that point $E = E_l(k)$, where l = 1,….. M. the parameter l indicates to the bond index. So, for each value of k, there could be M solutions to the eigenproblem, and thus M energy values. What following, by choosing multiple values for k, it is relatively simple to build up a band structure.

Therefore, to obtain the value of k in the scattering problem. Firstly, we have to find the value of E, instead of finding the E values at a given k. Secondly, we get the values of k at a given E, and this is approaching the problem from the opposite direction. Moreover, to complete successfully this problem, there is a root-finding that is used to perform

this, however, an enormous numerical effort is required due to the wave numbers are in general complex. Furthermore, the eigenvalue for this problem can be written down and resulted from the energy is the input, and then the wave numbers are as the results:

$$v_k = e^{-ikZ}\phi_k \tag{3.4.5}$$

By combining this equation with (Eq. 3.4.4):

$$\begin{pmatrix} H_1^{-1}(H_0 - E) & -H_1^{-1}H_1^{\dagger} \\ I & 0 \end{pmatrix}\begin{pmatrix} \phi_k \\ v_k \end{pmatrix} = e^{ikZ}\begin{pmatrix} \phi_k \\ v_k \end{pmatrix} \tag{3.4.6}$$

For a layer Hamiltonian H_0, the size of Hamiltonian matrix $M \times M$, equation (3.4.6) will yield *2M* eigenvalues, e^{ik_lZ} and eigenvectors ϕ_k of the size *M*. therefore, these states can be arranged to four parts depending on whether they are propagating or decaying, as well as whether they are left going or right going. For the case that is propagating, when it has a real number of k_l, and second case that is decay, if it has an imaginary part. That means, if the imaginary case of the wave number is positive and will be a left decay state. In contrast, if it has a negative imaginary part it is a right decaying state. Therefore, the propagating states are arranged according to the group velocity of the state:

$$v_{k_l} = \frac{1}{\hbar}\frac{\partial E_{k,l}}{\partial k} \tag{3.4.7}$$

If the group velocity v_{k_l} of the state is positive, then there will be a right propagating state, while if it is negative, a left propagating state will be found.

Table 3.4.1: Sorting of the eigenstates into left and right propagating and decaying states according to the wave number and group velocity.

Category	Left	Right
Decaying	$\mathrm{Im}(k_l) > 0$	$\mathrm{Im}(k_l) < 0$
Propagating	$\mathrm{Im}(k_l) = 0, \vartheta_{k_l} < 0$	$\mathrm{Im}(k_l) = 0, \vartheta_{k_l} > 0$

To understand and distinguish between the left and right propagating/decaying state, we would refer $\bar{k_l}$ to the left propagating/decaying set, and k_l indicates to the right propagating/decaying set. For the wave function, $\phi_{\bar{k}_l}$ and ϕ_{k_l} are associated to a left and right states, respectively. In addition, for H_1 case, if it is invertible, then there must be the same, *M*, of the left and right states. On other hand, if H_1 is singular, then the matrix in equation (3.4.6) cannot be constructed, since it relies of the inversion of H_1. Therefore, there are several methods which can be used to overcome this problem. The first method [10] which uses the decimation technique to create an effective non-singular H_1. There is other solution may be to populate a singular, H_1, with small random numbers which introduces an explicit numerical error. Therefore, this method is reasonable as the introduced numerical error might be as small as the numerical error introduced by decimation. Furthermore, another solution is re-written equation (3.4.6) such as H_1 need not be inverted:

$$\begin{pmatrix} H_0 - E & -H_1^{\dagger} \\ I & 0 \end{pmatrix} \begin{pmatrix} \phi_k \\ v_k \end{pmatrix} = e^{ikZ} \begin{pmatrix} H_1 & 0 \\ 0 & I \end{pmatrix} \begin{pmatrix} \phi_k \\ v_k \end{pmatrix} \qquad (3.4.8)$$

However, by solving this generalized eigenproblem is more computationally expensive, and the above-mentioned methods work reasonably in disrupting the problem of a singular H_1 matrix. And that means the number of the matrix must be the same of the left and right going states, whether H_1 is singular or not. Therefore, the solution of the equation (3.4.4) to the eigenproblem at a given energy *E*, there will not be exactly form an orthogonal set of states. And this is decisive because we might have to deal with non-orthogonality at constructing the Green's function, which is necessary to present the duals to ϕ_{k_l} and $\phi_{\bar{k}_l}$, which are given as:

$$\phi_{k_i}\tilde{\phi}^{\dagger}_{k_j} = \phi_{\bar{k}_i}\tilde{\phi}^{\dagger}_{\bar{k}_i} = \delta_{ij} \tag{3.4.9}$$

And this yields the generalized completeness relation:

$$\sum_{l=1}^{M} \tilde{\phi}^{\dagger}_{k_l}\,\phi_{k_l} = \sum_{l=1}^{M} \tilde{\phi}^{\dagger}_{\bar{k}_l}\,\phi_{\bar{k}_l} = I \tag{3.4.10}$$

By calculating the Green's function for the infinity system, and we are in possession of the whole set of eigenstates at a given energy and by satisfying the proper boundary conditions for the semi-infinite electrodes at their surface. At condition $\mathcal{Z} \neq \mathcal{Z}'$, the Green's function satisfies the Schrödinger equation, and we will build up the Green's function from the mixture of the eigenstates ϕ_{k_l} and $\phi_{\bar{k}_l}$.

$$g(z,z') = \begin{cases} \sum_{l=1}^{M} \phi_{k_l} e^{ik_l(z-z')} w^{\dagger}_{k_l} & z \geq z' \\ \\ \sum_{l=1}^{M} \phi_{\bar{k}_l} e^{i\bar{k}_l(z-z')} w^{\dagger}_{\bar{k}_l} & z \leq z' \end{cases} \tag{3.4.11}$$

Hence, the *M*-component vectors w_{k_l} and $w_{\bar{k}_l}$ are to be determined, also there are similarities of structures between this equation and equation (3.3.10), as well as all the degrees of freedom in the transverse direction are involved in the vectors ϕ_k and w_k. So, the priority is to obtain the w vectors. As mentioned in the section (3.3.1), the

equation (3.4.11) must be continuous when $z \neq z'$, and should achieve the Green's function (Eq. 3.3.9). The first condition is given as:

$$\sum_{l=1}^{M} \phi_{k_l} w_{k_l}^{\dagger} = \sum_{l} \phi_{\bar{k}_l} w_{\bar{k}_l}^{\dagger} \tag{3.4.12}$$

The second condition is:

$$\sum_{l=1}^{M} \left[(E - H_0)\phi_{k_l} w_{k_l}^{\dagger} + H_1 \phi_{k_l} e^{ik_l} w_{k_l}^{\dagger} + H_1^{\dagger} \phi_{\bar{k}_l} e^{-i\bar{k}_l} w_{\bar{k}_l}^{\dagger} \right] = I$$

And these two conditions employ the following equation:

$$\sum_{l=1}^{M} \left[(E - H_0)\phi_{k_l} w_{k_l}^{\dagger} + H_1 \phi_{k_l} e^{ik_l} w_{k_l}^{\dagger} + H_1^{\dagger} \phi_{\bar{k}_l} e^{-i\bar{k}_l} w_{\bar{k}_l}^{\dagger} + H_1^{\dagger} \phi_{k_l} e^{-ik_l} w_{k_l}^{\dagger} \right.$$

$$\left. + H_1^{\dagger} \phi_{k_l} e^{-ik_l} w_{k_l}^{\dagger} \right] = I$$

$$\sum_{l=1}^{M} \left[H_1^{\dagger} \phi_{-\bar{k}_l} e^{-i\bar{k}_l} w_{\bar{k}_l}^{\dagger} + H_1^{\dagger} \phi_{k_l} e^{-ik_l} w_{k_l}^{\dagger} \right]$$

$$+ \sum_{l=1}^{M} \left[(E - H_0) + H_1 e^{ik_l} + H_1^{\dagger} e^{-ik_l} \right] \phi_{k_l} w_{k_l}^{\dagger} = I \tag{3.4.13}$$

From the Schrödinger equation (Eq. 3.4.4), it is known;

$$\sum_{l=1}^{M} \left[(E - H_0) + H_1 e^{ik_l} + H_1^{\dagger} e^{-ik_l} \right] = \phi_{k_l} = 0 \tag{3.4.14}$$

And this yields:

$$\sum_{l=1}^{M} H_1^{\dagger} \left(\phi_{\bar{k}_l} e^{-i\bar{k}_l} w_{\bar{k}_l}^{\dagger} - \phi_{k_l} e^{-ik_l} w_{k_l}^{\dagger} \right) = I \tag{3.4.15}$$

By using dual vectors defined in Eq. (3.4.9), and multiplying Eq. (3.4.10) by $\tilde{\phi}_{k_p}$, which is given:

$$\sum_{l=1}^{M} \tilde{\phi}_{k_p}^{\dagger} \phi_{\bar{k}_l} w_{\bar{k}_l}^{\dagger} = w_{k_p}^{\dagger} \tag{3.4.16}$$

and similarly multiplying by $\tilde{\phi}_{\bar{k}_l}$ yields:

$$\sum_{l=1}^{M} \tilde{\phi}_{\bar{k}_p}^{\dagger} \phi_{k_l} w_{k_l}^{\dagger} = w_{\bar{k}_p}^{\dagger} \tag{3.4.17}$$

Also, utilizing the continuity Eq. (3..4.12), Eq. (3.4.16), Eq. (3.4.17), then the Green's function

Eq. (3.4.15) becomes:

$$\sum_{l=1}^{M} \sum_{p=1}^{M} H_1^{\dagger} \left(\phi_{k_l} e^{-ik_l} \tilde{\phi}_{k_l}^{\dagger} - \phi_{\bar{k}_l} e^{-i\bar{k}_l} \tilde{\phi}_{\bar{k}_l}^{\dagger} \right) \phi_{\bar{k}_p} w_{\bar{k}_p}^{\dagger} = I \tag{3.4.18}$$

And what follows:

$$\sum_{l=1}^{M} \left[H_1^{\dagger} \left(\phi_{k_l} e^{-ik_l} \tilde{\phi}_{k_l}^{\dagger} - \phi_{\bar{k}_l} e^{-i\bar{k}_l} \tilde{\phi}_{\bar{k}_l}^{\dagger} \right) \right]^{-1} = \sum_{p=1}^{M} \phi_{\bar{k}_p} w_{\bar{k}_p}^{\dagger} = \sum_{p=1}^{M} \phi_{k_p} w_{k_p}^{\dagger} \tag{3.4.19}$$

This directly gives us an expression for $w_k^{\dagger}$:

$$w_k^{\dagger} = \tilde{\phi}_k^{\dagger} v^{-1} \tag{3.4.20}$$

Hence, v is defined as:

$$v = \sum_{l=1}^{M} H_1^{\dagger} \left(\phi_{k_l} e^{-ik_l} \tilde{\phi}_{k_l}^{\dagger} - \phi_{\bar{k}_l} e^{-i\bar{k}_l} \tilde{\phi}_{\bar{k}_l}^{\dagger} \right) \tag{3.4.21}$$

In the equation (3.4.20), the wave function denotes to both left and right states. By substituting Eq. (3.60) into Eq. (3.51), gives the Green's function of an infinite system:

$$g_{z,z'}^{\infty} = \begin{cases} \sum_{l=1}^{M} \phi_{k_l} e^{ik_l (z - z')} \tilde{\phi}_k^{\dagger} v^{-1} & z \geq z \\ \sum_{l=1}^{M} \phi_{\bar{k}_l} e^{i\bar{k}_l (z - z')} \tilde{\phi}_{\bar{k}}^{\dagger} v^{-1} & z \leq z' \end{cases} \tag{3.4.22}$$

In addition, to get the Green's function for a semi-infinite lead, a wave function can be added to the Green's function, and the boundary conditions should satisfy at the edge of the lead, as with the one-dimensional (1-D) case. The boundary condition hence is that the Green's function must disappear at a given place, $z = z_0$. Therefore, in order to perform that $(g = g^{\infty} + \Delta)$ has been added to the Green's function (Eq. 3.4.22).

$$\Delta = \sum_{l,p=1}^{M} \phi_{\bar{k}_l} e^{i\bar{k}_l(z-z)} \tilde{\phi}^{\dagger}_{\bar{k}_l} \phi_{k_p} e^{ik_p(z-z_0)} \tilde{\phi}^{\dagger}_{k_p} v^{-1} \qquad (3.4.23)$$

For going left:

$$g_L = \left(I - \sum_{l,p} \phi_{\bar{k}_l} e^{-i\bar{k}_l} \tilde{\phi}^{\dagger}_{\bar{k}_l} \phi_{k_p} e^{ik_p} \tilde{\phi}^{\dagger}_{k_p}\right) v^{-1} \qquad (3.4.24)$$

And for going right:

$$g_R = \left(I - \sum_{l,p} \phi_{\bar{k}_l} e^{i\bar{k}_l} \tilde{\phi}^{\dagger}_{\bar{k}_l} \phi_{k_p} e^{-ik_p} \tilde{\phi}^{\dagger}_{k_p}\right) v^{-1} \qquad (3.4.25)$$

Therefore, we have a versatile method for calculating the surface Green's functions Eqs. (3.4.24) and (3.4.25)) for a semi-infinite lead utilizing the numerical approach in Eq. (3.4.6). in summary of all that is to obtain the Hamiltonian of the scattering region, and using DFT and combine this with the surface Green's function by Dyson's equation. So, to obtain the total Green's function, as shown:

$$G_T = [g^{-1} - H]^{-1} \qquad (3.4.26)$$

Where,

$$g = \begin{pmatrix} g_L & 0 \\ 0 & g_R \end{pmatrix} \qquad (3.4.27)$$

Here, g_L and g_R represent the surface Green's functions of left and right leads that are given in equations (3.4.24) and (3.4.24), respectively.

3.4.2 Scattering Matrix and the Transport coefficients

To calculate the scattering amplitudes, and deposing on the generalization of the Fisher-Lee relation [7,13,14], and it is assumed that states which are normalized to carry unit flux, which gives the transmission amplitude from the left to right lead, as shown:

$$t_{hl} = \tilde{\phi}^{\dagger}_{k_h} G_{01} v_L \phi_{k_l} \sqrt{\left|\frac{v_h}{v_l}\right|} \qquad (3.4.28)$$

Here, ϕ_{k_h} represents a right moving state in the right lead, and ϕ_{k_l} is a right moving state in the left lead. As well as, v_h and v_l express the corresponding group velocities. For the reflection amplitudes in the left lead, which is given as:

$$r_{hl} = \tilde{\phi}^{\dagger}_{\bar{k}_h} (G_{00} v_L - I) \phi_{k_l} \sqrt{\left|\frac{v_h}{v_l}\right|} \qquad (3.4.29)$$

All the states in the left lead are shown, $\phi_{\bar{k}_h}$ is a left moving state, ϕ_{k_l} is a right moving state and v_L is the *v* operator which mentioned in Eqn. (3.4.5) for the left lead.

For the right lead, we can define the scattering amplitude of particles coming from this side, as shown:

$$t'_{hl} = \tilde{\phi}^{\dagger}_{k_h} G_{10} v_R \phi_{\bar{k}_l} \sqrt{\left|\frac{v_h}{v_l}\right|} \qquad (3.4.30)$$

And

$$r'_{hl} = \tilde{\phi}^{\dagger}_{k_h} (G_{11} v_R - I) \phi_{\bar{k}_l} \sqrt{\left|\frac{v_h}{v_l}\right|} \qquad (3.4.31)$$

The group velocities and state vectors can be defined similarly as for electrons moving from the left to right lead. Therefore, the scattering matrix can be defined as the collections of transmission and reflection amplitudes connecting propagating states.

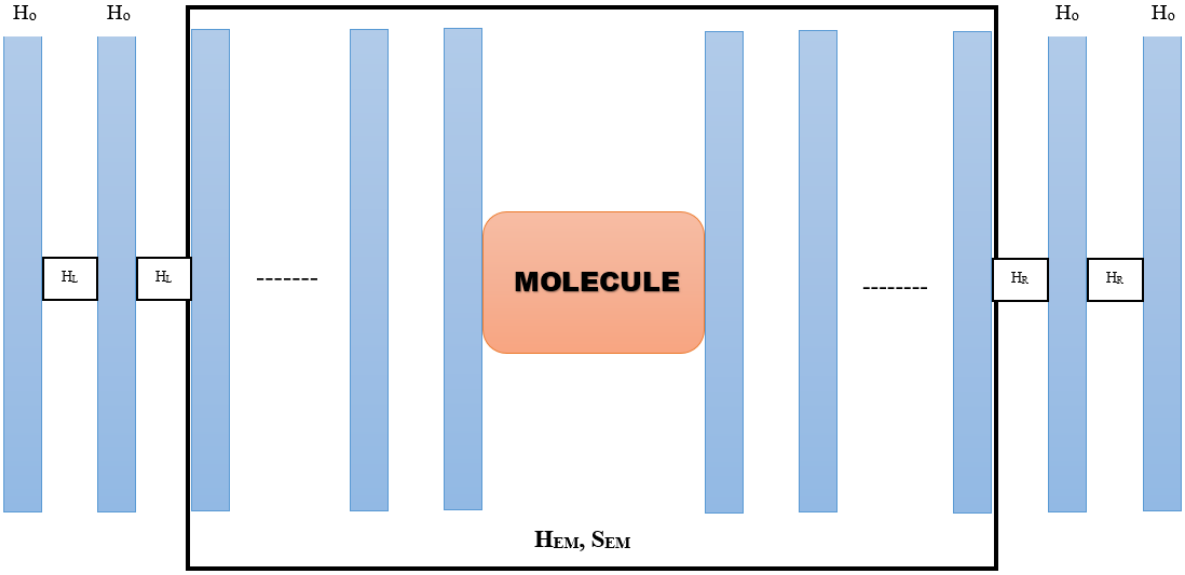

***Figure 3.4.2**: A Schematic representation of a two terminal device, showing the leads connected to the extended molecule of the scattering region, this includes the molecule plus some layers of the leads.*

The total transmission can be calculated for the system by summing over all channels, which can be written in terms of the trace of the transmission matrix [15].

$$T = \sum_{lh}^{M} |t_{lh}|^2 = \sum_{lh} t_{lh}\, t_{hl}^{*} = Tr\,(tt^{\dagger}) \qquad (3.4.32)$$

3.4.3. Effective Hamiltonian of the Scattering Region

In section, I have shown in the last section a coupling matrix between the surface of the semi-infinite leads, and the Dyson equation (3.3.6) that can be utilized to calculate the Green's function of the scatterer. Therefore, the scattering region is not usually described simply as a coupling matrix between surfaces. Thus, it is useful to use the decimation trichinae to reduce the Hamiltonian down to such a structure. Other methods

have been developed [11, 12]. The decimation trichinae has been used in this thesis. We re-write again the Schrödinger equation:

$$\sum_j H_{ij}\Psi_j = E\Psi_i \qquad (3.4.33)$$

If we separate the *lth* degree of freedom in the system:

$$H_{il}\Psi_l + \sum_{j\neq l} H_{ij}\Psi_j = E\Psi_i \qquad i \neq l \qquad (3.4.34)$$

$$H_{ll}\Psi_l + \sum_{j\neq l} H_{lj}\Psi_j = E\Psi_l \qquad i = l \qquad (3.4.35)$$

From last equation, we can express Ψ_l as shown:

$$\Psi_l = \sum_{j\neq l} \frac{H_{lj}\Psi_j}{E - H_{ll}} \qquad (3.4.36)$$

Now, if we substitute Eq. (3.4.29) into Eq. (3.4.27) yields:

$$\sum_{j\neq l} \left[H_{ij}\Psi_j + \frac{H_{il}H_{lj}\Psi_j}{E - H_{ll}}\right] = E\Psi_i \qquad i \neq l \qquad (3.4.37)$$

On other hand, equation (3.4.30) can be considered as an effective Schrödinger equation, where the number of degree of freedom is lowered by one compared to equation (3.66). Therefore, the new effective Hamiltonian, H', as shown:

$$H'_{ij} = H_{ij} + \frac{H_{il}H_{lj}}{E - H_{ll}} \qquad (3.4.38)$$

This Hamiltonian is the decimated Hamiltonian produced by simple Gaussian elimination. A notable characteristic of the decimated Hamiltonian is that is energy dependent, which suits the method presented in former section very well. Without the decimation method, the Hamiltonian describing the system in general would take the form, as given:

$$H = \begin{pmatrix} H_L & V_L & 0 \\ V_L^\dagger & H_{scatt} & V_R \\ 0 & V_R^\dagger & H_R \end{pmatrix} \tag{3.4.39}$$

Now, if we look to parameters in this equation, it can have defined as H_L and H_R indicate to the semi-infinite leads, H_{scatt} indicates the Hamiltonian of the scatterer, V_L and V_R are the coupling Hamiltonians which couple the original scattering region to the leads. Therefore, an new effectively equivalent Hamiltonian has been produced after decimation.

$$H = \begin{pmatrix} H_L & V_c \\ V_c^\dagger & H_R \end{pmatrix} \tag{3.4.40}$$

Hence, V_c indicates an effective coupling Hamiltonian, which now describes the whole scattering process. Now the same steps as with the one-dimensional case can be applied; using Dyson's equation (3.3.26). Hence, the Green's function for the whole system is described by the surface Green's function (Eqns. 3.64 and 3.65), and the effective coupling Hamiltonian from equation (3.4.33).

$$G = \begin{pmatrix} g_L^{-1} & V_c \\ V_c^\dagger & g_R^{-1} \end{pmatrix}^{-1} = \begin{pmatrix} G_{00} & G_{01} \\ G_{10} & G_{11} \end{pmatrix} \tag{3.4.41}$$

3.5. Thermoelectric coefficients

The thermoelectric effect in a system can be defined as conversion between thermal and electric energies, when there is a temperature difference ΔT and voltage difference ΔV across it. This leads to an electric current I and heat current $\dot{Q}$ passing through a device. Therefore, the linear response for both currents (electric and heat) are related to the temperature ΔT and voltage ΔV differences through the thermoelectric coefficients G, L, and K [16-17].

$$\begin{pmatrix} I \\ \dot{Q} \end{pmatrix} = \frac{1}{h} \begin{pmatrix} e^2 L_0 & \frac{e}{T} L_1 \\ eL_1 & \frac{1}{T} L_2 \end{pmatrix} \begin{pmatrix} \Delta V \\ \Delta T \end{pmatrix} \quad (3.5.1)$$

Here, T represents the reference temperature, also at room temperature the transport through single-molecules is phase-coherent, with moments $L_n = L_n^{\uparrow} + L_n^{\downarrow}$ (n=0,1,2), where L_n is written as:

$$L_n^{\sigma} = \int_{-\infty}^{\infty} (E - E_F)^n T^{\sigma}(E) \left(-\frac{\partial f(E,T)}{\partial E} \right) dE \quad (3.5.2)$$

where $T^{\sigma}(E)$ is the transmission coefficient, and σ represents spin [↑,↓] of transport of electrons passing through the single-molecule from one electrode to another [18], *f (E,T)* is the Fermi distribution function that is defined $f(E,T) = [e^{(E-E_F)/k_B T} + 1]^{-1}$ where k_B is Boltzmain's constant. We can rewrite equation (3.5.2) in the terms of the electrical conductance (*G*), thermopower (*S*), Peltier coefficient (*Π*), and the electronic contribution to the thermal conductance (k_e), as shown:

$$\begin{pmatrix} \Delta V \\ \dot{Q} \end{pmatrix} = \begin{pmatrix} 1/G & S \\ \Pi & k_e \end{pmatrix} \begin{pmatrix} I \\ \Delta T \end{pmatrix} \quad (3.5.1)$$

The electrical conductance, G is given by the Landauer formula:

$$G = \frac{2e^2}{h} L_0 \quad (3.5.2)$$

Here, h is Planck's constant. The thermopower in this case is given:

$$S = -\frac{\Delta V}{\Delta T} = \frac{1}{eT} \frac{L_1}{L_0} \quad (3.5.3)$$

The Peltier coefficient (Π),

$$\Pi = \frac{1}{e} \frac{L_1}{L_0} \quad (3.5.4)$$

And the electronic contribution to the thermal conductance (κ_e) is given:

$$k_e = \frac{1}{hT}\left(L_2 - \frac{L_1^2}{L_0}\right) \tag{3.5.5}$$

From the above equations, the figure of merit $ZT_e = S^2GT/k_e$ [17-20] can be written as:

$$ZT_e = \frac{1}{\frac{L_0 L_2}{L_1^2} - 1} \tag{3.5.6}$$

We can see the figure of merit *ZT* determines the efficiency of conversion heat into electricity. In the case when *E* is closed to Fermi energy, E_F, then if transmission, *T(E),* changes slowly with, *E,* on the of scale K_BT, and then the equations of conductance and thermopower take the form of the well-known formula[20,21]:

$$G(T) \approx \left(\frac{2e^2}{h}\right) T(E_F) \tag{3.5.7}$$

$$S(T) \approx -\propto eT \left(\frac{d\ lnT(E)}{dE}\right)_{E=E_F} \tag{3.5.8}$$

where $\propto = \left(\frac{K_B}{h}\right)^2 \frac{\pi^2}{3}$ is the Lorentz number. Therefore, from Eq. (3.5.7) it is seen that the thermopower *S* is enhanced by increasing the slope of lnT(E) close to $E=E_F$.

3.6 Phonon Thermal Conductance

To calculate the thermal conductance of a system for different vibrational modes through a molecular junction, the xyz-coordinates of the molecule were relaxed, and these coordinates were displaced for each atom in this system in positive and negative

directions by force δq′ = 0.01 Å. The forces were then calculated in three directions qi = (x_i, y_i, z_i) for each atom by using the siesta implementation DFT method without geometry relaxation. Thus, to construct the dynamical matrix from the values is constructed of the forces $F_i^q = \left(F_i^x, F_i^y, F_i^z\right)$ by using the formula:

$$D_{ij} = \frac{K_{ij}^{qq'}}{\sqrt{M_i M_j}} \tag{3.6.1}$$

where $K_{ij}^{qq'} i \neq j$ is the interatomic force constant that is obtained from the second derivation of total energy, i and j are label atomic sides, *q* and *q'* are Cartesian coordinates, M_i is the mass of labelled atom. We can obtain $K_{ij}^{qq'}$ from the finite difference of the forces on atoms *i* and *j* from:

$$K_{ij}^{qq'} = \frac{F_i^q(\delta q_j') - F_j^q(\delta q_j')}{2\delta q_j'} \tag{3.6.2}$$

Here, $\delta q_j'$ is displacement of atom *j* in the directions *q'*. So, the mass matrix M can be written $M = (M_i M_j)^{1/2}$. To satisfy the conservation of momentum, the K for $i = j$ (diagonal terms) is calculated from $K_{ii} = -\sum_{i \neq j} K_{ij}$. Therefore, the phonon thermal conductance κ_{ph} at room temperature T can be calculated from the formula as given[22]:

$$k_{ph}(T) = \frac{1}{2\pi}\int_0^\infty \hbar\omega T_{ph}(\omega)\frac{\partial f_{BE}(\omega,T)}{\partial T}d\omega \tag{3.6.3}$$

Here, $f_{BE}(\omega, T) = (e^{\frac{\hbar\omega}{k_B T}} - 1)^{-1}$ is Bose–Einstein distribution function, $\hbar$ is reduced Planck's constant, as well as $k_B = 8.6 \times 10^{-5}$ eV/K is Boltzmann's constant.

Bibliography

[1] Landauer, Rolf. "Spatial variation of currents and fields due to localized scatterers in metallic conduction." IBM Journal of Research and Development 1, no. 3 (1957): 223-231.

[2] Büttiker, M., Y. Imry, R. Landauer, and S. Pinhas. "Generalized many-channel conductance formula with application to small rings." Physical Review B 31, no. 10 (1985): 6207.

[3] Datta, Supriyo. Electronic transport in mesoscopic systems. Cambridge university press, 1997.

[4] Brouwer, P. W. "Scattering approach to parametric pumping." Physical Review B 58, no. 16 (1998): R10135.

[5] Economou, Eleftherios N. Green's functions in quantum physics. Vol. 3. New York: Springer, 1983.

[6] Mello, Pier A., and Narendra Kumar. Quantum transport in mesoscopic systems: complexity and statistical fluctuations, a maximum-entropy viewpoint. No. 4. Oxford University Press on Demand, 2004.

[7] Fisher, Daniel S., and Patrick A. Lee. "Relation between conductivity and transmission matrix." Physical Review B 23, no. 12 (1981): 6851.

[8] Visontai, D. Quantum and Classical Dynamics of Molecule Size Systems. PhD thesis, Lancaster University, 2011.

[9] Finch, C. M. An understanding of electrical characteristics of organic molecular devices, in Physics Department, Lancaster University, 2008.

[10] S, Sanvito. Giant magnetoresistance and quantum transport in mag-netic hybrid nanostructures. PhD thesis, University of Lancaster, 1999.

[11] White, Halbert. "A heteroskedasticity-consistent covariance matrix estimator and a direct test for heteroskedasticity." Econometrica: Journal of the Econometric Society (1980): 817-838.

[12] Ryndyk, D. A., R. Gutiérrez, B. Song, and G. Cuniberti. "Green function techniques in the treatment of quantum transport at the molecular scale." In Energy Transfer Dynamics in Biomaterial Systems, pp. 213-335. Springer Berlin Heidelberg, 2009.

[13] Sparks, E. R. MECHANICAL AND ELECTRICAL CONTROL OF TRANSPORT THROUGH SINGLE MOLECULES. PhD thesis, University of Lancaster, 2012.

[14] Dávid ,V. Quantum and Classical Dynamics of Molecular Scale Systems. PhD thesis, University of Lancaster, 2013.

[15] Stone, A. Douglas, and P. A. Lee. "Effect of inelastic processes on resonant tunneling in one dimension." Physical review letters 54, no. 11 (1985): 1196.

[16] N. Claughton, C. Lambert. *Physical Review B*, 1996. 53 (10). pp. 6605-6612.

[17] Sivan, U., and Y. Imry. "Multichannel Landauer formula for thermoelectric transport with application to thermopower near the mobility edge." Physical Review B 33, no. 1 (1986): 551.

[18] Giant thermopower and figure of merit in single-molecule devices. CM Finch, VM Garcia-Suarez, CJ Lambert, Physical Review B 79 (3), (2009): 033405

[19] Noori, Mohammed, Hatef Sadeghi, and Colin J. Lambert. "High-performance thermoelectricity in edge-over-edge zinc-porphyrin molecular wires." Nanoscale 9, no. 16 (2017): 5299-5304.

[20] García-Suárez, Víctor M., Colin J. Lambert, David Zs Manrique, and Thomas Wandlowski. "Redox control of thermopower and figure of merit in phase-coherent molecular wires." Nanotechnology 25, no. 20 (2014): 205402.

[21] Al-Galiby, Qusiy H., Hatef Sadeghi, Laith A. Algharagholy, Iain Grace, and Colin Lambert. "Tuning the thermoelectric properties of metallo-porphyrins." Nanoscale 8, no. 4 (2016): 2428-2433.

[22] Sadeghi, Hatef, Sara Sangtarash, and Colin J. Lambert. "Oligoyne molecular junctions for efficient room temperature thermoelectric power generation." Nano Letters 15, no. 11 (2015): 7467-7472.

[23] A Kambili, G Fagas, VI Fal'ko, CJ Lambert. "Phonon-mediated thermal conductance of mesoscopic wires with rough edges" Physical Review B 60 (23), (1999): 15593

[24] G. Fagas, A.G. Kozorezov, C.J. Lambert, J.K. Wigmore, A. Peacock,A. Poelaert, R. den Hartog, "Lattice dynamics of a disordered solid-solid interface," Phys. Rev. B60, (1999): 6459

Chapter 4

Effect of substituent and inter-ring torsion in 4,4'-bipyridine molecular junctions

In this chapter, the effect of substituent and torsion angle between two rings of 4,4'-bipyridine molecular junction on electrical conductance, will be examined both theoretically and experimentally. Here, I demonstrate that varying the chemical groups of bipyridine leads to different torsion angle between phenyl rings.

This study is a collaborative work and the experiment has been carried out in the Liverpool University (Prof. Richard J. Nichols group).

4.1 Introduction

The transport characteristics of molecular scale circuits and the fundamental understanding of their structure-property relationships are key to the future design and implementation of molecular-scale electronics. Measurements of electronic properties of single-molecules have demonstrated that the conductance of a molecular junction is sensitive to the electrode structure, molecule-metal contact geometry, conformation of the molecular backbone [1-3], presence of dopants [4-7] and/or solvents [8-10], electrochemical potential [11-13], UV or visible illumination [14-17], temperature [18-19], and many others. In the last decade, a series of experimental [14-17] and theoretical [21-22] studies performed on substituted 1,1'-biphenyl-4,4'-dithiols single-molecule junctions showed that the conductance of Au/molecule/Au junctions follows a simple $\cos^2\alpha$ dependence, where α is the inter-ring torsional angle. The same effect was also found in substituted benzidines (1,1'-biphenyl-4,4'-diamine) [23], confirming that the phenomenon is not ascribable to the nature of the molecule-metal contact and/or electrode structure. Instead, it is a general rule, which arises from the varying degree of π-electron delocalization (in the molecular backbone) with α, and a fully broken conjugation (reduced π overlap) for $\alpha \approx 90^{o}$ suppresses the conductance by roughly 2 orders of magnitude, while locking the two phenyl rings in a coplanar conformation resulted in a little increase in conductance. This rule was also found to be valid in the case of 3,3'-substituted 5,5'-bis(methylthio)-2,2'-bithiophenes, where the ring-locking resulted in a conductance increase, and ring staggering resulted in its decrease [3]. Since the rule only applies when the Fermi energy of the gold electrodes lies within the HOMO-LUMO gap [22], these studies confirm that electron transport in these molecules takes place via off-resonance tunneling.

Therefore, in this chapter, I will present the switching behavior of substituted bipyridine attached to gold, which could form the basis of a new kind of single-molecule switch. The chemical structure of the molecules being investigated can be seen in figure 4.1.

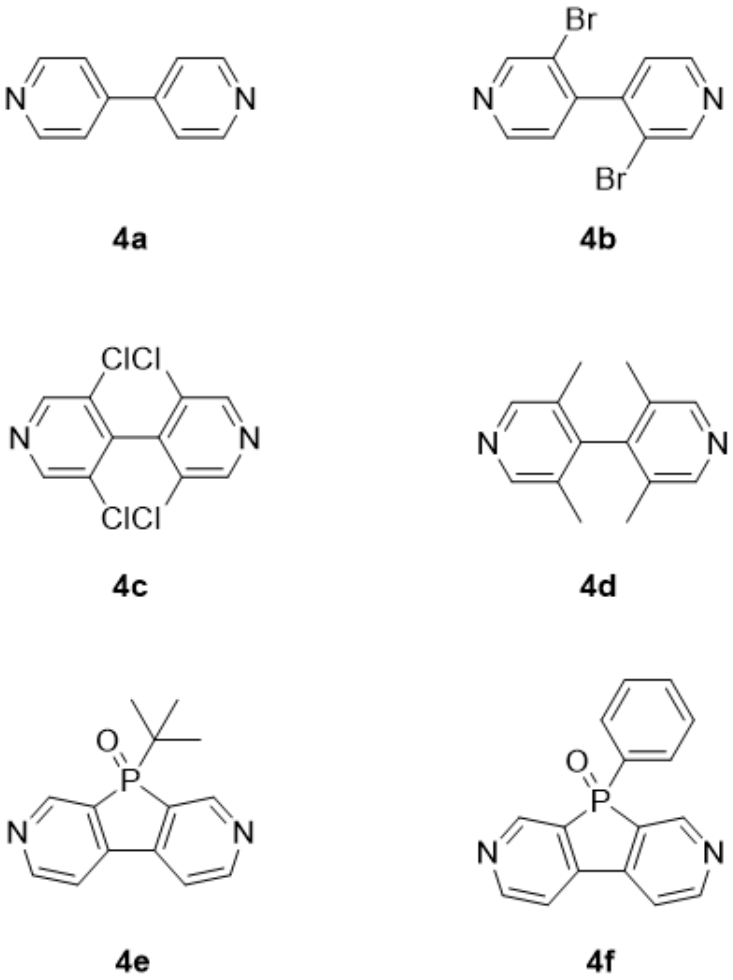

Figure 4.1: *Family of molecular wires discussed in this chapter.*

4.2. Theoretical Methods

4.2.1 Geometry of molecules and angles between the two rings

The DFT code (SIESTA) was employed to obtain fully relaxed geometries of the isolated molecules (figure 4.1) 4,4'-bipyridine (4a**)**, 3,3'-dibromo-4,4'-bipyridine (4b), 3,3',5,5'-tetrachloro-4,4'-bipyridine (4c), 3,3',5,5'-tetramethyl-4,4'-bipyridine (4d), tert-butyl phosphabipy (4e) and phenyl phosphabipy (4f), and their torsion angles as shown in figures 4.2.1-4.2.4 (right). It is well known that DFT is not able to distinguish between the local minima and global minima, which means that a typical relaxation calculation stops at the first total minima energy whether it is local or global. To find the global minima I fixed one of the rings and rotated the other with 360^{o} degrees around the molecule axis, and at each angle I calculated the ground state energy. After finding the global minima (the lowest energy), I let the molecules to be fully relaxed around the global minima angle so that I can obtain the most accurate torsion angle of the molecule.

I am going to start with 4a (4,4'-bipyridyl), where literature [2, 24-25] approximates the angle between the two rings to be around 34^{o}. In my DFT calculations I find the global minima energy to be at 40^{o}. For 4b (3,3'-dibromo-4,4'-bipyridine) my calculations of torsion angle is 78.5^{o}, 4c (3,3',5,5'-tetrachloro-4,4'-bipyridine) the global minima energy at 83.7^{o}. Same as in 4c there are local and global minima, the global one at 83.7^{o}. For 4d (3,3',5,5'-tetramethyl-4,4'-bipyridine) torsion angle is 86.5^{o}, all torsion angles are shown in figures 4.2.1-4.2.4 (left). The increase in the torsion angle is related to the steric effects induced by the bulky substituents. Furthermore, for 4e and 4f the angle between the two rings is zero due to a bridging atom (4e and 4f molecules) between two phenyl rings in these molecules, as shown in figure 4.1.

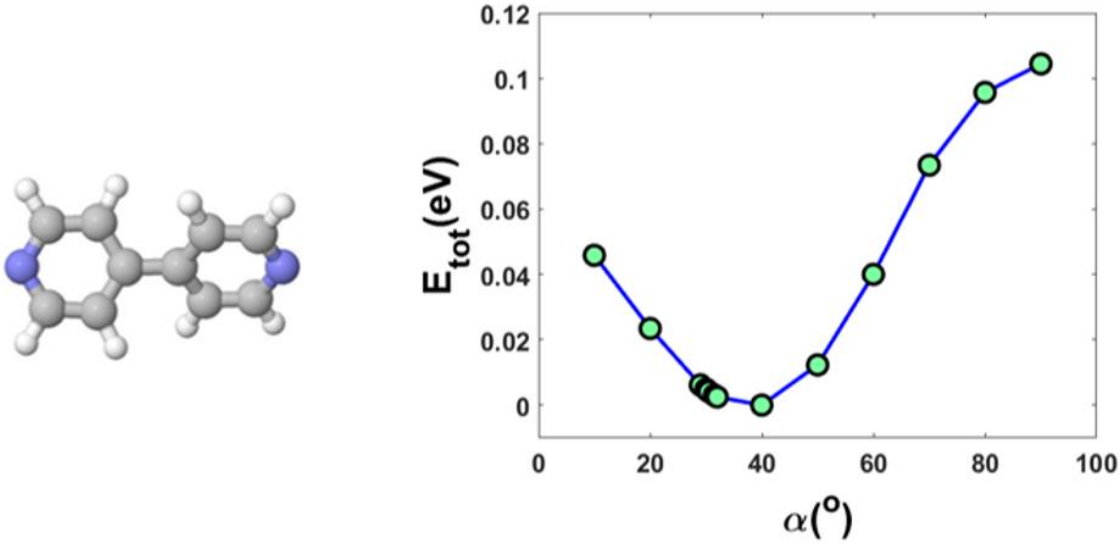

Figure 4.2.1: *illustrates the fully optimised geometry of the isolated molecule with the right angle 40° for 4,4'-bipyridine (4a) on the right of figure, and the global minimum energy.*

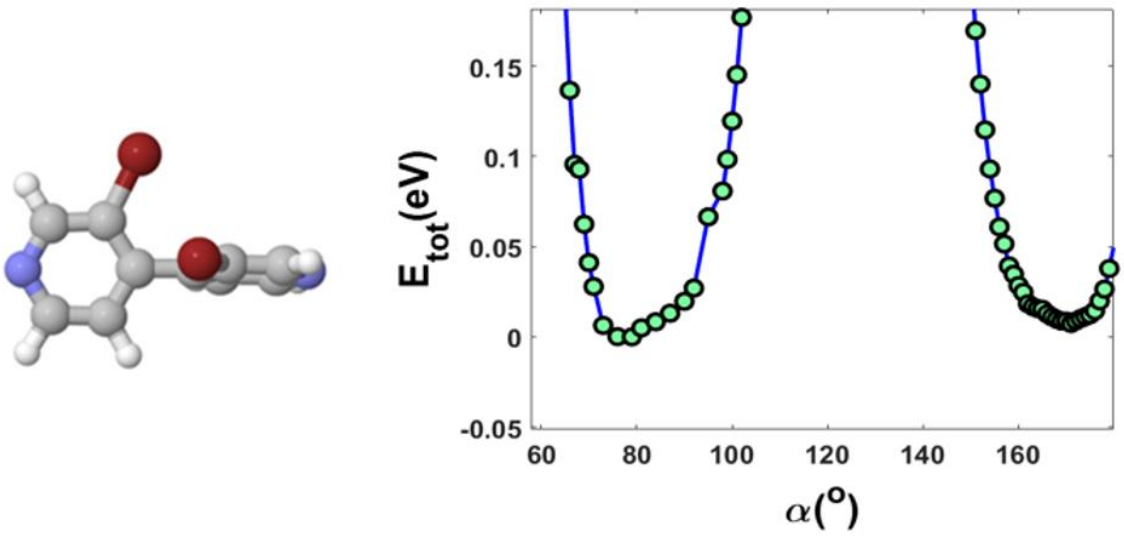

Figure 4.2.2: *illustrates the fully optimised geometry of the isolated molecule with the right angle 78.5° for 3,3'-dibromo-4,4'-bipyridine (4b) on the right of figure, and the global minimum energy.*

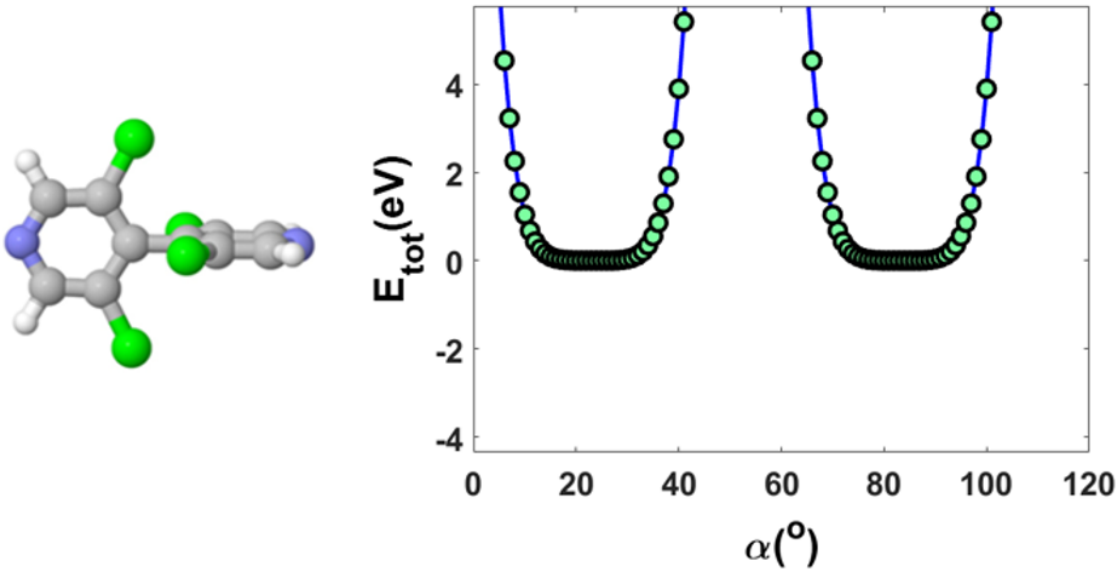

Figure 4.2.3: *illustrates the fully optimised geometry of the isolated molecule with the right angle 83.7° for 3,3',5,5'-tetrachloro-4,4'-bipyridine (4c) on the right of figure, and the global minimum energy.*

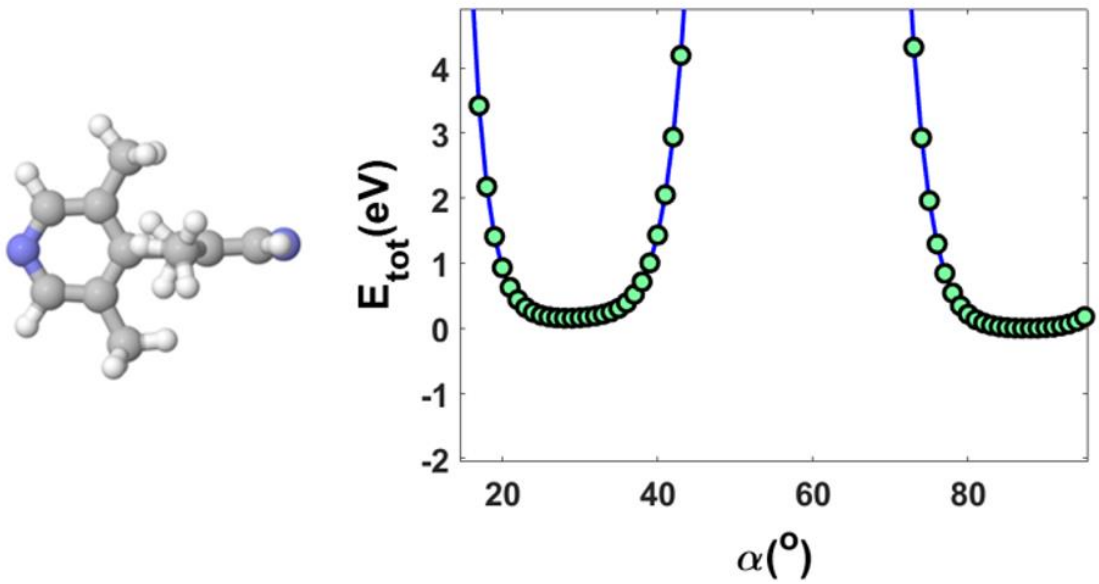

Figure 4.2.4: *illustrates the fully optimised geometry of the isolated molecule with the right angle 86.5° for 3,3',5,5'-tetramethyl-4,4'-bipyridine (4d) on the right of figure, and the global minimum energy.*

4.2.2. Frontier Orbitals

In this section, I present the electronic structures of 4a-4f molecules to help understand the electrical behavior of the junctions which have been investigated by using (DFT) SIESTA code. The electronic structures 4a-4f were carried out at the GAUSSIAN 09W using B3LYP function [26] with the 6-31G** [27] basis set used to appear the effect of various side groups, and torsion angle for each molecule on the distribution of the frontier molecular orbitals. Plots of the HOMOs and LUMOs are given in figure 4.2.5 of all molecules (4a-4f). It is clear that the frontier orbitals are distributed almost evenly across the molecular backbone, and this delocalization means there is a π-conjugated pathway between the two rings.

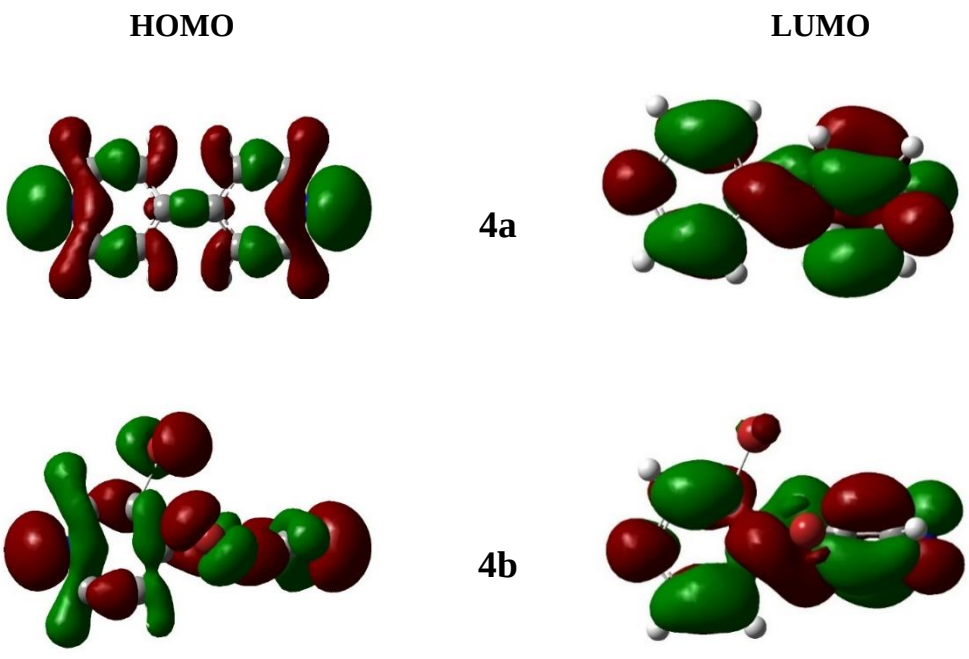

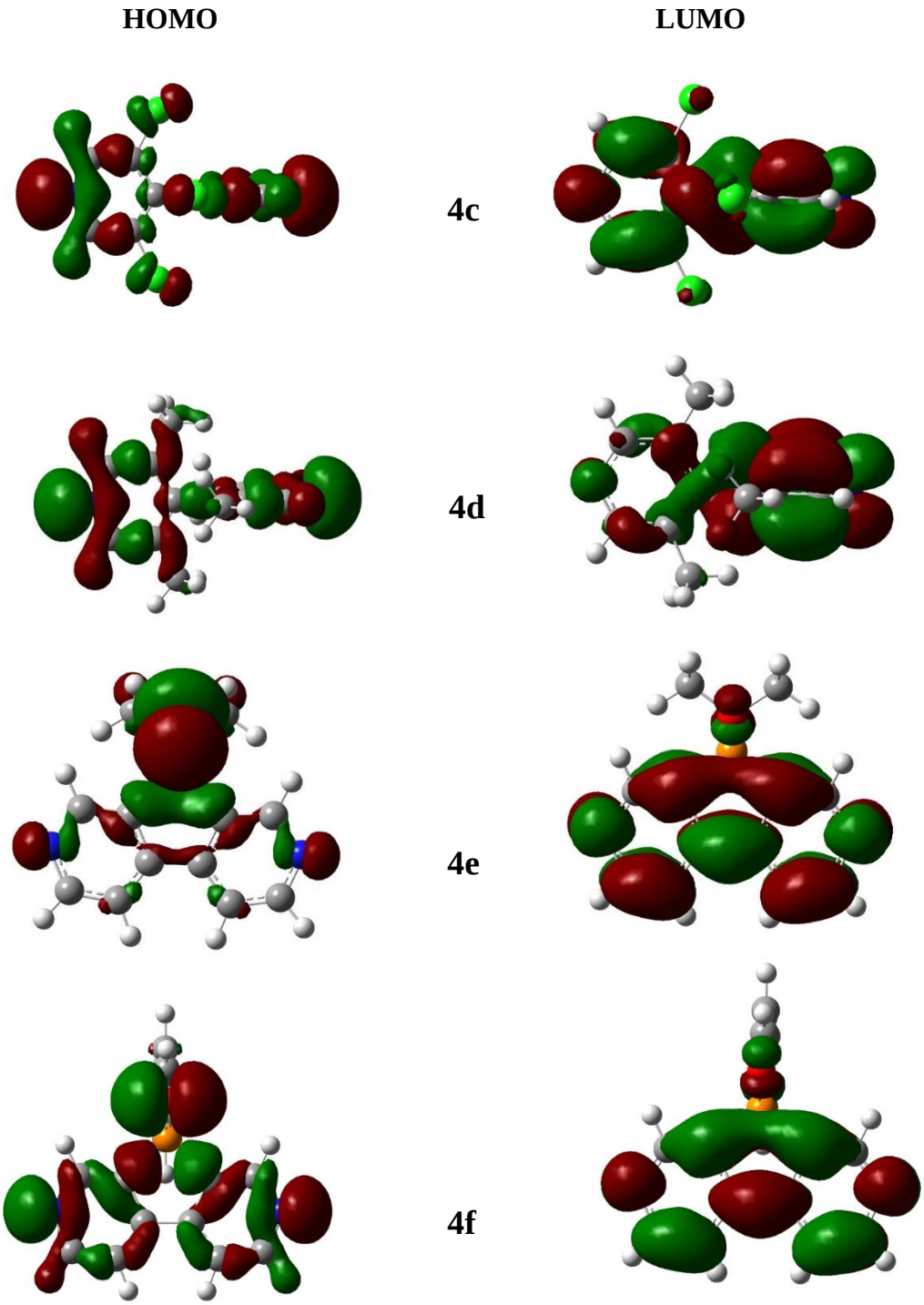

Figure 4.2.5: *Plots of the HOMO and LUMO of 4a, 4b, 4c, 4d, 4e, and 4f left panel are HOMOs and right are LUMOs.*

4.2.3 Binding distance of 4,4'-bipyridine on a gold surface

To calculate the optimum distance for 4,4'-bipyridine between two gold electrodes surfaces, I used DFT with a Generalized Gradient Approximation (GGA)–PBE functional [29-30] and the counterpoise method described in chapter 2. The binding distance d is defined as the distance between the gold surface and the nitrogen atom of the pyridyl group. Here 4,4'-bipyridine (4a) molecule is defined as entity A and the gold electrodes as entity B. The ground state energy of the total system is calculated using SIESTA and is denoted E_{AB}^{AB}. Here the gold leads consist of 3 layers of 25 atoms. The energy of each entity is then calculated in a fixed basis, which is achieved through the use of ghost atoms in SIESTA. Hence the energy of the individual *4a* molecule in the presence of the fixed basis is defined as E_A^{AB} and for the gold as E_B^{AB}. The binding energy is then calculated using the following equation:

$$\text{Binding Energy} = E_{AB}^{AB} - E_A^{AB} - E_B^{AB} \qquad (4.1)$$

Figure 4.2.6 shows that for the optimum binding distance d is 2.3 Å for 4a and the binding energy is approximately -0.42 (eV).

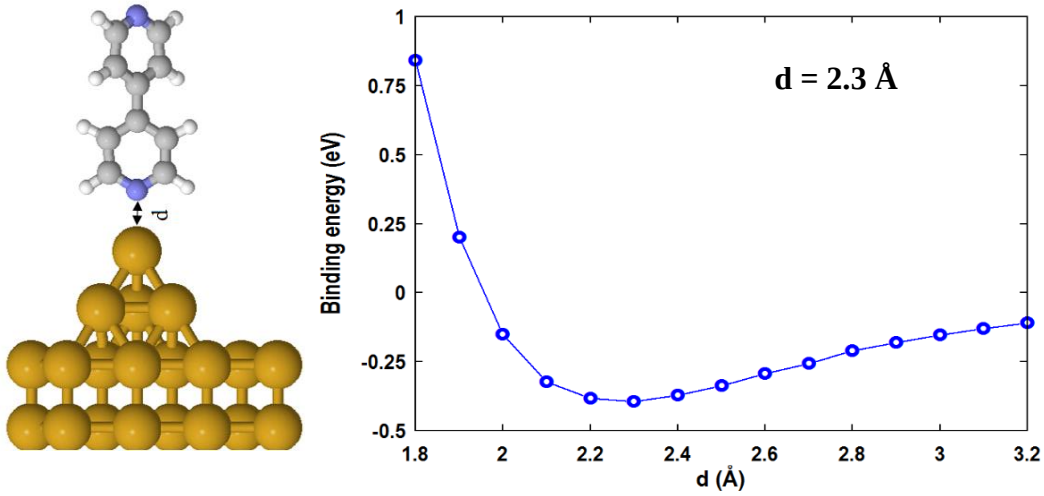

***Figure 4.2.6**. Left panel: Orientation of the 4a with respect to the gold leads. (Right) illustrates binding energy of 4,4'-bipyridine (4a) on a gold surface.*

4.2.4 Transmission coefficient T(E)

To calculate the electronic properties of family of 4,4'-bipyridine's molecules, I used the DFT-based GOLLUM code to compute T(E) [31]. Geometrical optimizations that have carried out using DFT SIESTA [28] code, as well as a Generalized Gradient Approximation (GGA)–PBE functional, double-ξ polarized basis set, and mesh cutoff 250 Ry. All molecules that have been studied in this chapter were freely relaxed in isolation to yield optimized geometries, which are presented in figure 4.1. For each molecular structure, the transmission coefficient of electrons T(E), which describes the propagation of energy of electrons from one electrode to the other was calculated by first calculating the Hamiltonian from SIESTA code, and then using GOLLUM code [31] to compute T(E), and I calculated electrical conductance at room temperature using the formula:

$$G = G_0 \int_{-\infty}^{\infty} \mathrm{dE}\, \mathrm{T}(E) \left(-\frac{df(E)}{dE}\right) \qquad (4.2)$$

where $f(E) = \left[e^{\beta(E-E_F)} + 1\right]^{-1}$ is the Fermi function with $\beta = \frac{1}{k_\beta T}$, E_F is the Fermi energy, $G_0 = \frac{2e^2}{h}$ is the quantum of conductance. To investigate the conductance in more detail, I performed DFT simulations to examine how the conductance of molecules 4a, 4b, 4c, 4d, 4e and 4f depend on three angles, the first one is torsion angle which defines the angle between two rings shown in figure 4.2.8(a), the second one is θ, which defines the tilt angle of the molecule away from normal, and the last one is ϕ, which defines the rotation of the whole molecule about its long axis. As an example, figure 4.2.8(a) shows the case α= 40º, θ=180º and ϕ=0º, where the end phenyl ring is oriented perpendicular to the tip gold surface, and figure 4.2.8(b) shows the case α= 40º, θ=145º and ϕ=50º in which the end phenyl ring is oriented parallel to a surface of the gold tip.

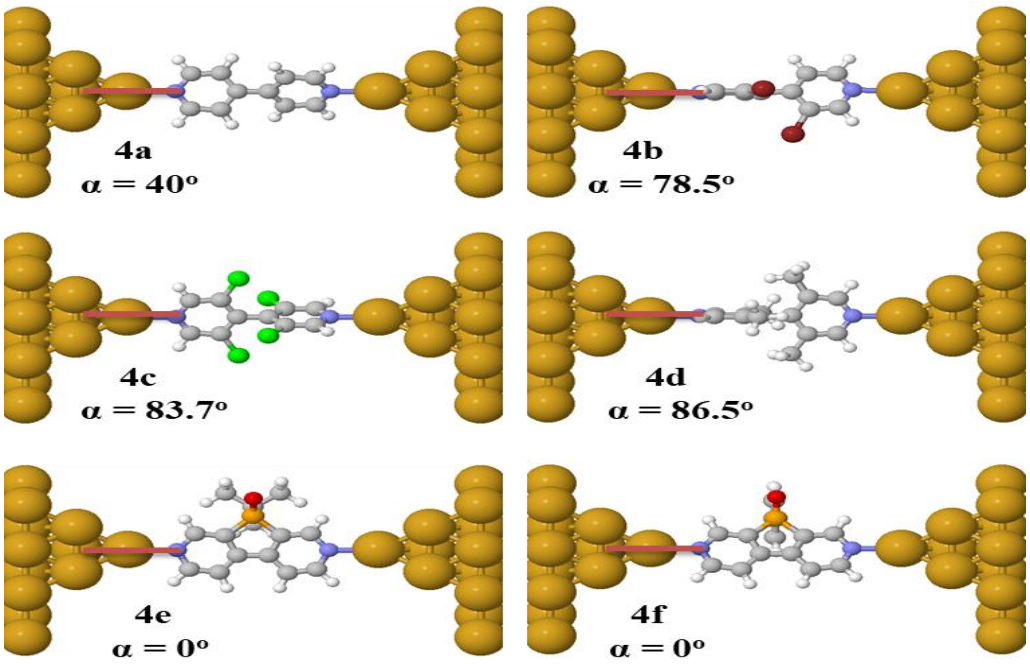

***Figure 4.2.7**: Molecular geometries of family of 4,4'-Bipridine molecules between two gold electrodes at various torsion angles and at θ =180º and ϕ=0º.*

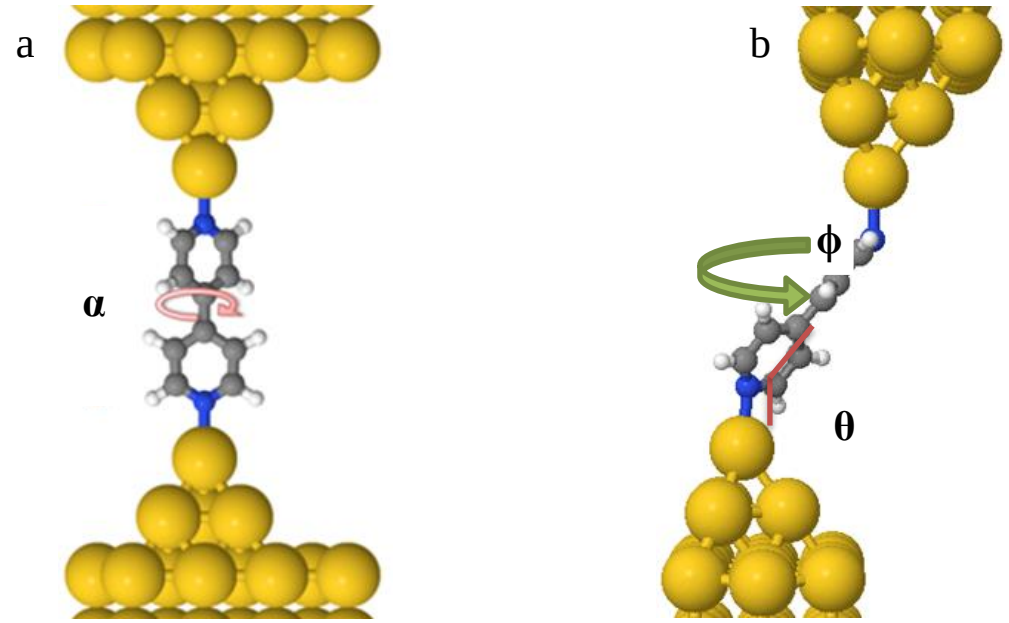

***Figure 4.2.8**: Examples geometries of 4,4'-Bipridine (4a) between two electrodes: a) α = 0°-90°, θ =180°, ϕ=0°. b) α = 40°, θ =145°, ϕ=50°.*

Before performing transport calculations, the isolated molecules were first fully relaxed, and then a further relaxation step was performed after placing the molecules in the electrode-molecule-electrode junctions. The transmission coefficient T(E) for the geometries discussed in figure 4.2.8 are shown in figure 4.2.9. For the first case, when the bipyridine molecule is normal to the gold surface with a tilt angle of θ=180°, I calculate T(E) for a range of values of ϕ between 0 and 90° and find that the conductance does not vary with ϕ and has a value of approximately $3*10^{-4}G_0$ at the Fermi energy ($E-E_F$=-0.4eV). The conductance is unchanged because the coupling strength between the molecule and the gold is constant [32] when the molecule rotates about its axis. In contrast, when the molecule is tilted to an angle of θ =145° the behaviour changes significantly as shown in the transmission coefficients in figures 4.2.9(b). Here the conductance at $E-E_F$=-0.4eV varies between $10^{-4}G_0$ and $10^{-3}G_0$ as ϕ is varied, which is due to the interaction between the end phenyl-ring π systems and the electrode surfaces

changing [33-34], depending on the geometry this can increase or decrease the coupling between nitrogen and the electrodes [32].

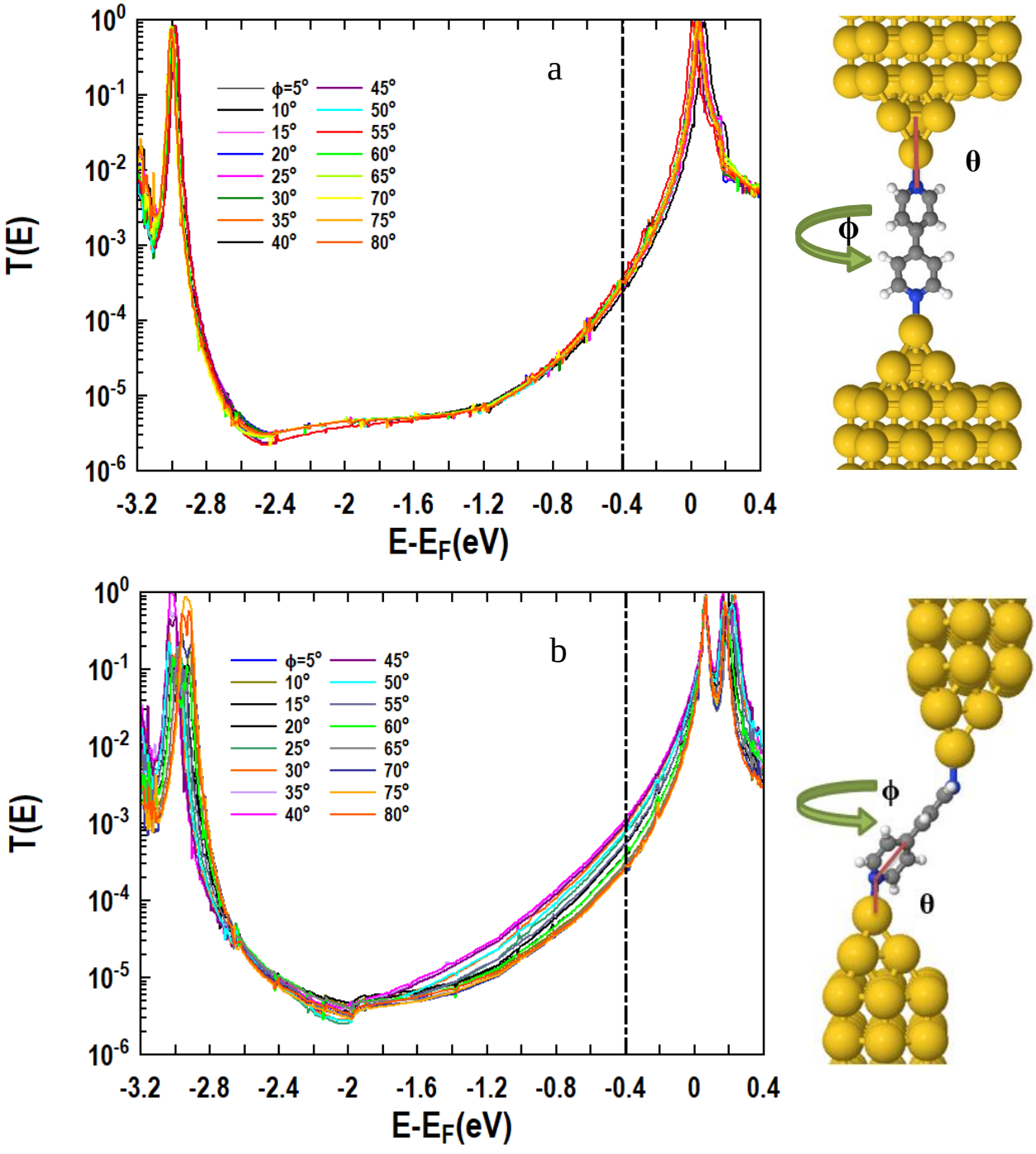

Figure 4.2.9: *Transmission coefficient and orientation of 4,4'-Bipridine (4a) between two electrodes conducts at: a) θ =180°, ϕ=5°-80° and α=40°. b) θ =145°, ϕ=5°-80° and α=40°.*

Next, I investigate that the dependence of conductance on the torsion angle α (0°-90°), to do this I continuously varied α for molecule 4a (fixing θ=180 ϕ=0°) and computed the transmission T(E) versus Fermi energy as shown in figure 4.2.10. This shows that a $\cos^2\alpha$ dependence is obtained over a wide range of Fermi energies within the HOMO-LUMO gap, shown in figure 4.2.10(a).

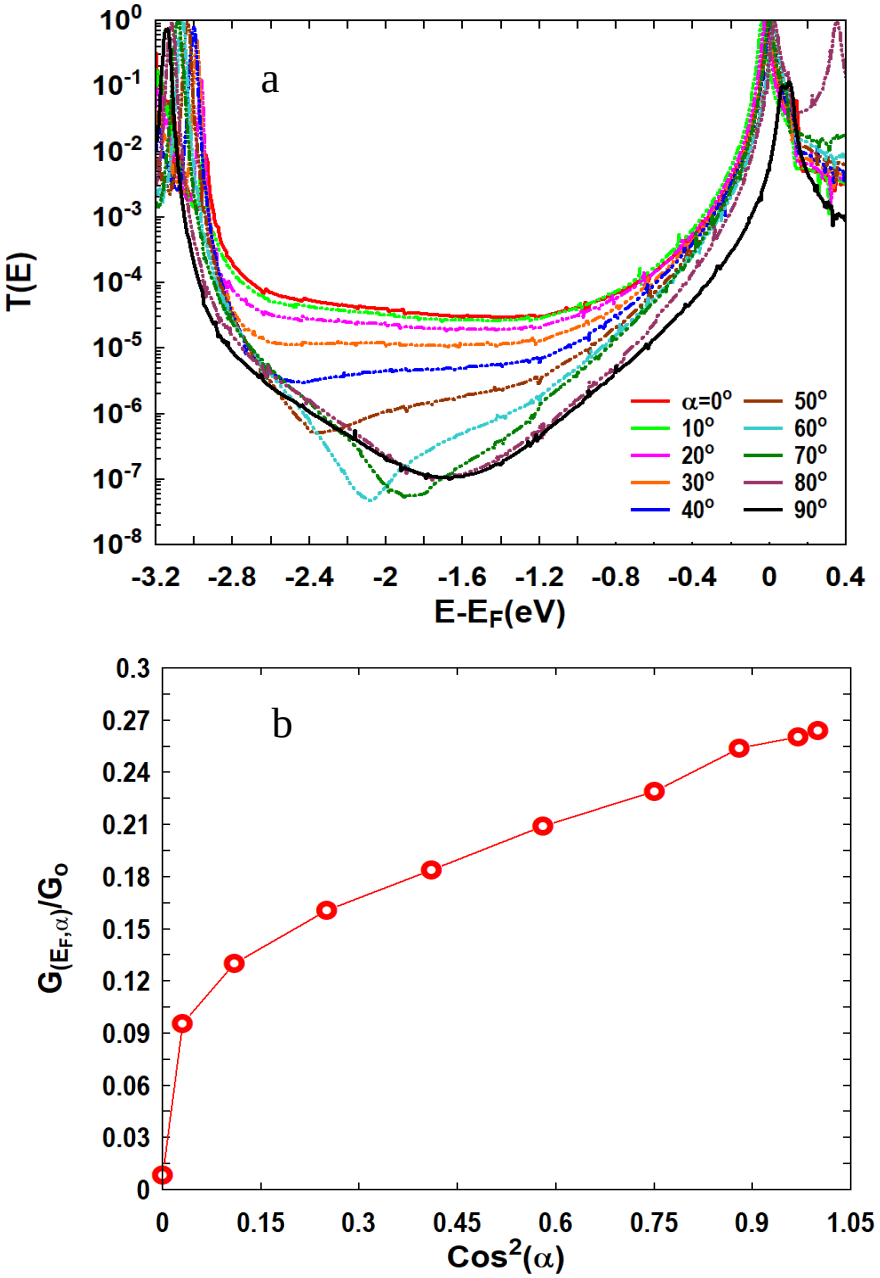

Figure 4.2.10: *(a) DFT results for transmission coefficient as a function of Fermi energy for 4,4'-bipyridine 4a at various torsion angles (α = 0°-90°, θ =180° and ϕ=0°). b) electrical conductance as a function of cos^2(α) at various torsion angles (α = 0°-90°, θ =180° and ϕ=0°*

While the behavior holds in the HOMO-LUMO gap, the DFT-predicted Fermi energy E_F^{DFT} (corresponding to E_F-E_F^{DFT} =0 eV in fig 4.2.10) lies close to the LUMO transport resonance (a well-known property of molecules with pyridine anchor groups) [1, 10, 20-21]. Therefore, at this energy the predicted conductance does not follow a $cos^2\alpha$ dependence [20] and are significantly higher than the measured values. However, by shifting the Fermi energy away from the LUMO to E_F-E_F^{DFT} = -0.4 (eV) gives the correct trend and I justify this shift by comparing to the experimental measurements (seen in section 4.3) which at this energy gives excellent agreement between theory and experiment. The next step is to see if the torsion angle dependence holds for the individual series 4a-f where the angle α is fixed by steric hindrance (The data for these molecules can be found in table 1). Figure 4.2.11 shows the resulting values of transmission coefficients versus Fermi energy for all six molecules. Again, taking the values at (E-E_F=-0.4 eV) the conductance follows a $\cos^2\alpha$ dependence at a tilt angle of θ=180°, showing that the transport is unaffected by the chemical substituents which produce the steric effects.

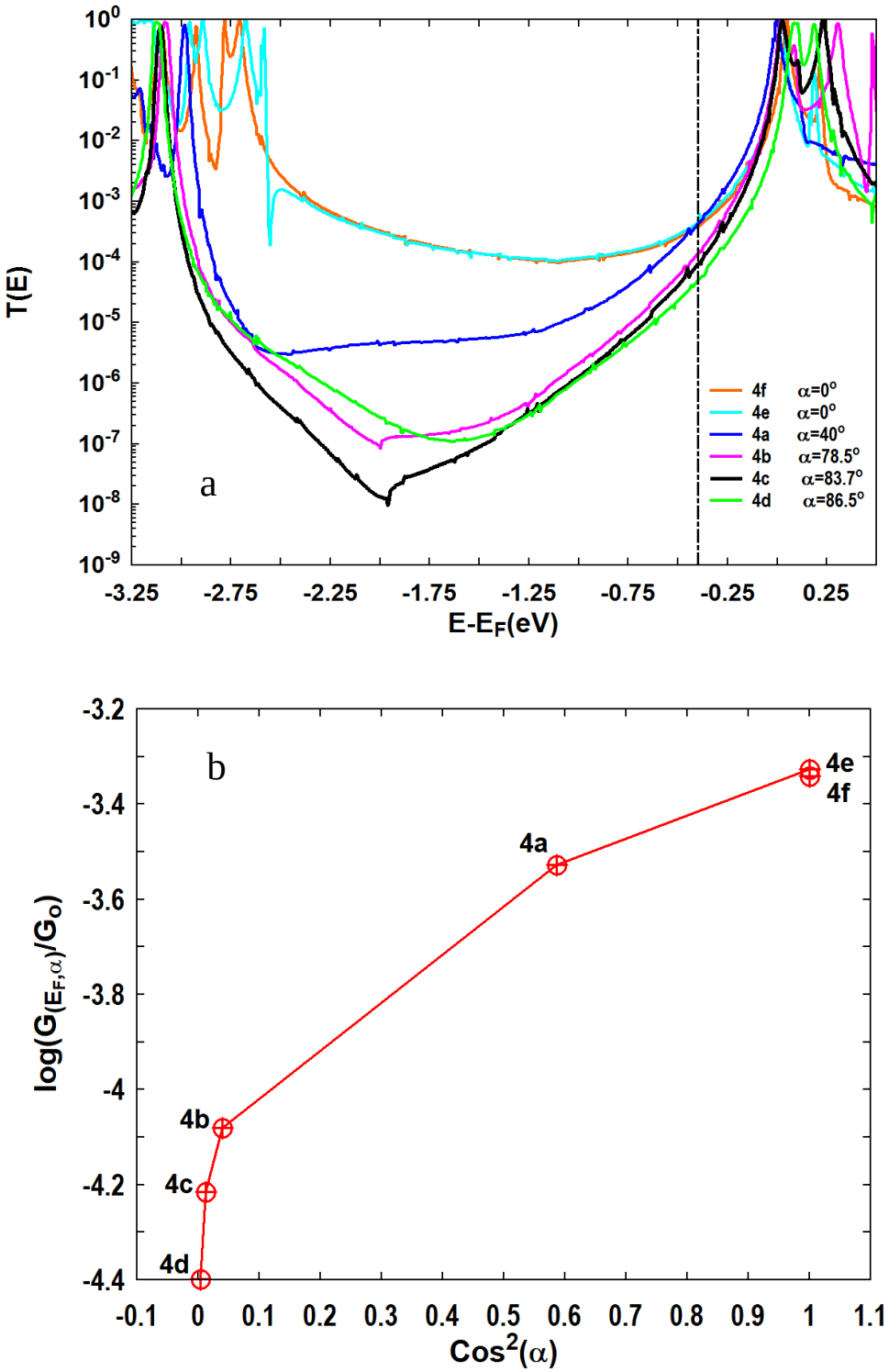

***Figure 4.2.11**: a) The transmission coefficient as a function of energy of election for series of molecules at their respective torsion angles α (θ=180° and ϕ=0°). b) Electrical conductance as a function of cos^2(α) for series of molecules at various torsion angles α (θ =180° and ϕ=0°)*

I now repeat the calculations for the series 4b-4f, varying α and θ in the same way as was carried out for 4a. The resulting transmission coefficients can be seen in figures 4.2.12-4.2.17. These molecules show the same behavior as molecule 4a with the tilt angle of θ=180° showing no dependence on α (left panels labelled a) whereas for the tilted geometry θ=145° the value of T(E) at E-E_F=-0.4eV shows a strong dependence on torsion angle *α*.

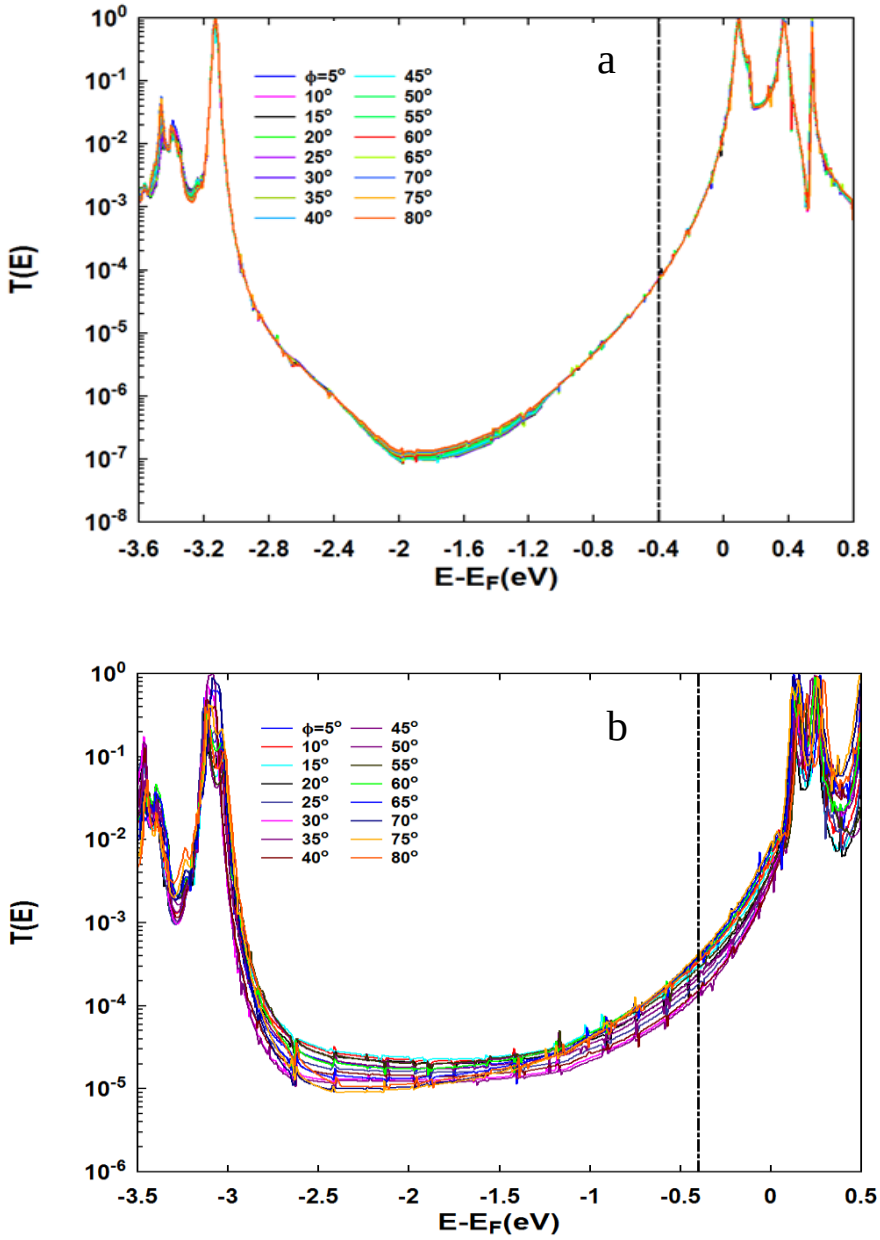

***Figure 4.2.12**: Transmission coefficient as a function of electron energy of 3,3'-dibromo-Bipridine -4,4' (4b) at: a) θ =180º, ϕ=5º-80º and α=78.5º. b) θ =145º, ϕ=5º-80º and α=78.5º.*

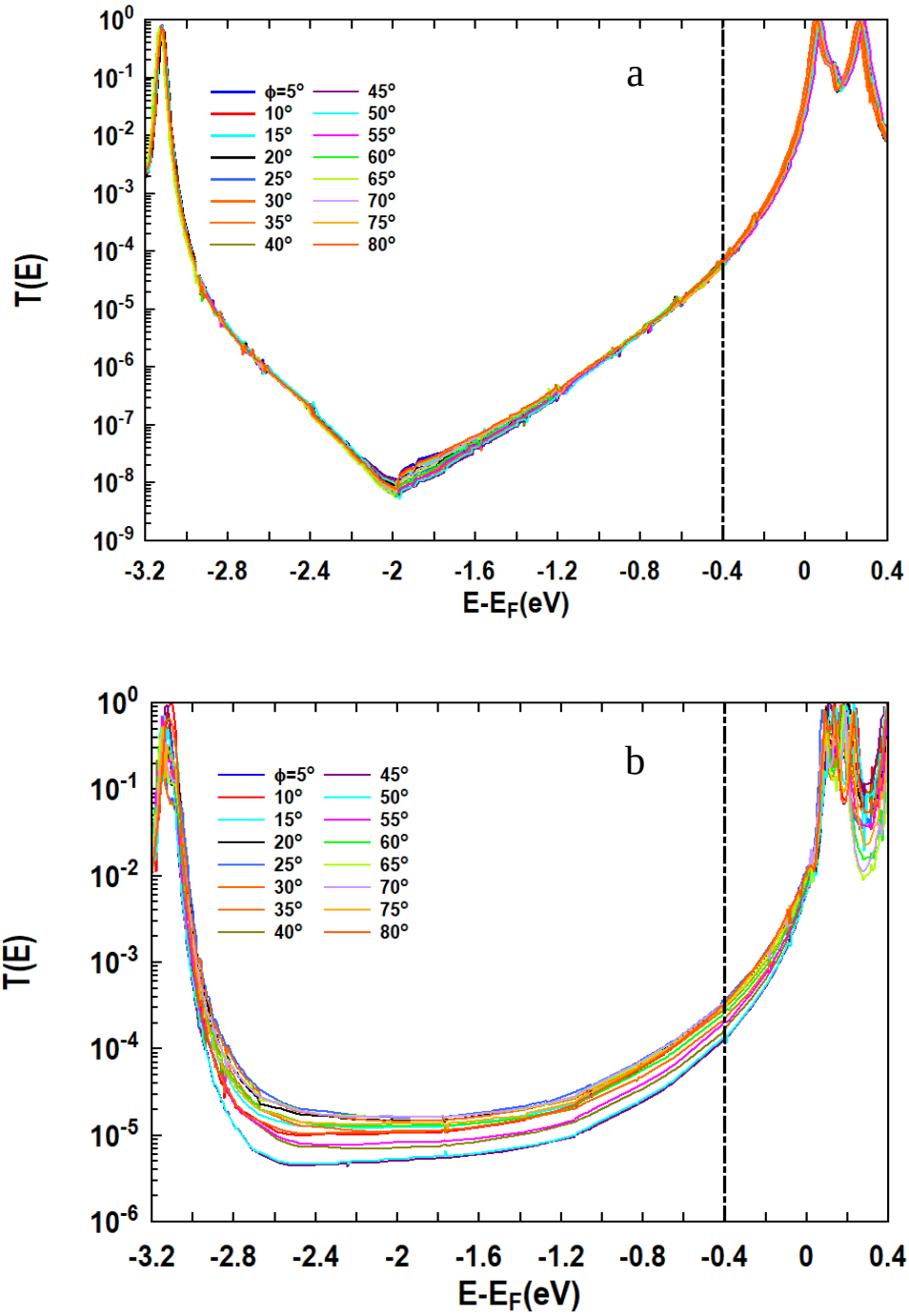

Figure 4.2.13: *Transmission coefficient as a function of electron energy of 3,3',5,5'-tetrachloro-4,4'-bipyridine (4c) at: a) θ =180º, ϕ=5º-80º and α=83.7º. b) θ =145º, ϕ=5º-80º and α=83.7º.*

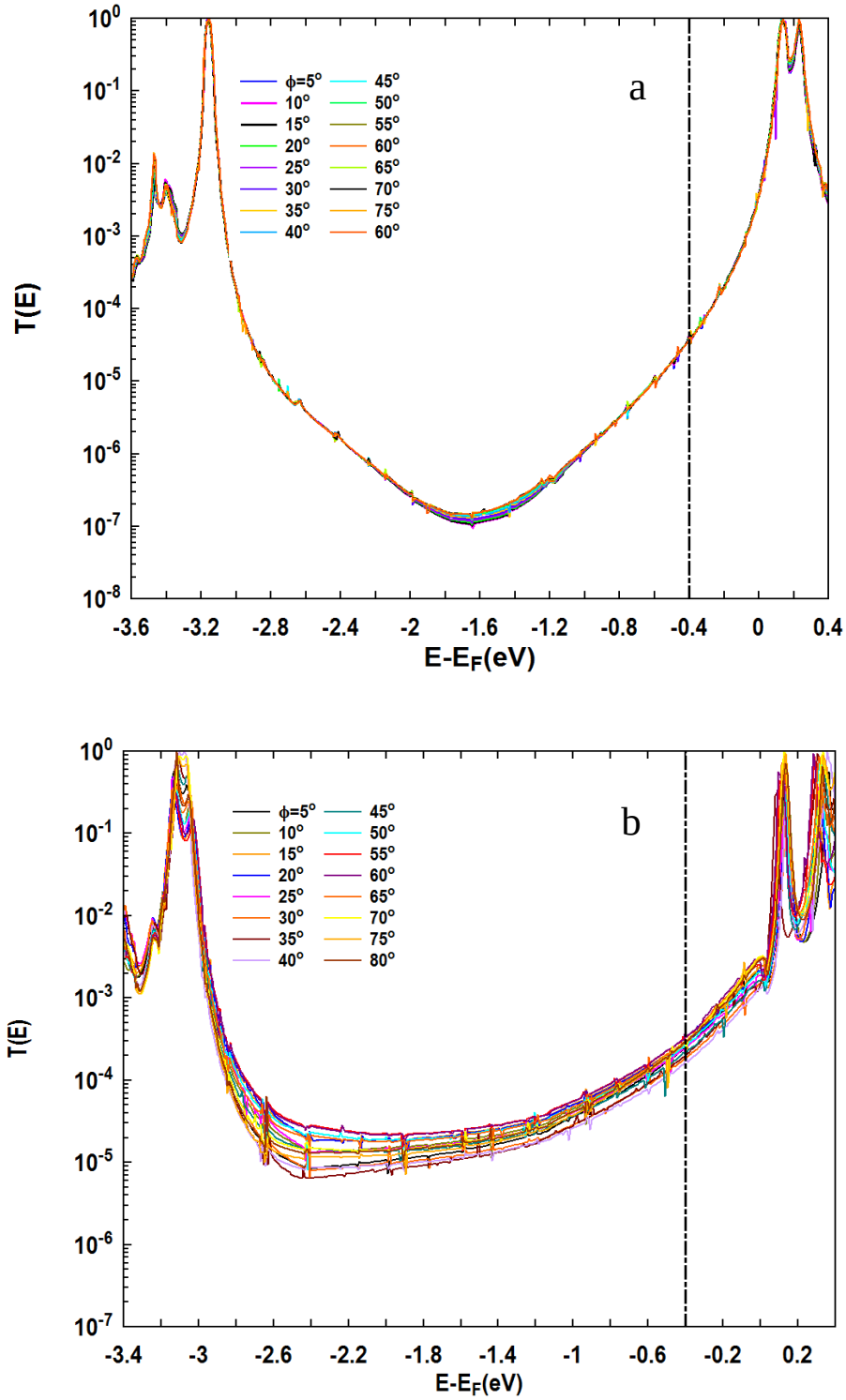

Figure 4.2.14: *Transmission coefficient as a function of electron energy of 3,3',5,5'-tetramethyl-4,4'-bipyridine (4d) at: a) θ =180º, ϕ=5º-80º and α=86.5º. b) θ =145º, ϕ=5º-80º and α=86.5º.*

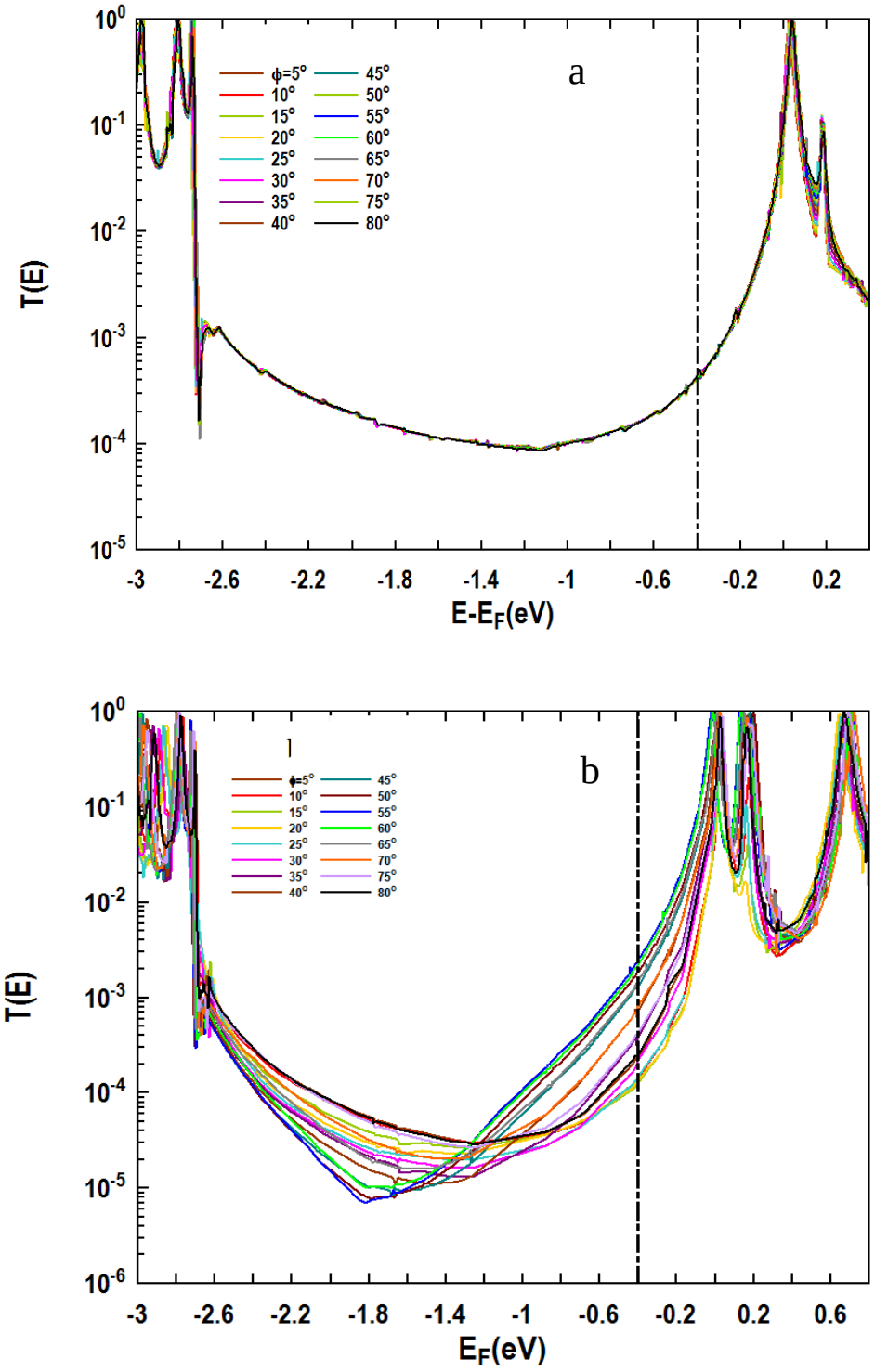

Figure 4.2.15*: Transmission coefficient as a function of electron energy of tert-Butyl-phospho-4,4'-bipyridine (4e) at: a) θ =180º, ϕ=5º-80º and α=0º. b) θ =145º, ϕ=5º-80º and α=0º.*

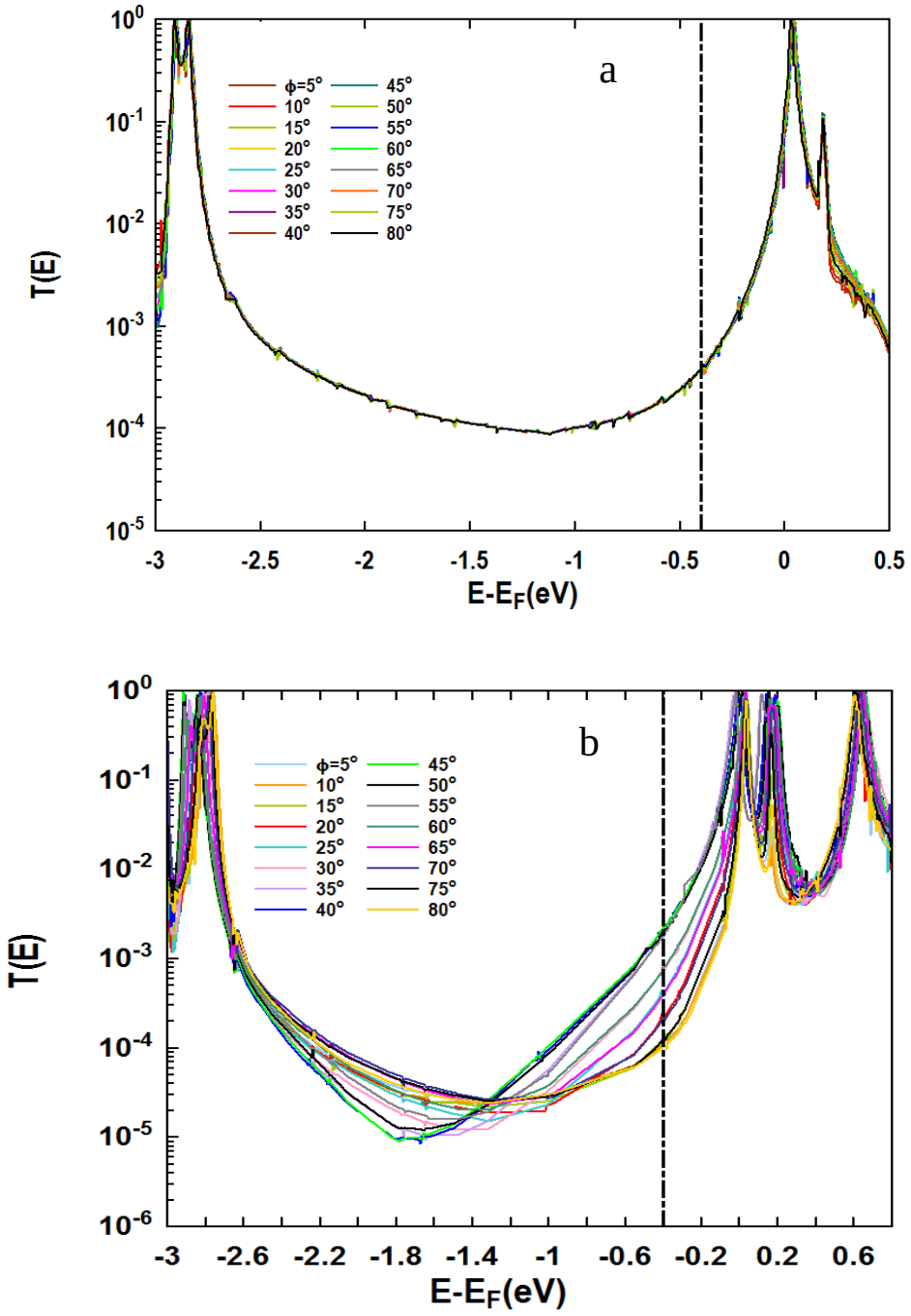

Figure 4.2.16*: Transmission coefficient as a function of electron energy of phospho-4,4'-bipyridine (4f) at: a) θ =180º, ϕ=5º-80º and α=0º. b) θ =145º, ϕ=5º-80º and α=0º.*

To understand how the value of α can change the variation in conductance, I plot the extracted conductance at (E-E_F=-0.4eV) for each of the different torsion angles shown in Figures 4.2.17. This is again done for the two different tilt angles *θ =180º* (left panel a) and *θ =145º* (right panel b). Here the individual circles represent a different value of

α between 0 and 90°. These two figures show that for the elongated junction (a) where there is no tilt angle, the conductance is largely unaffected, and it also has a value lower than the compressed junction (b) where the molecule is tilted. Figure 4.2.17 also shows the distribution of conductance values is strongly dependent on torsion angle when the molecule is tilted. For molecules which have a large torsion angle (4b, 4c and 4d), varying α causes the conductance to change by approximately a factor of 2. Whereas, for 4e and 4f where the torsion angle is 0° the conductance can change by almost an order of magnitude. This behaviour can be explained by the coupling between the terminal pyridine rings and the tips of the gold electrodes; when the molecule is tilted the π-system of the molecule interacts with the gold enhancing the coupling strength which explains the larger conductance for the tilted systems. The parameter α controls the amount of overlap between the π-system and gold and therefore for molecules with a torsion angle of 0, symmetry means that coupling to both electrodes is identical. For molecules with a large torsion angle, this symmetry is broken so that if the coupling is strong at one side it will be weak at the other meaning that they produce a much smaller range of conductance values as seen in Figure 4.2.17.

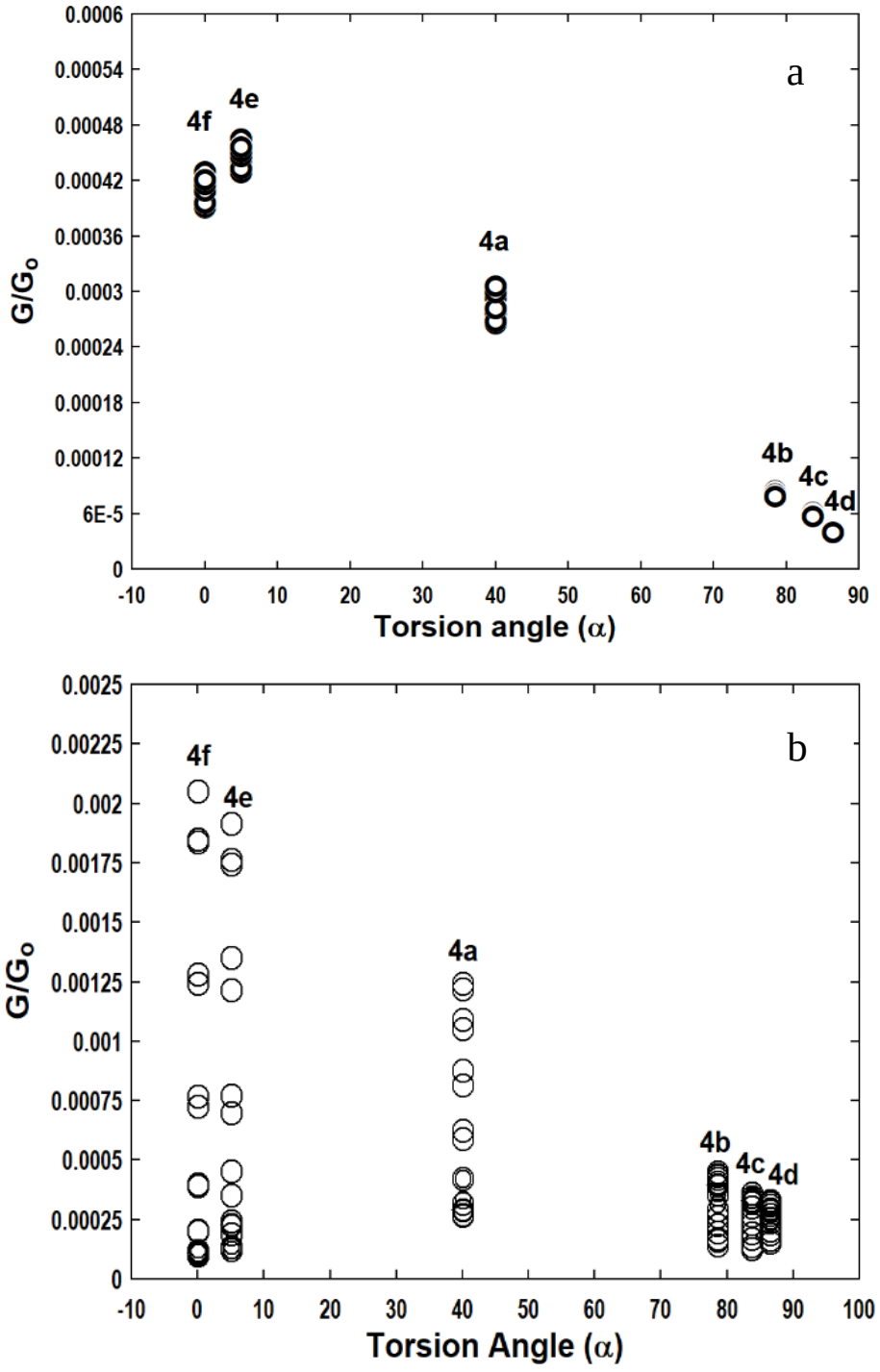

Figure 4.2.17*: Shows Junction conductance of all molecules at: a) θ =180°, ϕ=5°-80°. b) θ =145°, ϕ=5°-80°.*

4.3. Experimental methods and measurements

Having performed a detailed theoretical study of the geometry parameters controlling this series of molecule I now compare the results to experiment. These were performed at the University of Liverpool and used the STM-Break Junction technique [24]. The transport characteristics were measured in solution at room temperature, this method was first described in 2003 [35]. In this technique, a gold STM tip is pushed into a gold substrate under constant bias, and then retracted while the current flowing between the two electrodes is measured. Interestingly, 4,4'-bipyridine and 4-pyridyl terminated molecular wire generally show two conductance states depending on the contact geometry [32], the consensus being that a high conductance value is measured with the molecule tilted between the two electrodes, with electrons injected directly into the ring π-system, and a lower conductance is measured when the molecule is sitting upright in the junction, with electron injected into the N-end of the pyridyl ring. Furthermore, mechanical control of electrode separation allows cycling between the two conductance's states [32].

Being able to introduce substituents in such positions allows control of the inter-ring torsional angle, and therefore to further test the validity of the $cos^2\alpha$ dependence. We applied these recent synthetic findings to prepare and characterize a series of 4,4'-bipyridines with α varying from 0 to ≈ 90º. In our study, we found that, while the $cos^2\alpha$ dependence found in the biphenyl system is still valid for the 4,4'-bipyridines, locking the two rings in a coplanar geometry ($\alpha = 0$) results in the suppression of one of the two conductance states. Moreover, the $cos^2\alpha$ dependence suggests that the bridged bipyridyls sit in the junction in the low (upright) conductance state, greatly increased in its conductance value by inter-ring locking.

Brominated 4,4'-bipyridines were synthesized by using copper [33] or iodine [34] catalyzed coupling of brominated 4-lithiopyridine, prepared by treating the appropriate pyridine with LDA at -94º C. This allowed our collaborator group to prepare 3,3'-dibromo- and 3,3',5,5'-tetrabromo-4,4'-bipyridine, that can be further functionalized by lithium-halogen exchange (with ^{n}BuLi or ^{t}BuLi) and subsequent quench with an electrophile to give the compounds presented in figure 4.1.

The compounds were characterized by H NMR [1], C NMR [15] and mass spectrometry, and their purity assessed by CHN microanalysis. The conductances were measured (as current /voltage) using the *STM-BJ* technique. In this method, Au-Au point contacts were repeatedly formed and broken by moving the STM Au tip in and out of contact with a Au substrate. In the presence of a mesitylene (1,3,5-trimethylbenzene) 1 mM solution of the desired molecular wire, under constant bias (100 mV). Thousands of current-distance traces are recorded while moving the tip, and these were then compiled in histograms, bearing a statistical distribution of conductance values, and 2d "density" plots, showing the distribution of conductance values as a function of electrodes separation. Conductance is given as a function of G_0 (quantum of conductance, 77.48 μS). All the non-bridged compounds showed two distinct conductance values (two separate peaks in the histograms), ascribed to the possibility of high- and low-conductance geometry in the *Au/molecule/Au junction*, and the values follow indeed the general $cos^2\alpha$ rule. In contrast the two bridged (α locked to 0º, orange and blue trace in figure 4.3.1a) bipyridyls showed only one sharp peak. A comparison between theoretical and experimental results of conductance and torsion angle (α) are shown in table1.

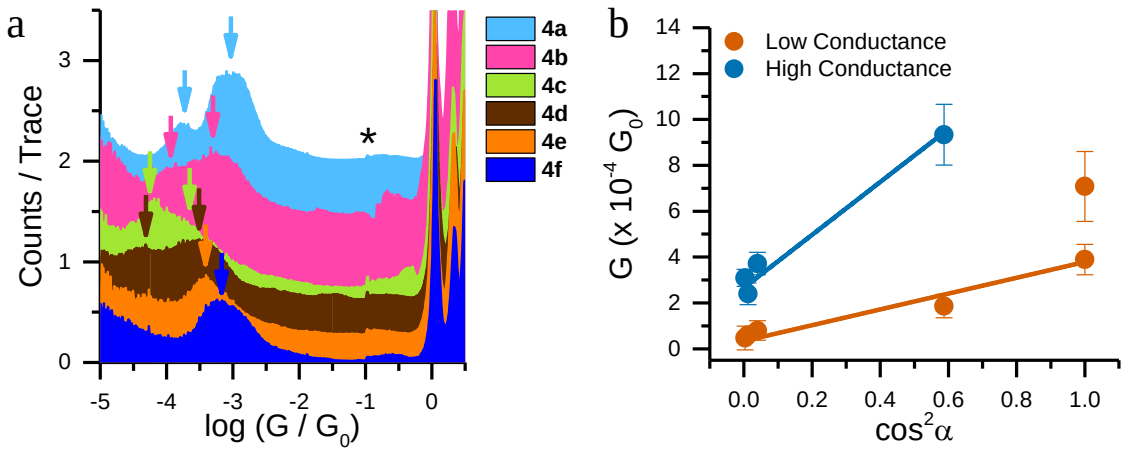

Figure 4.3.1: *a) Semilogarithmic conductance histogram of the molecular wires presented in this study. 100 mV bias voltage, normalized to counts / trace. * is an artifact introduced by the channel switch in the STM preamplifier used in this study. b) Cos²α dependence of conductance.*

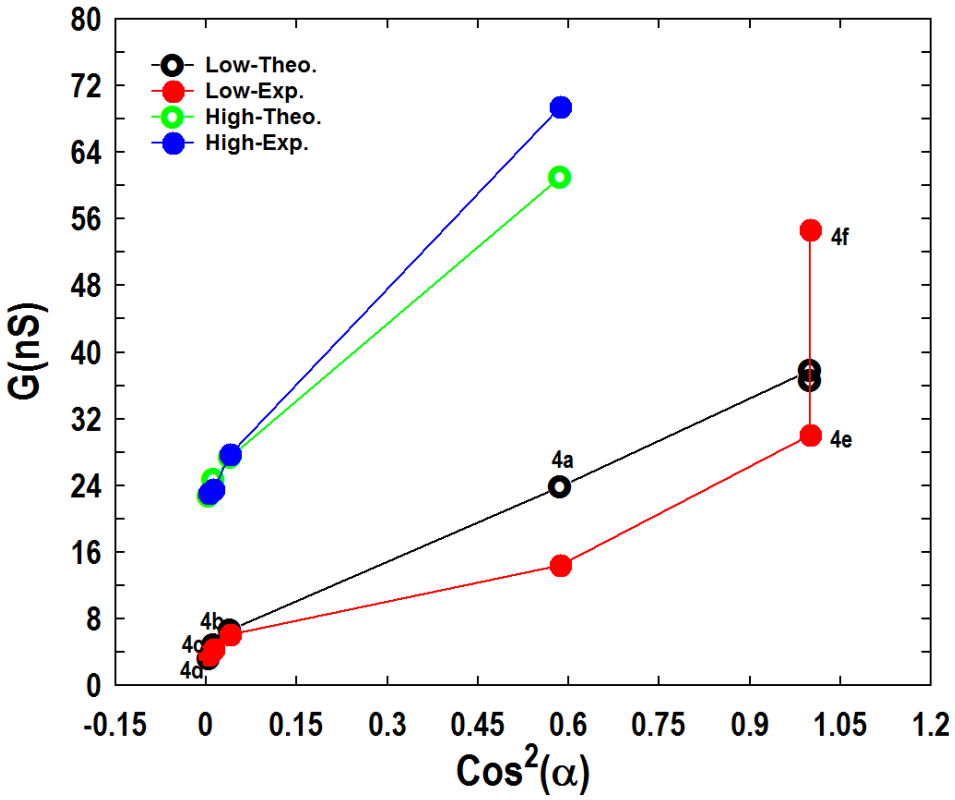

Figure 4.3.2*: Theoretical (black and green) and experimental (red and blue) results for high and low conductances as a function of cos²α.*

Table 1 | Measured and theoretical properties of six molecules with their structures.

No. Molecules	Structure	Conductance (nS) Measured	Calculated	Torsion angle (α)
4f	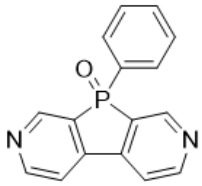	**60.0**	**35.33**	**0º**
4e	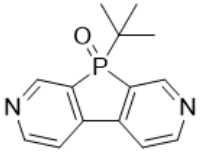	**31.0**	**36.5**	**0º**
4a	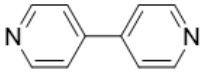	**14.0**	**23.02**	**40º**
4b	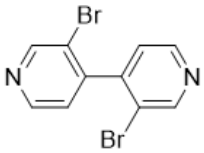	**4.4**	**6.43**	**78.5º**
4c	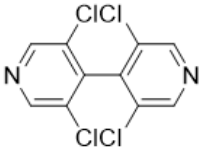	**4.3**	**4.751**	**83.7º**
4d	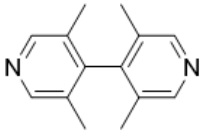	**3.4**	**3.132**	**86.5º**

As shown in Table 1, molecules 4a, 4b, 4c, and 4d that have torsion angles as 40º, 78.5º, 83.7º and 86.5º, respectively. Furthermore, when these torsion angles are used to plot their conductances versus $\cos^2\alpha$, both theory and experiment confirm the $\cos^2\alpha$ rule. Figure 4.3.2 shows a plot of the above experimental and theoretical results for the low and high conductance groups.

4.5 Conclusions

We have studied the transport properties of a family of 4,4-bipyridine molecules, with a series of sterically-induced twist angles α between the two pyridyl rings. Experiment reveals the presence of high and low conductance peaks, which are attributed to different molecule orientations within the junctions. Both experimental measurements using the using the *STM-BJ* technique and DFT-based theory calculations reveal that their conductances are proportional to $\cos^2(\alpha)$ confirming that for both geometries (tilted and non-tilted), the electrical current flows through the C-C bond linking the pi systems of the two rings. In common with many calculations of electron transport through pyridyl-terminated molecules, DFT predicts that the Fermi energy of the gold electrodes lies close to the LUMO transmission peak, in which case there would be no $\cos^2(\alpha)$ dependence. However, shifting this to lower energies corrects this error and confirms that the Fermi energy of gold lies within the HOMO-LUMO gap. The fact that no high conductance values are measured for the $\alpha=0°$ can be theoretically attributed to the large spread of conductance values these systems produce meaning they may be difficult to measure.

Bibliography:

[1] Shaporenko, Andrey, Mark Elbing, Alfred Błaszczyk, Carsten von Hänisch, Marcel Mayor, and Michael Zharnikov. "Self-assembled monolayers from biphenyldithiol derivatives: Optimization of the deprotection procedure and effect of the molecular conformation." The Journal of Physical Chemistry B 110, no. 9 (2006): 4307-4317.

[2] Mishchenko, Artem, David Vonlanthen, Velimir Meded, Marius Burkle, Chen Li, Ilya V. Pobelov, Alexei Bagrets et al. "Influence of conformation on conductance of biphenyl-dithiol single-molecule contacts." Nano letters 10, no. 1 (2009): 156-163.

[3] Dell, Emma J., Brian Capozzi, Kateri H. DuBay, Timothy C. Berkelbach, Jose Ricardo Moreno, David R. Reichman, Latha Venkataraman, and Luis M. Campos. "Impact of molecular symmetry on single-molecule conductance." Journal of the American Chemical Society 135, no. 32 (2013): 11724-11727.

[4] Vezzoli, Andrea, Iain Grace, Carly Brooke, Kun Wang, Colin J. Lambert, Bingqian Xu, Richard J. Nichols, and Simon J. Higgins. "Gating of single molecule junction conductance by charge transfer complex formation." Nanoscale 7, no. 45 (2015): 18949-18955.

[5] Ismael, Ali K., Iain Grace, and Colin J. Lambert. "Increasing the thermopower of crown-ether-bridged anthraquinones." Nanoscale 7, no. 41 (2015): 17338-17342.

[6] Zhang, Wei, Shiyu Gan, Andrea Vezzoli, Ross J. Davidson, David C. Milan, Konstantin V. Luzyanin, Simon J. Higgins et al. "Single-Molecule Conductance of Viologen–Cucurbit [8] uril Host–Guest Complexes." ACS nano 10, no. 5 (2016): 5212-5220.

[7] García, Raúl, M. Ángeles Herranz, Edmund Leary, M. Teresa González, Gabino Rubio Bollinger, Marius Bürkle, Linda A. Zotti et al. "Single-molecule conductance of a chemically modified, π-extended tetrathiafulvalene and its charge-transfer complex with F4TCNQ." Beilstein journal of organic chemistry 11 (2015): 1068.

[8] Choi, Bonnie, Brian Capozzi, Seokhoon Ahn, Ari Turkiewicz, Giacomo Lovat, Colin Nuckolls, Michael L. Steigerwald, Latha Venkataraman, and Xavier Roy. "Solvent-dependent conductance decay constants in single cluster junctions." Chemical Science 7, no. 4 (2016): 2701-2705.

[9] Milan, David C., Oday A. Al-Owaedi, Marie-Christine Oerthel, Santiago Marqués-González, Richard J. Brooke, Martin R. Bryce, Pilar Cea et al. "Solvent dependence of the single molecule conductance of oligoyne-based molecular wires." The Journal of Physical Chemistry C 120, no. 29 (2015): 15666-15674.

[10] Fatemi, V., M. Kamenetska, J. B. Neaton, and L. Venkataraman. "Environmental control of single-molecule junction transport." Nano letters 11, no. 5 (2011): 1988-1992.

[11] Baghernejad, Masoud, David Zsolt Manrique, Chen Li, Thomas Pope, Ulmas Zhumaev, Ilya Pobelov, Pavel Moreno-García et al. "Highly-effective gating of single-molecule junctions: an electrochemical approach." Chemical communications 50, no. 100 (2014): 15975-15978.

[12] Osorio, Henrry M., Samantha Catarelli, Pilar Cea, Josef BG Gluyas, František Hartl, Simon J. Higgins, Edmund Leary et al. "Electrochemical single-molecule transistors with optimized gate coupling." Journal of the American Chemical Society 137, no. 45 (2015): 14319-14328.

[13] Li, Yonghai, Masoud Baghernejad, Al-Galiby Qusiy, David Zsolt Manrique, Guanxin Zhang, Joseph Hamill, Yongchun Fu et al. "Three-State Single-Molecule Naphthalenediimide Switch: Integration of a Pendant Redox Unit for Conductance Tuning." Angewandte Chemie International Edition 54, no. 46 (2015): 13586-13589.

[14] Löfås, Henrik, Andreas Orthaber, Burkhard O. Jahn, Alvi M. Rouf, Anton Grigoriev, Sascha Ott, Rajeev Ahuja, and Henrik Ottosson. "New class of molecular conductance switches based on the [1, 3]-silyl migration from silanes to silenes." The Journal of Physical Chemistry C 117, no. 21 (2013): 10909-10918.

[15] Roldan, Diego, Veerabhadrarao Kaliginedi, Saioa Cobo, Viliam Kolivoska, Christophe Bucher, Wenjing Hong, Guy Royal, and Thomas Wandlowski. "Charge transport in photoswitchable dimethyldihydropyrene-type single-molecule junctions." Journal of the American Chemical Society 135, no. 16 (2013): 5974-5977.

[16] Jia, Chuancheng, Agostino Migliore, Na Xin, Shaoyun Huang, Jinying Wang, Qi Yang, Shuopei Wang et al. "Covalently bonded single-molecule junctions with stable and reversible photoswitched conductivity." Science 352, no. 6292 (2016): 1443-1445.

[17] Taherinia, Davood, and C. Daniel Frisbie. "Photoswitchable hopping transport in molecular wires 4 nm in length." The Journal of Physical Chemistry C 120, no. 12 (2016): 6442-6449.

[18] Luo, Liang, Ahmed Benameur, Pierre Brignou, Seong Ho Choi, Stéphane Rigaut, and C. Daniel Frisbie. "Length and temperature dependent conduction of ruthenium-containing redox-active molecular wires." The Journal of Physical Chemistry C 115, no. 40 (2011): 19955-19961.

[19] Selzer, Yoram, Marco A. Cabassi, Theresa S. Mayer, and David L. Allara. "Thermally activated conduction in molecular junctions." Journal of the American Chemical Society 126, no. 13 (2004): 4052-4053.

[20] Bürkle, Marius, Janne K. Viljas, David Vonlanthen, Artem Mishchenko, Gerd Schön, Marcel Mayor, Thomas Wandlowski, and Fabian Pauly. "Conduction mechanisms in biphenyl dithiol single-molecule junctions." Physical Review B 85, no. 7 (2012): 075417.

[21] Pauly, Fabian, Janne K. Viljas, Juan Carlos Cuevas, and Gerd Schön. "Density-functional study of tilt-angle and temperature-dependent conductance in biphenyl dithiol single-molecule junctions." Physical Review B 77, no. 15 (2008): 155312.

[22] Finch, Christopher M., Skon Sirichantaropass, Steven W. Bailey, Iain M. Grace, Victor M. Garcia-Suarez, and Colin J. Lambert. "Conformation dependence of molecular conductance: chemistry versus geometry." Journal of Physics: Condensed Matter 20, no. 2 (2007): 022203.

[23] Xu, Bingqian, and Nongjian J. Tao. "Measurement of single-molecule resistance by repeated formation of molecular junctions." Science 301, no. 5637 (2003): 1221-1223.

[24] Venkataraman, Latha, Jennifer E. Klare, Colin Nuckolls, Mark S. Hybertsen, and Michael L. Steigerwald. "Dependence of single-molecule junction conductance on molecular conformation." Nature 442, no. 7105 (2006): 904-907.

[25] Artacho, Emilio, Eduardo Anglada, Oswaldo Diéguez, Julian D. Gale, Alberto García, Javier Junquera, Richard M. Martin et al. "The SIESTA method; developments and applicability." Journal of Physics: Condensed Matter 20, no. 6 (2008): 064208.

[26] a) Becke, Axel D. "Becke's three parameter hybrid method using the LYP correlation functional." J. Chem. Phys 98 (1993): 5648-5652; b) Stephens, P. J., F. J. Devlin, CFn Chabalowski, and Michael J. Frisch. "Ab initio calculation of vibrational absorption and circular dichroism spectra using density functional force fields." The Journal of Physical Chemistry 98, no. 45 (1994): 11623-11627.

[27] Petersson, G. A., and Mohammad A. Al-Laham. "A complete basis set model chemistry. II. Open-shell systems and the total energies of the first-row atoms." The Journal of chemical physics 94, no. 9 (1991): 6081-6090.

[28] Soler, José M., Emilio Artacho, Julian D. Gale, Alberto García, Javier Junquera, Pablo Ordejón, and Daniel Sánchez-Portal. "The SIESTA method for ab initio order-N materials simulation." Journal of Physics: Condensed Matter 14, no. 11 (2002): 2745.

[29] Kim, Kwang S., P. Tarakeshwar, and Jin Yong Lee. "Molecular clusters of π-systems: theoretical studies of structures, spectra, and origin of interaction energies." Chemical reviews 100, no. 11 (2000): 4145-4186.

[30] Watson, Mark D., Andreas Fechtenkötter, and Klaus Müllen. "Big is beautiful−"aromaticity" revisited from the viewpoint of macromolecular and supramolecular benzene chemistry." Chemical Reviews 101, no. 5 (2001): 1267-1300.

[31] Ferrer, Jaime, Colin J. Lambert, Víctor Manuel García-Suárez, D. Zs Manrique, D. Visontai, L. Oroszlany, Rubén Rodríguez-Ferradás et al. "GOLLUM: a next-generation simulation tool for electron, thermal and spin transport." New Journal of Physics 16, no. 9 (2014): 093029.

[32] Quek, Su Ying, Maria Kamenetska, Michael L. Steigerwald, Hyoung Joon Choi, Steven G. Louie, Mark S. Hybertsen, J. B. Neaton, and Latha Venkataraman. "Mechanically controlled binary conductance switching of a single-molecule junction." Nature nanotechnology 4, no. 4 (2009): 230-234.

[33] Haiss, Wolfgang, Changsheng Wang, Rukkiat Jitchati, Iain Grace, Santiago Martin, Andrei S. Batsanov, Simon J. Higgins et al. "Variable contact gap single-molecule conductance determination for a series of conjugated molecular bridges." Journal of Physics: Condensed Matter 20, no. 37 (2008): 374119.

[34] Haiss, Wolfgang, Changsheng Wang, Iain Grace, Andrei S. Batsanov, David J. Schiffrin, Simon J. Higgins, Martin R. Bryce, Colin J. Lambert, and Richard J. Nichols. "Precision control of single-molecule electrical junctions." Nature materials 5, no. 12 (2006).

[35] Kim, Taekyeong, Pierre Darancet, Jonathan R. Widawsky, Michele Kotiuga, Su Ying Quek, Jeffrey B. Neaton, and Latha Venkataraman. "Determination of energy level alignment and coupling strength in 4, 4′-Bipyridine single-molecule junctions." Nano letters 14, no. 2 (2014): 794-798.

Chapter 5

Oscillating Seebeck coefficient in π-stacked molecular junctions

In this chapter, I perform a theoretical investigation into the Seebeck coefficient S of π-stacked molecular junctions using a first principles quantum transport method. Using oligo (phenyleneethynylene) (OPE)-type molecules as a model system, I have showed that quantum interference produces antiresonances in the gap between the HOMO and LUMO resonances and the stacking geometry can control the position of these destructive interference features. The shifting of this antiresonance leads to an enhancement of the thermopower *S* when the geometry of the stacking is altered. The sign of *S* also oscillates with the overlap of the two molecules. This behaviour is dependent on the connectivity of the molecule as a meta-connected molecule produces a destructive QI feature which dominates and reduces the sensitivity to destructive interference through the pi-stacking geometry.

5.1 Introduction

Measurement of the Seebeck coefficient *S* in single-molecule junctions [1-9] has opened up the possibility of utilizing such devices in novel thermoelectric materials. A wide variety of molecules have been measured and the value of *S* is typically low in single molecules with values much less than 100μV/K [9]. One important property of *S* is that it helps to determine the nature of the transport in the HOMO-LUMO gap of the molecule; with a positive *S* determining the position of the Fermi energy is close to the HOMO resonance and a negative *S* means it is closer to the LUMO. In addition, molecules have been shown to display bi-thermoelectric behaviour and this has been attributed to both geometric changes [10] and the application of pressure [11]. In both these cases, the sign change in *S* changes due to shifting positions of the molecular resonances. Another important property in single molecule transport is quantum interference which has shown great promise in the control of quantum transport through design of the molecular structure [12-19]. The increase and decrease in conductance (i.e. constructive or destructive interference) is due to multiple transmission paths that an electron can take through a molecule.

One type of molecular junction that has shown quantum interference is stacked molecules [20-23] where the molecules bridge the gap between the electrodes by attaching one anchor at each end and the electron path from one electrode to the other is through the overlap π-orbitals of the molecules overlap. In this scenario the junction shows destructive interference at certain geometries due to the different transmission paths. Experimental evidence that such junctions form can be seen in situations where molecules only have one anchor group [20,22], but also improved methods of analyzing conductance data [24] show they may occur in any junction with molecules that has a

preference to stack through their π-systems. In this work we analyze the importance that π-stacked junctions may have on future thermoelectric materials with the aim of maximising *S*. The efficiency of a device is usually calculated from the dimensionless figure of merit [25, 26] $ZT = S^2G\tau/k$, where G is the electrical conductance, k is the thermal conductance, and τ the temperature. *S* is squared in the numerator so controlling this term is a possible route to improving performance. We also show that careful consideration should be taken into the measurement of *S*, especially where a molecule displays both positive and negative *S* as this could simply be attributed to transport through multiple molecules and quantum interference. And the aim in maximising *S*, is because there is now a world-wide race to develop molecular materials with a high thermoelectric efficiency [25].

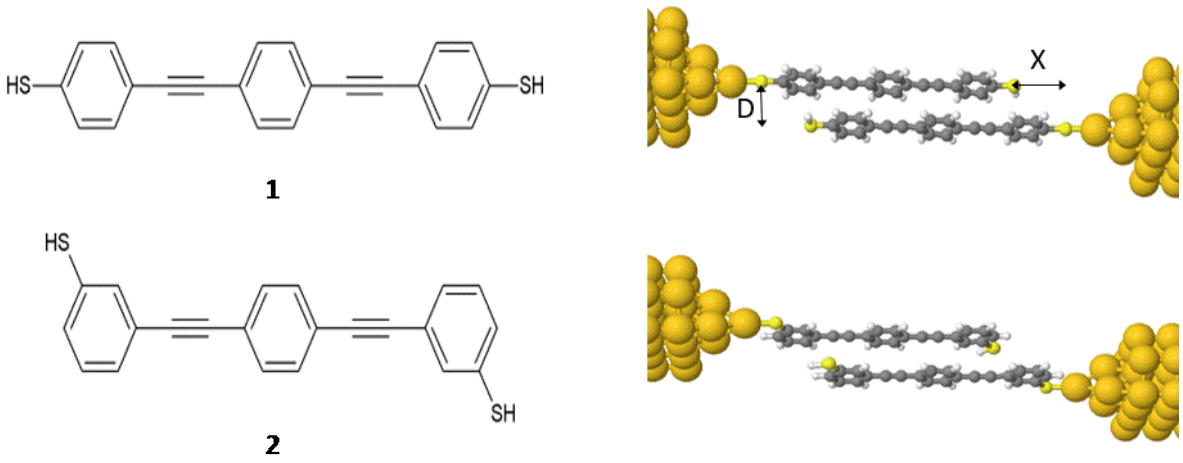

Figure 5.1*: (Left) Molecular structures for oligophenyleneethynylene (OPE) molecules with thiol achor groups connected in the para (1) and meta (2) position. (Left) Example stacking geometries for* ***1*** *and* ***2*** *connected between gold electrodes determined by the parameters X and D which is the overlap and separation respectively.*

5.2 Theoretical Methods

To calculate the electronic transport properties of OPE π-conjugated molecules shown in figure 5.1, I use a combination of the density functional SIESTA code [27] and the quantum transport code GOLLUM [28]. The optimum geometry was calculated for molecules **1** and **2** by relaxing them to a force tolerance of 0.01eV/Å using Troullier–Martins pseudopotentials to represent the potentials of the atomic cores [29], a generalized gradient approximation (GGA–PBE) functional to describe the exchange correlation [30, 31], double-ξ polarized basis set, and a real-space grid was defined with an energy cutoff 250 Rydbergs.

The optimal stacking geometry for both molecules was calculated by minimizing the ground state energy by altering the overlap length X, and the displacement distance D of identical molecules as shown in figure 5.1. I define X to be the distance between the sulfur atoms along the axis of the molecule, i.e. when X = 0 nm the overlap of the molecules is a maximum and X = L (L is the length of the molecule which for 1= 0.01 nm and 2 = 0.02 nm) is the minimum. D is the distance between the molecules in the stacking direction in the case of both OPEs 1 and 2 the values found are X=0.161 nm and D=0.33 nm, and this configuration has a binding energy of -0.77 eV (see fig. 5.4). Each molecule is then attached to one gold electrode as shown in figure 5.1. The lead consists of 6 layers of (111) gold each containing 25 gold atoms which is terminated by a pyramid of gold atoms. The terminating sulfur atom of the thiol group loses it hydrogen atom and the gold-sulfur binding distance is optimized to 2.4 Å. The hydrogen atom of the unattached thiol group remains. The zero-bias transmission coefficient T(E), which is the probability for an electron of energy *E* of electrons to transfer from left-to-right of electrodes was calculated by extracting a Hamiltonian using the SIESTA code, and then using GOLLUM to compute T(E). The transmission

coefficient was then utilized to compute the Seebeck coefficient *S* which has been shown to depend on the magnitude and derivative of the transmission at the Fermi level of the electrodes [32].

$$S = \frac{\pi^2 k_B^2 \tau}{3e} \frac{dlnT(E)}{dE}\Big|_{E=E_F} \qquad (5.1)$$

where k_B is the Boltzmann constant, τ is the temperature of the junction and e is the electron charge.

5.3 Results and discussion

Taking the optimum molecule separation D = 0.33 nm, we vary the overlap length of the molecule X from 0 to L (figure 5.1) and calculate the transmission coefficient T(E). Figure 5.2 shows the results for X varying between (0 nm to 0.09 nm) for the *para* connected molecule 1, (transmission data for a larger range of X can be seen in Figure 5.3). At a value of X = 0.1610 nm (which is the optimum stacking geometry see in fig. 5.4) the Fermi energy ($E-E_F$=0 eV) lies close to the HOMO resonance, and there is an antiresonance feature ($E-E_F$ = 0.5 eV) in the gap between the HOMO and LUMO resonances. This destructive interference is attributed to the multiple transport paths through the stacked molecule (Fabry-Perot type behaviour) and suggests that by altering the overlap length *X* the interference behaviour should change.

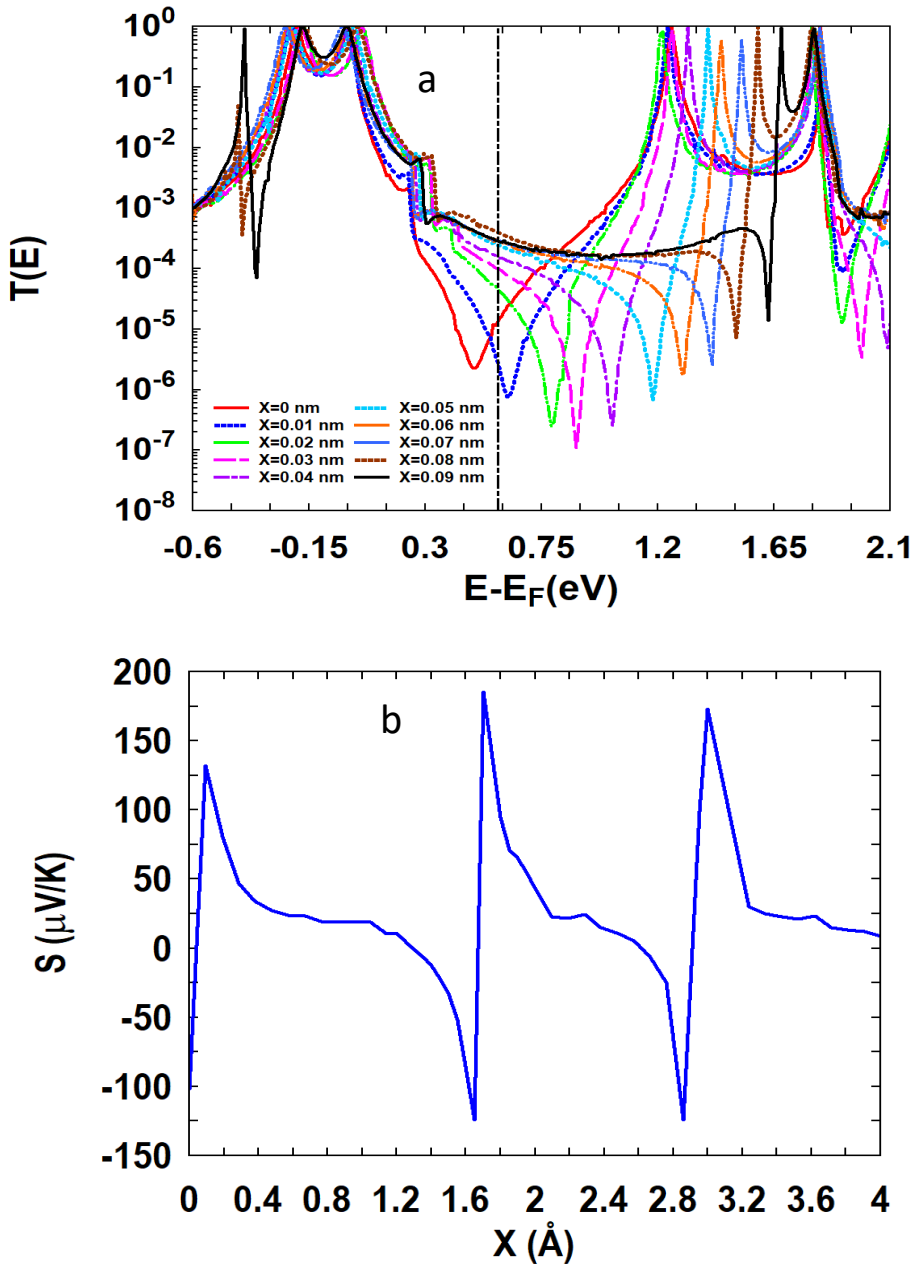

Figure 5.2*: (a) Zero bias transmission coefficient T(E) against electron energy E for different overlap lengths X and fixed separation D = 0.33nm. (b) Seebeck coefficient S as a function of overlap length X (D=0.33 nm).*

Figure 5.2 shows that as the value of X is increased the antiresonance moves towards the LUMO resonance and at value of X=0.09 nm the minimum sits at E-E_F = 1.6 eV. The transmission data also shows the HOMO-LUMO gap increasing as the overlap length is increased, this is due to the splitting between the two LUMO resonances of the

individual molecules decreasing because the coupling between the two molecules becomes weaker.

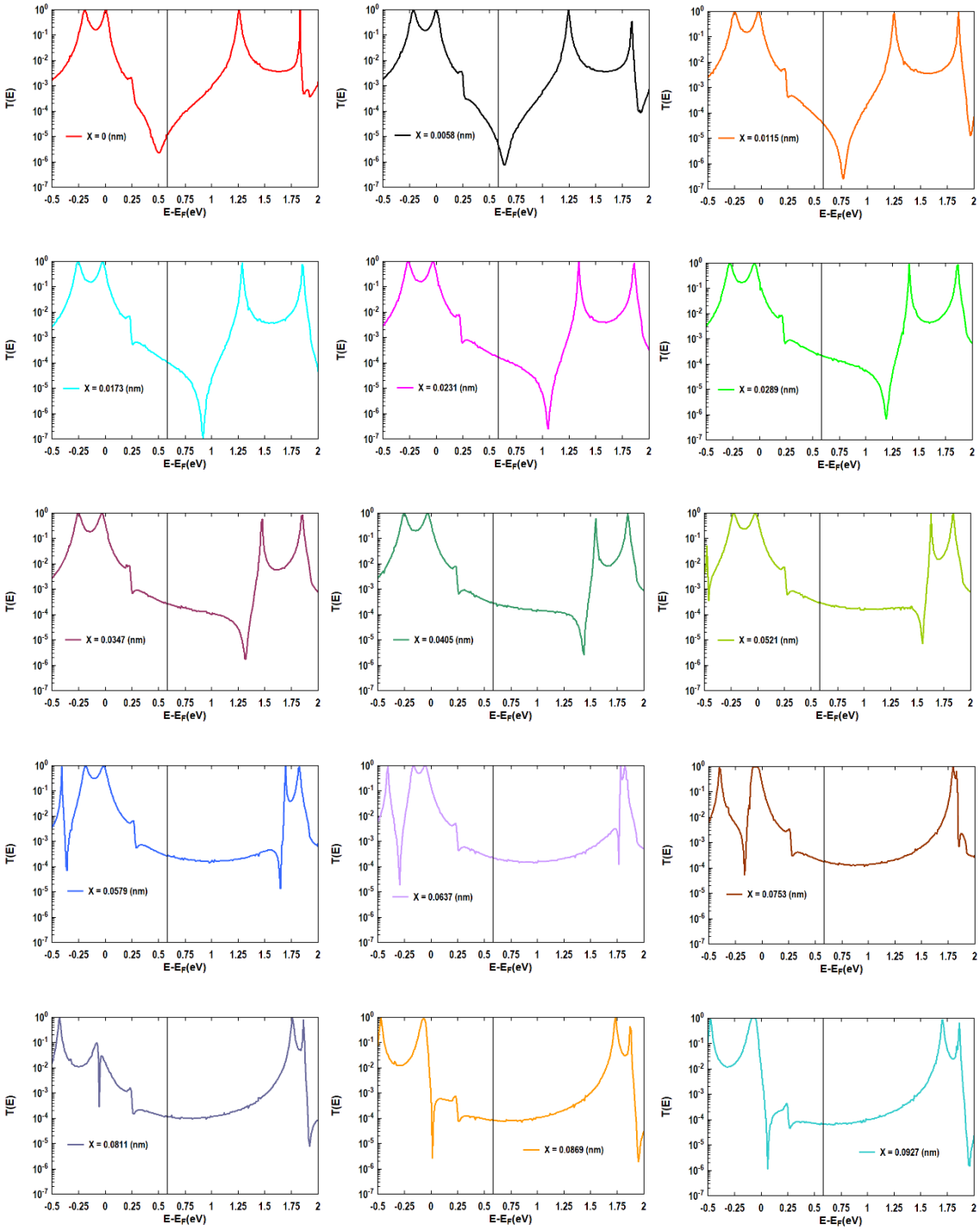

***Figure 5.3**: Illustrates moving of transmission coefficient with displacements (X = 0 - 0.4 nm) of π- π stacked S-OPE3-S molecules at various distances at Fermi energy (E_F).*

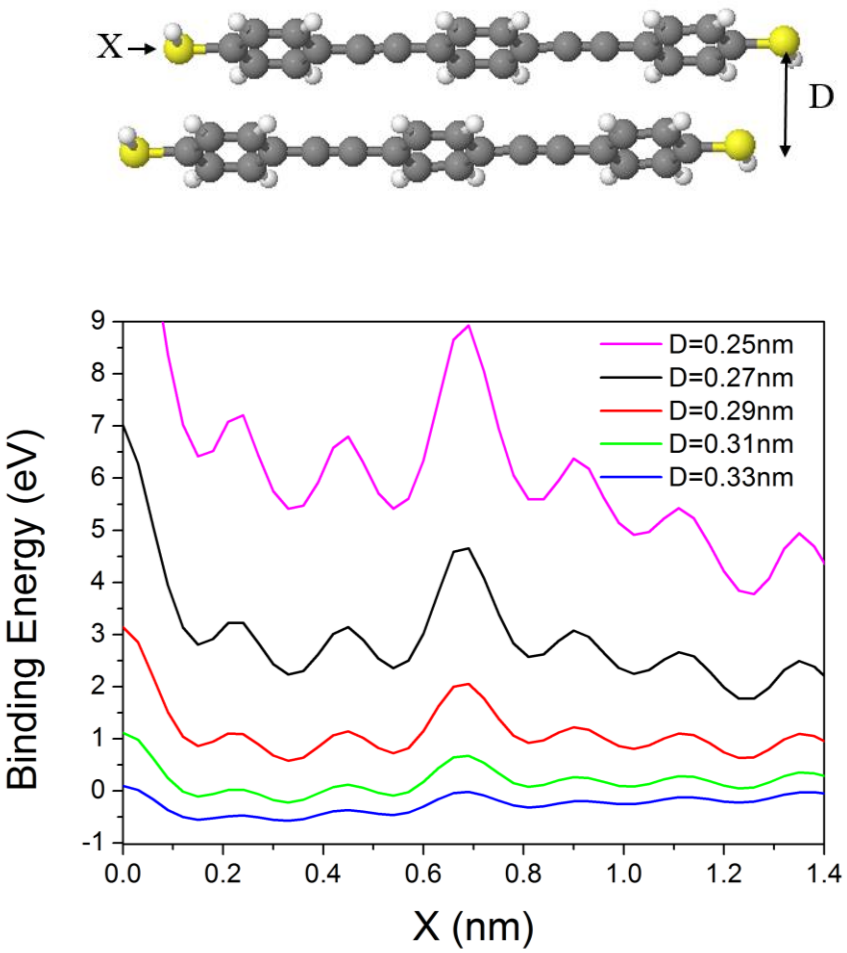

Figure 5.4. *Binding energy of molecule* ***1*** *as a function of parameters X and D.*

When an anti-resonance passes through the Fermi Energy the gradient of T(E) changes sign, which suggests that the Seebeck coefficient S is sensitive to the stacking geometry. Figure 5.2 shows the calculated value of S at room temperature, for a Fermi energy of $E-E_F$=0.5eV and a separation of D=0.33nm for values of X between 0 and 0.4nm. At X=0 nm the sign of S is negative and has a magnitude of -100 μV/K as the overlap length X is increased the sign of S is switched and at a value of S at X=0.02 nm is 100 μV/K. The antiresonance then moves away from the Fermi energy and S remains positive with a value of approximately 25μV/K. At further separations the sign of S oscillates.

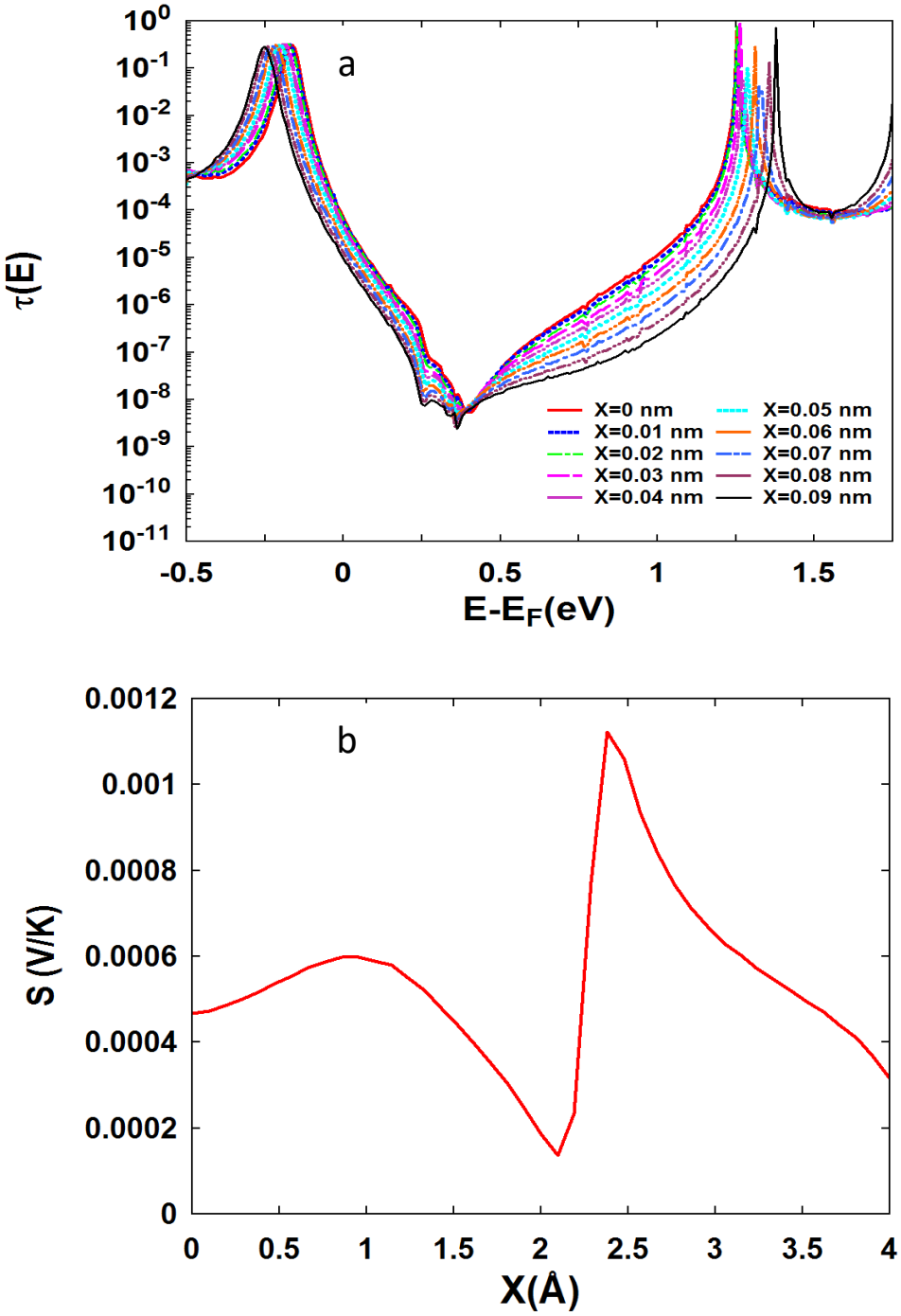

Figure 5.5*: (a) Zero bias transmission coefficient T(E) for molecule 2 for different overlap lengths X and fixed separation D = 0.33nm. (b) Seebeck coefficient S as a function of overlap length X (D=0.33nm)*

The calculation is then repeated for the meta-connected molecule **2** and the results can be seen on figure 5.5 (the separation D=0.33 nm and the overlap X is varied between 0 and 0.09nm). Here the transmission T(E), shows an antiresonance at 0.3 eV which does

not move across the HOMO-LUMO gap as the overlap length X is increased. The value of the Seebeck coefficient is therefore positive for all values of X between 0nm and 0.4nm. This suggests that the interference due to the meta-connectivity of the molecule dominates and the additional destructive interference from the stacked geometry is negligible.

5.4 Conclusion

I have shown theoretically that the transmission through molecules which are π-stacked leads to destructive quantum interference. The role it plays in determining the sign of the Seebeck coefficient is then dependent on the connectivity of the individual molecules. In para-connected systems, the shifting of this resonance can lead to molecules displaying both signs of S whereas for meta-connected molecules the oscillation of the sign does not occur. This novel behaviour may have important consequences in the design of SAM based thermoelectric materials and in the role of single molecule measurements where a molecule may show a measured S with both signs.

Bibliography

[1] Rincón-García, Laura, Charalambos Evangeli, Gabino Rubio-Bollinger, and Nicolás Agraït. "Thermopower measurements in molecular junctions." Chemical Society Reviews 45, no. 15 (2016): 4285-4306.

[2] Cui, Longji, Ruijiao Miao, Chang Jiang, Edgar Meyhofer, and Pramod Reddy. "Perspective: Thermal and thermoelectric transport in molecular junctions." The Journal of Chemical Physics 146, no. 9 (2017): 092201.

[3] Reddy, Pramod, Sung-Yeon Jang, Rachel A. Segalman, and Arun Majumdar. "Thermoelectricity in molecular junctions." Science 315, no. 5818 (2007): 1568-1571.

[4] Aradhya, Sriharsha V., and Latha Venkataraman. "Single-molecule junctions beyond electronic transport." Nature nanotechnology 8, no. 6 (2013): 399-410.

[5] Tan, Aaron, Janakiraman Balachandran, Seid Sadat, Vikram Gavini, Barry D. Dunietz, Sung-Yeon Jang, and Pramod Reddy. "Effect of length and contact chemistry on the electronic structure and thermoelectric properties of molecular junctions." Journal of the American Chemical Society 133, no. 23 (2011): 8838-8841.

[6] Tan, Aaron, Seid Sadat, and Pramod Reddy. "Measurement of thermopower and current-voltage characteristics of molecular junctions to identify orbital alignment." Applied Physics Letters 96, no. 1 (2010): 013110.

[7] Pfeiffer, M., A. Beyer, T. Fritz, and K. Leo. "Controlled doping of phthalocyanine layers by cosublimation with acceptor molecules: A systematic Seebeck and conductivity study." Applied Physics Letters 73, no. 22 (1998): 3202-3204.

[8] Tsutsui, Makusu, Takanori Morikawa, Yuhui He, Akihide Arima, and Masateru Taniguchi. "High thermopower of mechanically stretched single-molecule junctions." Scientific reports 5 (2015): 11519.

[9] Duan, Junxi, Xiaoming Wang, Xinyuan Lai, Guohong Li, Kenji Watanabe, Takashi Taniguchi, Mona Zebarjadi, and Eva Y. Andrei. "High thermoelectricpower factor in graphene/hBN devices." Proceedings of the National Academy of Sciences 113, no. 50 (2016): 14272-14276.

[10] Vacek, Jaroslav, Jana Vacek Chocholoušová, Irena G. Stará, Ivo Starý, and Yonatan Dubi. "Mechanical tuning of conductance and thermopower in helicene molecular junctions." Nanoscale 7, no. 19 (2015): 8793-8802.

[11] Rincón-García, Laura, Ali K. Ismael, Charalambos Evangeli, Iain Grace, Gabino Rubio-Bollinger, Kyriakos Porfyrakis, Nicolás Agraït, and Colin J. Lambert. "Molecular design and control of fullerene-based bi-thermoelectric materials." Nature materials 15, no. 3 (2015): nmat4487.

[12] Markussen, Troels, Jakob Schiötz, and Kristian S. Thygesen. "Electrochemical control of quantum interference in anthraquinone-based molecular switches." The Journal of chemical physics 132, no. 22 (2010): 224104.

[13] Geng, Yan, Sara Sangtarash, Cancan Huang, Hatef Sadeghi, Yongchun Fu, Wenjing Hong, Thomas Wandlowski, Silvio Decurtins, Colin J. Lambert, and Shi-Xia Liu. "Magic ratios for connectivity-driven electrical conductance of graphene-like molecules." Journal of the American Chemical Society 137, no. 13 (2015): 4469-4476.

[14] Sangtarash, Sara, Hatef Sadeghi, and Colin J. Lambert. "Exploring quantum interference in heteroatom-substituted graphene-like molecules." Nanoscale 8, no. 27 (2016): 13199-13205.

[15] Manrique, David Zsolt, Cancan Huang, Masoud Baghernejad, Xiaotao Zhao, Oday A. Al-Owaedi, Hatef Sadeghi, Veerabhadrarao Kaliginedi et al. "A quantum circuit rule for interference effects in single-molecule electrical junctions." arXiv preprint arXiv:1509.00990 (2015).

[16] Solomon, Gemma C., Carmen Herrmann, Thorsten Hansen, Vladimiro Mujica, and Mark A. Ratner. "Exploring local currents in molecular junctions." Nature chemistry 2, no. 3 (2010): 223-228.

[17] Gantenbein, Markus, Lin Wang, Alaa A. Al-jobory, Ali K. Ismael, Colin J. Lambert, Wenjing Hong, and Martin R. Bryce. "Quantum interference and heteroaromaticity of para-and meta-linked bridged biphenyl units in single molecular conductance measurements." Scientific Reports 7 (2017).

[18] Nozaki, Daijiro, and Cormac Toher. "Is the Antiresonance in Meta-Contacted Benzene Due to the Destructive Superposition of Waves Traveling Two Different Routes around the Benzene Ring?." The Journal of Physical Chemistry C (2017).

[19] Guédon, Constant M., Hennie Valkenier, Troels Markussen, Kristian S. Thygesen, Jan C. Hummelen, and Sense Jan Van Der Molen. "Observation of quantum interference in molecular charge transport." Nature nanotechnology 7, no. 5 (2012): 305-309.

[20] Martín, Santiago, Iain Grace, Martin R. Bryce, Changsheng Wang, Rukkiat Jitchati, Andrei S. Batsanov, Simon J. Higgins, Colin J. Lambert, and Richard J. Nichols. "Identifying diversity

in nanoscale electrical break junctions." Journal of the American Chemical Society 132, no. 26 (2010): 9157-9164.

[21] Frisenda, Riccardo, Vera AEC Janssen, Ferdinand C. Grozema, Herre SJ van der Zant, and Nicolas Renaud. "Mechanically controlled quantum interference in individual π-stacked dimers." Nature chemistry (2016).

[22] Wu, Songmei, Maria Teresa González, Roman Huber, Sergio Grunder, Marcel Mayor, Christian Schönenberger, and Michel Calame. "Molecular junctions based on aromatic coupling." Nature nanotechnology 3, no. 9 (2008): 569-574.

[23] Kiršanskas, Gediminas, Qian Li, Karsten Flensberg, Gemma C. Solomon, and Martin Leijnse. "Designing π-stacked molecular structures to control heat transport through molecular junctions." Applied Physics Letters 105, no. 23 (2014): 233102.

[24] Lemmer, Mario, Michael S. Inkpen, Katja Kornysheva, Nicholas J. Long, and Tim Albrecht. "Unsupervised vector-based classification of single-molecule charge transport data." Nature communications 7 (2016).

[25] Nolas, George S., Jeffrey Sharp, and Julian Goldsmid. Thermoelectrics: basic principles and new materials developments. Vol. 45. Springer Science & Business Media, 2013.

[26] Algharagholy, Laith A., Qusiy Al-Galiby, Haider A. Marhoon, Hatef Sadeghi, Hayder M. Abduljalil, and Colin J. Lambert. "Tuning thermoelectric properties of graphene/boron nitride heterostructures." Nanotechnology 26, no. 47 (2015): 475401.

[27] Soler, José M., Emilio Artacho, Julian D. Gale, Alberto García, Javier Junquera, Pablo Ordejón, and Daniel Sánchez-Portal. "The SIESTA method for ab initio order-N materials simulation." Journal of Physics: Condensed Matter 14, no. 11 (2002): 2745.

[28] Ferrer, Jaime, Colin J. Lambert, Víctor Manuel García-Suárez, D. Zs Manrique, D. Visontai, L. Oroszlany, Rubén Rodríguez-Ferradás et al. "GOLLUM: a next-generation simulation tool for electron, thermal and spin transport." New Journal of Physics 16, no. 9 (2014): 093029.

[29] Troullier, Norman, and José Luís Martins. "Efficient pseudopotentials for plane-wave calculations." Physical review B 43, no. 3 (1991): 1993.

[30] Kim, Kwang S., P. Tarakeshwar, and Jin Yong Lee. "Molecular clusters of π-systems: theoretical studies of structures, spectra, and origin of interaction energies." Chemical reviews 100, no. 11 (2000): 4145-4186.

[31] Watson, Mark D., Andreas Fechtenkötter, and Klaus Müllen. "Big is beautiful−"aromaticity" revisited from the viewpoint of macromolecular and supramolecular benzene chemistry." Chemical Reviews 101, no. 5 (2001): 1267-1300.

[32] Paulsson, Magnus, and Supriyo Datta. "Thermoelectric effect in molecular electronics." Physical Review B 67, no. 24 (2003): 241403.

[33] Simine, Lena, Wei Jia Chen, and Dvira Segal. "Can the Seebeck coefficient identify quantum interference in molecular conduction?." The Journal of Physical Chemistry C 119, no. 22 (2015): 12097-12108.

[34] Wu, Songmei, Maria Teresa González, Roman Huber, Sergio Grunder, Marcel Mayor, Christian Schönenberger, and Michel Calame. "Molecular junctions based on aromatic coupling." Nature nanotechnology 3, no. 9 (2008): 569-574.

[35] Batra, Arunabh, Gregor Kladnik, Héctor Vázquez, Jeffrey S. Meisner, Luca Floreano, Colin Nuckolls, Dean Cvetko, Alberto Morgante, and Latha Venkataraman. "Quantifying through-space charge transfer dynamics in π-coupled molecular systems." Nature Communications 3 (2012): ncomms2083.

[36] Lin, Li-Li, Jian-Cai Leng, Xiu-Neng Song, Zong-Liang Li, Yi Luo, and Chuan-Kui Wang. "Effect of aromatic coupling on electronic transport in bimolecular junctions." The Journal of Physical Chemistry C 113, no. 32 (2009): 14474-14477.

[37] Geng, Hua, Shiwei Yin, Ke-Qiu Chen, and Zhigang Shuai. "Effects of Intermolecular Interaction and Molecule− Electrode Couplings on Molecular Electronic Conductance." The Journal of Physical Chemistry B 109, no. 25 (2005): 12304-12308.

[38] He, Yuanyuan, Jinjiang Zhang, Hongmei Liu, and Jianwei Zhao. "Electron transport across π-stacked oligophenyls system: A density functional theory approach." Computational and Theoretical Chemistry 1043 (2014): 47-53.

[39] Noori, Mohammed, Hatef Sadeghi, and Colin J. Lambert. "High-performance thermoelectricity in edge-over-edge zinc-porphyrin molecular wires." Nanoscale 9, no. 16 (2017): 5299-5304.

Chapter 6

Designing thermoelectric materials

In chapter 5 I looked at a simple OPE molecule system to further investigate the thermopower in single molecule junctions. In this chapter, I will present theoretical work that is aimed at designing new types of thermoelectric materials. Here, I have investigated a set of molecules that have varying types of side branches attached to the main backbone and I study the electron and phonon transport through these nanoscale molecular junctions with the aim of developing high performance thermoelectric materials.

This study is a collaborative work with Marjan Famili (PhD student in Colin's group) who calculated the phonon properties, and the experiment were carried out at the University of Liverpool (Prof. Richard J. Nichols group).

6.1 Introduction

Recent studies of electron transport through molecular junctions have been underpinned by substantial improvements in electrical contacting techniques [1-4], which have identified a range of fundamental characteristics involving switching [5], and organic-based devices [6]. Molecular electronics has received great attention in investigating nanoscale thermoelectricity, with the hope that it will contribute to the design of new environmentally organic thermoelectric materials [7-8] through the use of individual molecular structures which as function electronics devices [9-10]. Therefore, the design of new organic thermoelectric materials for converting waste heat directly into electricity is a global challenge [11].

There are various strategies to improve the thermoelectric properties of inorganic [12] and organic materials [13-14], which yield quantum confinement of electrons and phonons [15]. Due to the attractive characteristics of single molecules, research groups have begun to measure and calculate the thermoelectric properties. Moreover, it is highly desirable to design new materials and build devices suitable for applications [7]. Therefore, the transport properties of single *metal-molecule-metal* junction is one of fundamental importance to develop functional nanoscale and organic-based devices [6, 16-17]. There are various features of these systems to control, including the chemical linking compounds [16, 18-23] and the contact geometry they form [24-25], which are important to study the electronic and phononic properties [1, 7] with nanoelectrode contacts.

When describing the electron transport properties through single-molecules which is controlled by the energy level alignment with the Fermi energy of the electrode, the conductance will be calculated for both electrons and phonon. The thermopower will

also be studied by calculation of the Seebeck coefficient. To investigate high-performance thermoelectric materials, which will eventually inform the design and synthesis of molecular structures [1, 26], a series of molecules have been studied to understand the factors which may govern the sign and magnitude of their thermopower. On such as the length of conjugated molecules and the kind of terminal group [16, 27]. In this work I examine a series of thiophene molecules where the bridging atoms vary: silicon, germanium, carbon, and tin. Thiophene-based molecules are π-conjugated compounds, which have been proven to give sensitive platforms in organic materials chemistry [28]. Linking systems with Si, Ge, C and Sn unit is interesting due to the interaction between the σ orbital of the linked-bridges and the π orbital of the molecule, which results in interesting properties such as enhanced conjugation [29-30].

Previous studies [31-33] have focused on calculating the electrical conductance and thermopower of single molecules only, which provided fundamental knowledge required to understand and enhance structures at the molecular scale. However, in this chapter I will study both the electronic and phononic properties. The efficiency of a thermoelectric device for power generation is characterized by the figure of merit $ZT = GS^2\tau/k$, where G is the electrical conductance, S is the Seebeck coefficient, τ is temperature, and κ (κ_e+ κ_{ph}) is the thermal conductance of the electronic and phonon contributions [27, 34]. The aim is to then produce thermoelectric organic materials that might be an attractive alternative to inorganic materials (i.e. have a higher ZT). To help increase ZT and overcome the limiting factors concerning organic materials, there have been recent studies into the behaviour of single organics at room temperature [8, 26, 35]. One possibility, is by utilizing the weak interaction between two parts of the molecule such as π-π stacking [36-37], which leads to a reduction of the thermal conductance (*k*) in molecular junctions (which should enhance efficiency because it is

in the denominator of ZT). In what follows, we present the comparative theoretical study of varying linked-bridge thiophenes, whose chemical structure is shown in figure 6.1.

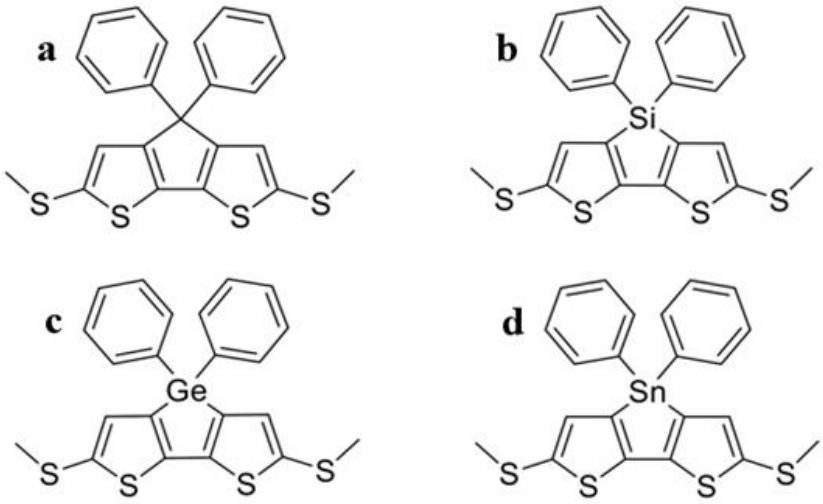

Figure 6.1: C*hemical structure of thiophene molecules with terminal group SMe with varying bridge-link atoms (Si, Ge, Sn, and C).*

6.2 Theoretical Method

The geometry of each structure of thiophene consisting of the gold electrodes and a single-molecule, which was relaxed to a force tolerance of 0.01 (eV $Å^{-1}$), SIESTA [38] implementation of density functional theory (DFT), with a double-ζ polarized basis set (DZP), as well as the Generalized Gradient Approximation (GGA) functional [39, 40], with Perdew− Burke−Ernzerhof (PBE) parametrization. The Hamiltonian and overlap matrices are calculated on a real-space grid defined by a plane-wave cut-off of 250 Ry.

To calculate the phononic thermal conductance for each structure, we use the harmonic approximation method discussed in chapter three (3.6), to build the dynamical matrix D for each molecule (shown in figure 6.1) contacted to gold electrodes. GOLLUM [41] is

then used to calculate $T_{ph}(\omega)$ which is the transport probability of a phonon. The phonon thermal conductance κ_{ph} at room temperature τ can be calculated from the formula:

$$k_{ph}(\tau) = \frac{1}{2\pi}\int_0^\infty \hbar\omega T_{ph}(\omega)\frac{\partial f_{BE}(\omega,\tau)}{\partial\tau}d\omega \qquad (6.1)$$

Here, $f_{BE}(\omega,\tau) = (e^{\frac{\hbar\omega}{k_B\tau}} - 1)^{-1}$ is Bose–Einstein distribution function, $\hbar$ is reduced Planck's constant, as well as $k_B = 8.6 \times 10^{-5}$ eV/K is Boltzmann's constant.

To calculate the transport of electrons through the molecule, contacted to gold electrodes, we take the electronic Hamiltonian from the converged DFT calculation, and again use GOLLUM to produce the transmission coefficient T_{el} (E) of electrons. The transmission coefficient can then be utilized to compute the Seebeck coefficient which has been shown to depend on the magnitude and derivative of the transmission at the Fermi level of the electrodes [42].

$$S = \frac{\pi\, k_B^2\, \tau}{3e}\frac{dlnT(E)}{dE}\Big|_{E=E_F} \qquad (6.2)$$

where k_B is the Boltzmann constant, τ is the temperature of the junction and e is the electron charge. The electrical conductance at room temperature is evaluated using the formula:

$$G = G_0\int_{-\infty}^{\infty} \mathrm{dE}\, \mathrm{T}(E)\left(-\frac{df(E)}{dE}\right) \qquad (6.3)$$

Here, $f(E) = \left[e^{(E-E_F)/k_B\tau} + 1\right]^{-1}$ is the Fermi function, E_F is the Fermi energy, $G_0 = \frac{2e^2}{h}$ is the quantum of conductance, τ is the temperature, and h is the Planck's constant. I now have all the parameters to compute ZT for these molecules.

6.3 Results and discussion

The compounds of thiophene that are shown in figure 6.1 were chosen to explore the behaviour of the varying side bridges to the molecules. The main influences are the mass of bridged atoms, and the resulting bond length between the backbone of molecule and the molecular bridge (C, Si, Ge, and Sn). First, the electronic structure of the molecules was calculated in the gas phase, including their Ionization Potential (IP) and the Electron Affinity (EA) which can give a more accurate calculation of the HOMO and LUMO energy levels. Here I calculate IP=E(N-1)-E(N) and EA=E(N)-E(N+1) where E(N) is the ground state energy of the neutral molecule, E(N-1) is the energy with one electron removed and E(N+1) is the energy with one electron added. The results can be seen in table 1, and show that the bridging atom only slightly affects the IP and EA. I also plot the frontier orbitals of the individual molecules in figure 6.4.2 which shows that the structure of the HOMO and LUMO wave functions are unaltered by changing the bridging atom.

Next, after connecting the molecules to gold electrodes via the SME anchor groups, I compute the electron transmission coefficient $T_{el}(E)$, where the binding distance between the gold tip and sulphur atom was calculated to be 0.24 nm. The results are shown in figure 6.4.3.

Table 1*: Variation of the Ionization Potential (IP) and Electron Affinity (EA) with central atom of molecules a-d in figure 6.4.2.*

Central atom	IP (eV)	EA (eV)
C	5.850395	-0.076025
Si	5.919914	0.134342
Ge	5.833446	0.128631
Sn	5.727306	0.034381

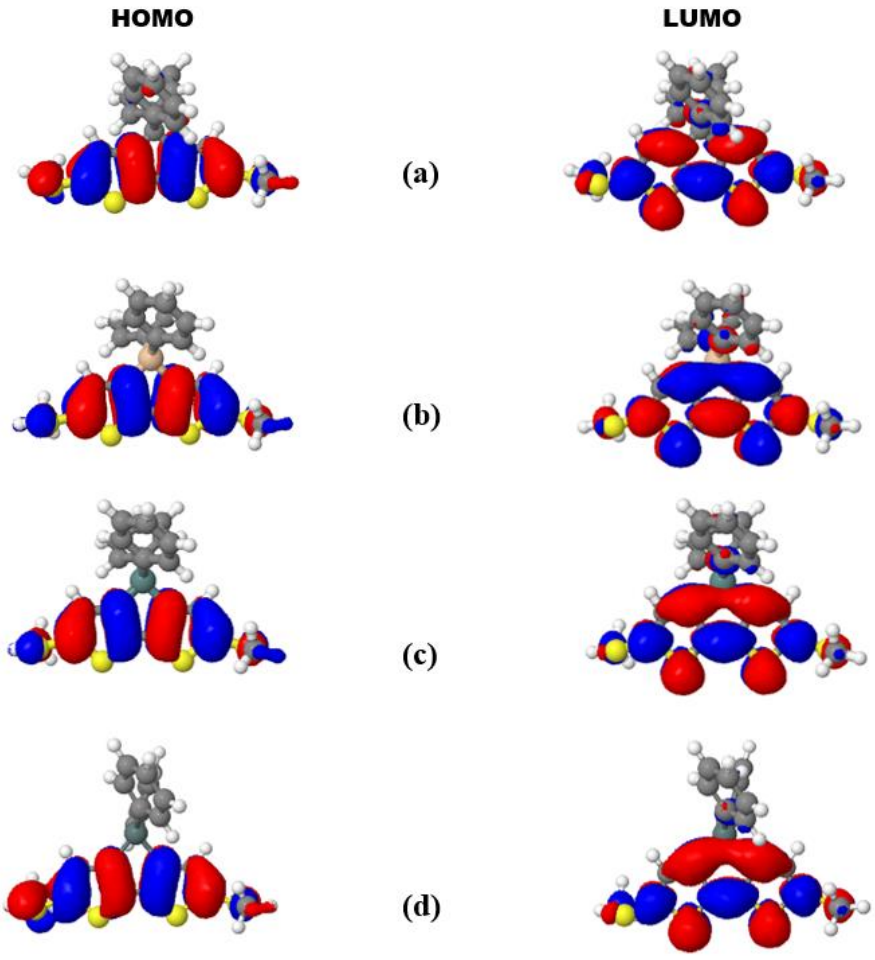

Figure 6.4.2: *Plots of the HOMO and LUMO of* ***a, b****,* ***c****, and* ***d*** *left panel are HOMOs and right are LUMOs.*

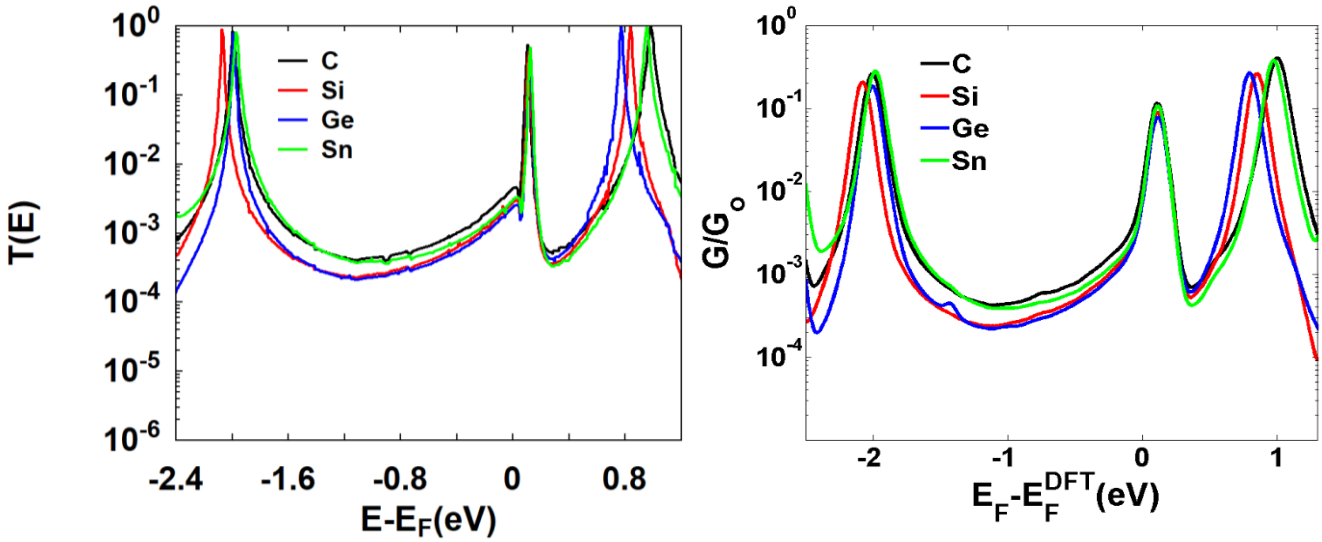

Figure 6.4.3: (left) *Electron Transmission coefficient as a function of electron energy at varied central bridge Si (red), Ge (blue), Sn (green) and C (black) of thiophene molecule. (right) Conductance versus Fermi energy evaluated at room temperature.*

The electron transmission shows that the DFT predicted Fermi energy ($E-E_F=0eV$) lies close to the LUMO resonances. The HOMO resonance for Sn (tin) sits at the highest energy and causes the value of the transmission $T(E_F)$ to be highest, whereas the Si (silicon) is at the lowest energy and has the lowest transmission in the gap. This behaviour directly relates to the calculated IP-EA gap. I can then use this transmission coefficient to evaluate the conductance and Seebeck coefficient using equations 6.2 and 6.3 at room temperature. The resulting values evaluated at the DFT predicted Fermi Energy can be seen in Figure 6.4.4.

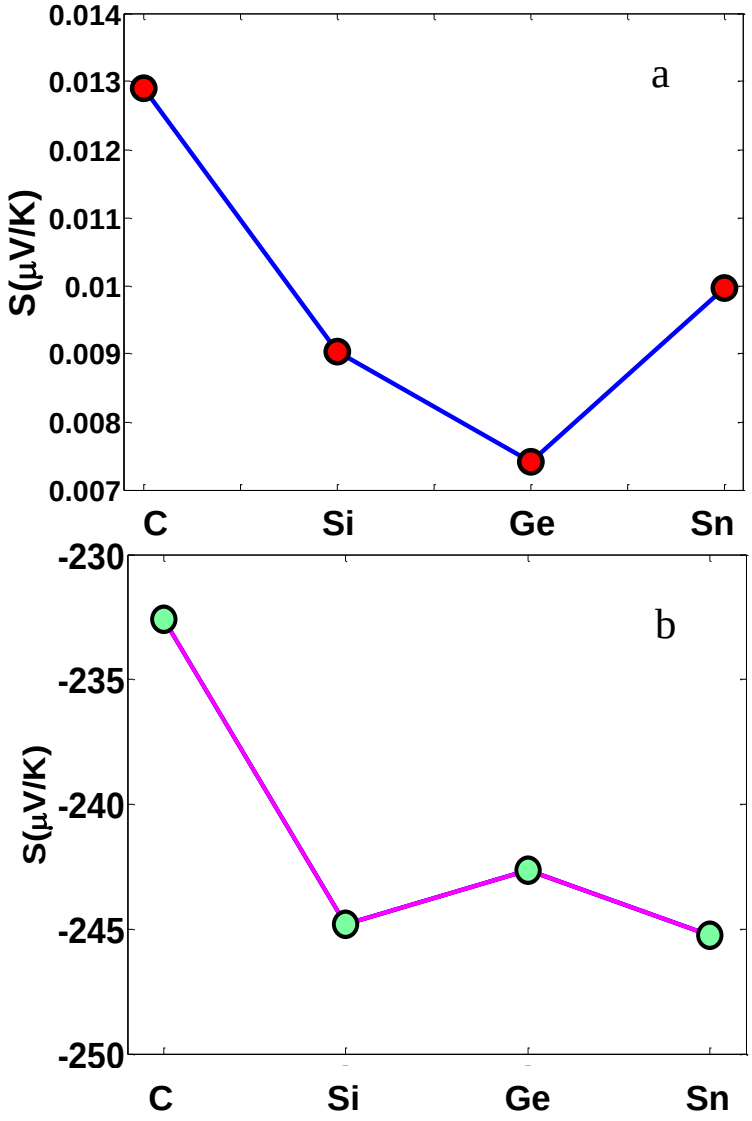

Figure 6.4.4*: (a) electrical conductance and (b) Seebeck coefficient as a function of Fermi energy (E_F) for the thiophene series at room temperature for varying link atom (C, Si, Ge, and Sn).*

In this work, we have demonstrated that introducing side bridged to molecules decreases the phonon conductance. This occurs due to appearance of antiresonances in the phonon transmission function when the frequency of incoming phonons happens to resonate with vibrational modes of the side branch. The four introduced molecules in figure 6.1, have side bridges of different shape and mass attached to the molecule backbone. These side branches are expected to lower the phonon conductance.

Table 2*: Mass of central atoms and bond length with Carbon in molecules a-d in figure 1*

Central atom	Side branches mass	Bond length with carbon X-C	Colour in plots
C	12.0107	1.53 Å	**black**
Si	28.0855	1.89 Å	**red**
Ge	72.64	1.98 Å	**blue**
Sn	118.71	2.18 Å	**green**

Therefore, we expect more scattering from the heavy atom and therefore lower conductance. While molecule with Si, Ge and Sn follow this trend, the molecule with the lightest central atom shows the lowest phonon conductance. This as explained in table 2, could be due to the fact that molecule *a* has the stiffest backbone. This can be understood by comparing the C-C bond length to C-Si, C-Ge, and C-Sn.

To study the electron and phonon thermal properties, we present contribution to the comparative theoretical study of the side-branched dependent of the thiophene molecule, which contains contributions from both electrons and phonons. The main unpredicted result from our study is that thermal conductance of Si-bridged atom is

higher than C-bridged (see fig. 6.4.5) due to each bridged atom in this molecule controls the thermal phonon conductance by the relatively weak coupling between this bridged atom and the backbone of molecule. We have found the bond length of Si-bridged atom is more floppy than C-bridge because the high-mass value of Si-bridge unit is higher than C-bridged atom, as shown in table 2. All these parameters that are demonstrated above lead to a change in the thermal phonon conductance.

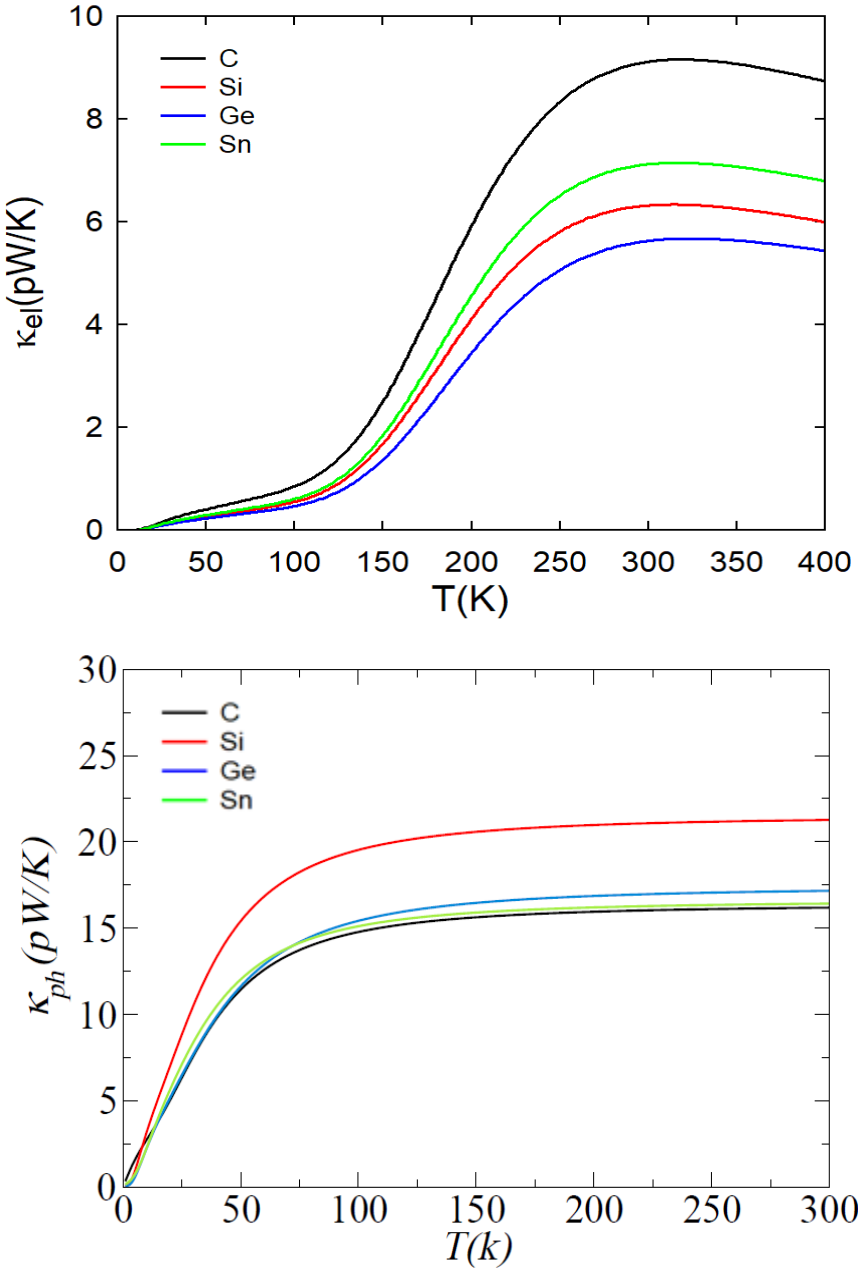

Figure 6.4.5*: Electron and phonon conductance (k) versus Temperature for molecules a (C, black), b (Si, red), c (Ge, blue), d (Sn, green) of figure 6.1.*

To compare the potential of these series of molecules for thermoelectricity, the electrical conductance and thermopower were calculated. The electrical conductance of Si-bridged atom is the lowest, while we have found its thermopower is the highest (see figs. 6.4.3 and 6.4.4(b)), this is because dependance on the Ionization Potential of Si-atom is lower (see table 1) and the width of HOMO-LUMO gap of Si-atom leads to low electrical conductance. Our results also show that the thermopower provides valuable information about the relative alignment between the molecular energy levels and the electrode Fermi energy.

We explore SMe-Au linked molecules that are predicted to conduct through the lowest unoccupied molecular orbital (LUMO) [44-46]. In addition, the Fermi energy lies in the tail of the LUMO resonance, and depending on the terminal group (see fig. 6.4.3) the value of the slope of transmission coefficient $T_{el}(E)$ of Si-bridged atom at Fermi energy (E_F=0 eV) is higher, which leads to higher thermopower.

In summary, we find the thermopower is negative for SMe-Au linked LUMO-conducting junctions.

In contrast, the highest conductance and the lowest thermopower is obtained with C-bridging. Therefore, the resulting combination of low electrical conductance, and high thermopower lead to a high value of ZT that is 1.77 shown in figure 6.4.6 , and make Si-bridging attractive for thermoelectric devices.

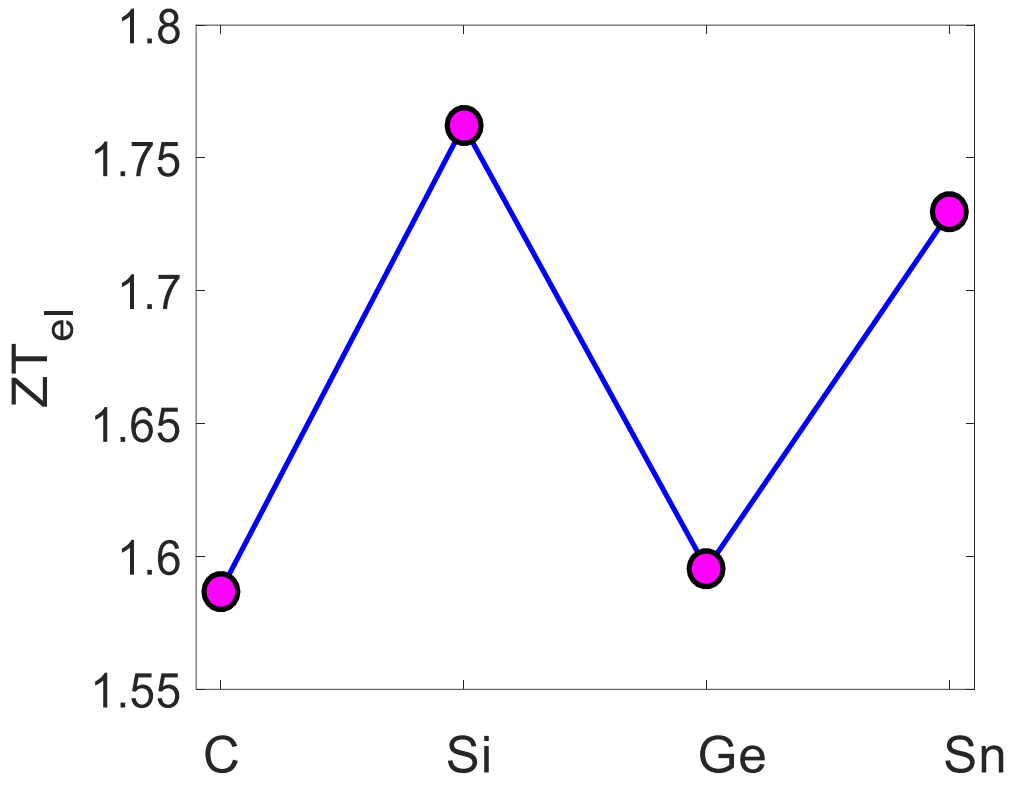

Figure 6.4.6*: shows electronic contribution to the figure of merit ZT_{el} at Fermi energy at room temperature for each central atom (C, Si, Ge, and Sn).*

6.4 Conclusion

Understanding electron transport and phonon through molecular junctions formed from single molecules attached to two electrodes is critical to the development of high-performance thermoelectric materials in nanoscale devices. In this chapter, we have studied the electronic and phononic properties in thiophene molecules that have various bridge atoms (C, Si, Ge, and Sn), and we find the thermal phonon conductance decreases monotonically with decreases bond length and mass for each bridged atom such that the C-bridged phonon thermal conductance is the lowest than other bridges, due to rigid nature of this bridge. In contrast, the thermal conductance of Si-bridged thiophenes increases with bond length and mass. For electrical properties, various results of conductance and thermopower were calculated for different bridges, which leads to variations in the value of figure of merit ZT_{el}, where Si-bridging has the highest value of ZT_{el} equal 1.77. Therefore, the Si-central unit is an attractive candidate for high-performance thermoelectric energy conversion.

Bibliography

[1] Finch, C. M., V. M. Garcia-Suarez, and C. J. Lambert. "Giant thermopower and figure of merit in single-molecule devices." Physical review b 79, no. 3 (2009): 033405.

[2] Lörtscher, Emanuel, Jacob W. Ciszek, James Tour, and Heike Riel. "Reversible and Controllable Switching of a Single-Molecule Junction." Small 2, no. 8-9 (2006): 973-977.

[3] Xu, Bingqian, and Nongjian J. Tao. "Measurement of single-molecule resistance by repeated formation of molecular junctions." Science 301, no. 5637 (2003): 1221-1223.

[4] Haiss, Wolfgang, Changsheng Wang, Iain Grace, Andrei S. Batsanov, David J. Schiffrin, Simon J. Higgins, Martin R. Bryce, Colin J. Lambert, and Richard J. Nichols. "Precision control of single-molecule electrical junctions." Nature materials 5, no. 12 (2006).

[5] Choi, Byoung-Young, Se-Jong Kahng, Seungchul Kim, Hajin Kim, Hyo Won Kim, Young Jae Song, Jisoon Ihm, and Young Kuk. "Conformational molecular switch of the azobenzene molecule: a scanning tunneling microscopy study." Physical review letters 96, no. 15 (2006): 156106.

[6] Nitzan, Abraham, and Mark A. Ratner. "Electron transport in molecular wire junctions." Science 300, no. 5624 (2003): 1384-1389.

[7] Rincón-García, Laura, Ali K. Ismael, Charalambos Evangeli, Iain Grace, Gabino Rubio-Bollinger, Kyriakos Porfyrakis, Nicolás Agraït, and Colin J. Lambert. "Molecular design and control of fullerene-based bi-thermoelectric materials." Nature materials 15, no. 3 (2015): nmat4487.

[8] Zhang, Qian, Yimeng Sun, Wei Xu, and Daoben Zhu. "Organic thermoelectric materials: emerging green energy materials converting heat to electricity directly and efficiently." Advanced Materials 26, no. 40 (2014): 6829-6851.

[9] Joachim, Ch, J. K. Gimzewski, and A. Aviram. "Electronics using hybrid-molecular and mono-molecular devices." Nature 408, no. 6812 (2000): 541-548.

[10] Bai, Ping, Erping Li, Peter A. Collier, Wee-Shong Chin, and Kian-Ping Loh. "Electron Conductance of Thiophene Dimers with Different Torsional Angles." In Emerging Technologies-Nanoelectronics, 2006 IEEE Conference on, pp. 173-178. IEEE, 2006.

[11] Snyder, G. Jeffrey, and Eric S. Toberer. "Complex thermoelectric materials." Nature materials 7, no. 2 (2008): 105-114.

[12] Kihou, Kunihiro, Hirotaka Nishiate, Atsushi Yamamoto, and Chul-Ho Lee. "Thermoelectric Properties of As-Based Zintl Compounds Ba1–x K x Zn2As2." Inorganic Chemistry 56, no. 6 (2017): 3709-3712.

[13] Zhang, Kun, Yue Zhang, and Shiren Wang. "Enhancing thermoelectric properties of organic composites through hierarchical nanostructures." Scientific reports 3 (2013): 3448.

[14] Bubnova, Olga, Magnus Berggren, and Xavier Crispin. "Tuning the thermoelectric properties of conducting polymers in an electrochemical transistor." Journal of the American Chemical Society 134, no. 40 (2012): 16456-16459.

[15] Jiang, Jian-Hua, and Yoseph Imry. "Enhancing Thermoelectric Performance Using Nonlinear Transport Effects." Physical Review Applied 7, no. 6 (2017): 064001.

[16] Widawsky, Jonathan R., Pierre Darancet, Jeffrey B. Neaton, and Latha Venkataraman. "Simultaneous determination of conductance and thermopower of single molecule junctions." Nano letters 12, no. 1 (2011): 354-358.

[17] Sadeghi, Hatef, Sara Sangtarash, and Colin Lambert. "Robust molecular anchoring to graphene electrodes." Nano Letters 17, no. 8 (2017): 4611-4618.

[18] Chen, Fang, Xiulan Li, Joshua Hihath, Zhifeng Huang, and Nongjian Tao. "Effect of anchoring groups on single-molecule conductance: comparative study of thiol-, amine-, and carboxylic-acid-terminated molecules." Journal of the American Chemical Society 128, no. 49 (2006): 15874-15881.

[19] Venkataraman, Latha, Jennifer E. Klare, Iris W. Tam, Colin Nuckolls, Mark S. Hybertsen, and Michael L. Steigerwald. "Single-molecule circuits with well-defined molecular conductance." Nano letters 6, no. 3 (2006): 458-462.

[20] Mishchenko, Artem, Linda A. Zotti, David Vonlanthen, Marius Bürkle, Fabian Pauly, Juan Carlos Cuevas, Marcel Mayor, and Thomas Wandlowski. "Single-molecule junctions based on nitrile-terminated biphenyls: a promising new anchoring group." Journal of the American Chemical Society 133, no. 2 (2010): 184-187.

[21] Martin, Christian A., Dapeng Ding, Jakob Kryger Sørensen, Thomas Bjørnholm, Jan M. van Ruitenbeek, and Herre SJ van der Zant. "Fullerene-based anchoring groups for molecular electronics." Journal of the American Chemical Society 130, no. 40 (2008): 13198-13199.

[22] Schneebeli, Severin T., Maria Kamenetska, Zhanling Cheng, Rachid Skouta, Richard A. Friesner, Latha Venkataraman, and Ronald Breslow. "Single-molecule conductance through multiple π− π-stacked benzene rings determined with direct electrode-to-benzene ring connections." Journal of the American Chemical Society 133, no. 7 (2011): 2136-2139.

[23] Cheng, Z-L., R. Skouta, H. Vazquez, J. R. Widawsky, S. Schneebeli, W. Chen, M. S. Hybertsen, R. Breslow, and L. Venkataraman. "In situ formation of highly conducting covalent Au-C contacts for single-molecule junctions." Nature nanotechnology 6, no. 6 (2011): 353-357.

[24] Haiss, Wolfgang, Changsheng Wang, Rukkiat Jitchati, Iain Grace, Santiago Martin,Andrei S. Batsanov, Simon J. Higgins et al. "Variable contact gap single-molecule conductance determination for a series of conjugated molecular bridges." Journal of Physics: Condensed Matter 20, no. 37 (2008): 374119.

[25] Haiss, Wolfgang, Santiago Martín, Edmund Leary, Harm van Zalinge, Simon J. Higgins, Laurent Bouffier, and Richard J. Nichols. "Impact of junction formation method and surface roughness on single molecule conductance." The Journal of Physical Chemistry C 113, no. 14 (2009): 5823-5833.

[26] Famili, Marjan, Iain Grace, Hatef Sadeghi, and Colin J. Lambert. "Suppression of Phonon Transport in Molecular Christmas Trees." ChemPhysChem 18, no. 10 (2017): 1234-1241.

[27] Noori, Mohammed, Hatef Sadeghi, and Colin J. Lambert. "High-performance thermoelectricity in edge-over-edge zinc-porphyrin molecular wires." Nanoscale 9, no. 16 (2017): 5299-5304.

[28] Murakami, Kazuya, Yousuke Ooyama, Hideyuki Higashimura, and Joji Ohshita. "Synthesis, Properties, and Polymerization of Spiro [(dipyridinogermole)(dithienogermole)]." Organometallics 35, no. 1 (2015): 20-26.

[29] Shang, Yan, LuQing Yang, GuiLing Zhang, Hui Zhang, and Bo Liu. "Theoretical studies on organosilicon oligomers containing ethenylene moieties." Journal of Polymer Research 18, no. 6 (2011): 1889-1902.

[30] Sanchez, Jason C., and William C. Trogler. "Hydrosilylation of diynes as a route to functional polymers delocalized through silicon." Macromolecular chemistry and physics 209, no. 15 (2008): 1527-1540.

[31] Manrique, David Zsolt, Cancan Huang, Masoud Baghernejad, Xiaotao Zhao, Oday A. Al-Owaedi, Hatef Sadeghi, Veerabhadrarao Kaliginedi et al. "A quantum circuit rule for interference effects in single-molecule electrical junctions." arXiv preprint arXiv:1509.00990 (2015).

[32] Milan, David C., Oday A. Al-Owaedi, Marie-Christine Oerthel, Santiago Marqués-González, Richard J. Brooke, Martin R. Bryce, Pilar Cea et al. "Solvent dependence of the single molecule conductance of oligoyne-based molecular wires." The Journal of Physical Chemistry C 120, no. 29 (2015): 15666-15674.

[33] Al-Galiby, Qusiy H., Hatef Sadeghi, Laith A. Algharagholy, Iain Grace, and Colin Lambert. "Tuning the thermoelectric properties of metallo-porphyrins." Nanoscale 8, no. 4 (2016): 2428-2433.

[34] Sadeghi, Hatef, Sara Sangtarash, and Colin J. Lambert. "Oligoyne molecular junctions for efficient room temperature thermoelectric power generation." Nano letters 15, no. 11 (2015): 7467-7472.

[35] Majumdar, Shubhaditya, Jonatan A. Sierra-Suarez, Scott N. Schiffres, Wee-Liat Ong, C. Fred Higgs III, Alan JH McGaughey, and Jonathan A. Malen. "Vibrational mismatch of metal leads controls thermal conductance of self-assembled monolayer junctions." Nano letters 15, no. 5 (2015): 2985-2991.

[36] Kiršanskas, Gediminas, Qian Li, Karsten Flensberg, Gemma C. Solomon, and Martin Leijnse. "Designing π-stacked molecular structures to control heat transport through molecular junctions." Applied Physics Letters 105, no. 23 (2014): 233102.

[37] Li, Qian, and Gemma C. Solomon. "Exploring coherent transport through π-stacked systems for molecular electronic devices." Faraday discussions 174 (2014): 21-35.

[38] Soler, José M., Emilio Artacho, Julian D. Gale, Alberto García, Javier Junquera, Pablo Ordejón, and Daniel Sánchez-Portal. "The SIESTA method for ab initio order-N materials simulation." Journal of Physics: Condensed Matter 14, no. 11 (2002): 2745.

[39] Kim, Kwang S., P. Tarakeshwar, and Jin Yong Lee. "Molecular clusters of π-systems: theoretical studies of structures, spectra, and origin of interaction energies." Chemical reviews 100, no. 11 (2000): 4145-4186.

[40] Watson, Mark D., Andreas Fechtenkötter, and Klaus Müllen. "Big is beautiful−"aromaticity" revisited from the viewpoint of macromolecular and supramolecular benzene chemistry." Chemical Reviews 101, no. 5 (2001): 1267-1300.

[41] Ferrer, Jaime, Colin J. Lambert, Víctor Manuel García-Suárez, D. Zs Manrique, D. Visontai, L. Oroszlany, Rubén Rodríguez-Ferradás et al. "GOLLUM: a next-generation simulation tool for electron, thermal and spin transport." New Journal of Physics 16, no. 9 (2014): 093029.

[42] Paulsson, Magnus, and Supriyo Datta. "Thermoelectric effect in molecular electronics." Physical Review B 67, no. 24 (2003): 241403.

[43] Gantenbein, Markus, Lin Wang, Alaa A. Al-jobory, Ali K. Ismael, Colin J. Lambert, Wenjing Hong, and Martin R. Bryce. "Quantum interference and heteroaromaticity of para-and meta-linked bridged biphenyl units in single molecular conductance measurements." Scientific Reports 7 (2017).

[44] Davidson, Ross, Oday A. Al-Owaedi, David C. Milan, Qiang Zeng, Joanne Tory, František Hartl, Simon J. Higgins, Richard J. Nichols, Colin J. Lambert, and Paul J. Low. "Effects of Electrode–Molecule Binding and Junction Geometry on the Single-Molecule Conductance of bis-2, 2′: 6′, 2 ″-Terpyridine-based Complexes." Inorganic chemistry 55, no. 6 (2016): 2691-2700.

[45] Al-Owaedi, Oday A., David C. Milan, Marie-Christine Oerthel, Sören Bock, Dmitry S. Yufit, Judith AK Howard, Simon J. Higgins et al. "Experimental and Computational Studies of the Single-Molecule Conductance of Ru (II) and Pt (II) trans-Bis (acetylide) Complexes." Organometallics 35, no. 17 (2016): 2944-2954.

[46] Hüser, Falco, and Gemma C. Solomon. "From chemistry to functionality: Trends for the length dependence of the thermopower in molecular junctions." The Journal of Physical Chemistry C 119, no. 25 (2015): 14056-14062.

Chapter 7

Conclusions and Future Works

7.1. Conclusions

I have studied the electronic and thermoelectric properties of 12 different organic molecules, using density functional theory DFT, and the Green's function formalism which are reported in chapters 2 and 3, respectively.

Chapter 4 presents studies of the charge transport of 4,4-bipyridine molecules, with a series of sterically-induced twist angles α between the two pyridyl rings. Experiment reveals the presence of high and low conductance peaks, which are attributed to different molecule orientations within the junctions. Both experimental measurements using the STM-BJ technique and DFT-based theory reveal that their conductances are proportional to $\cos^2(\alpha)$, confirming that for both geometries, the electrical current flows through the C-C bond linking the pi systems of the two rings. In common with many calculations of electron transport through pyridyl-terminated molecules, DFT predicts that the Fermi energy of the gold electrodes lies close to the LUMO transmission peak, in which case there would be no $\cos^2(\alpha)$ dependence. Shifting this to lower energies

corrects this error and confirms that the Fermi energy of gold lies within the HOMO-LUMO gap.

Chapter 5 demonstrated that the electronic properties and thermopower of π -stacked molecules are enhanced by increasing π-stacking length. Intermolecular π- π stacking between (OPE)-type molecules has a strong effect on thermopower and can change both the magnitude and sign of the Seebeck coefficient. The increase of the conjugation length of the system is predicted to enhance the thermoelectric response. In the case of fully identical of OPE-molecules, the coupling between two molecules results in the appearance of destructive interference features, which results in lower transmission which leads to an increase in the thermopower. However, dislocated molecules yield higher transmission, because such interference effects disappear. The displacements of two molecules relative each another yield to change the behaviour of transmission curves, and leads to oscillations in the Seebeck coefficient, and furthermore this behaviour can be switched on or off.

Chapter 6 presented theoretical studies of electron and phonon transport through molecular junctions formed from single molecules attached to two electrodes, which could be critical to the development of high-performance thermoelectric materials in nanoscale devices. In this chapter, we studied electronic and phononic properties in thiophene-based molecules that contain various bridges (C, Si, Ge, and Sn), and found that the thermal phonon conductance decreased monotonically with decrease of bond length and mass for each bridge atom. The phonon thermal conductance with a C-bridging atom is lower than other bridges, due to the rigid nature of this bridge. Whereas, the thermal conductance with Si-bridges increases with bond length and mass.

For electrical properties, various results of conductance and thermopower that are calculated at different bridges due to variation in the central atom, which leads to variations in the value of the figure of merit ZT_{el}, with Si-bridges possessing the highest value of ZT_{el} equal 1.76. Therefore, thiophenes with a Si-central bridge are attractive candidates for high-performance thermoelectric energy conversion.

7.2. Future Works

In this thesis, it would be of interest to investigate the electrical conductance of molecular wires attached to gold electrodes. For the future, one can conceive of a number of possibilities for extending this work in new directions. First, it would be interesting to examine how results change when 4,4-bipyridine molecules are terminated by other anchor group [1-5], as well as the examined effect of different torsion angles between phenyl rings with different connectivities (para and meta) to the terminal groups [6], which is known to control electrical conductance and may also be a useful method of controlling thermoelectricity [7]. Secondly, it would be interesting to examine the conductance of bipyridine and thiophene derivatives [8] with torsion angle by using the same side groups. Also, the varied bridged atoms of thiophene molecules may lead to new features and change the behaviour of electrical conductances. It would also be of interest to study the effect of varying the electrode material using alternative materials such as graphene [9], silicene [10, 11], platinum, palladium [12], or even superconducting electrodes [13,14], which introduce their own novel interference effects.

Bibliography

[1] Chen, Fang, Xiulan Li, Joshua Hihath, Zhifeng Huang, and Nongjian Tao. "Effect of anchoring groups on single-molecule conductance: comparative study of thiol-, amine-, and carboxylic-acid-terminated molecules." Journal of the American Chemical Society 128, no. 49 (2006): 15874-15881.

[2] Frisenda, Riccardo, Simge Tarkuç, Elena Galán, Mickael L. Perrin, Rienk Eelkema, Ferdinand C. Grozema, and Herre SJ van der Zant. "Electrical properties and mechanical stability of anchoring groups for single-molecule electronics." Beilstein journal of nanotechnology 6 (2015): 1558.

[3] Obersteiner, Veronika, David A. Egger, and Egbert Zojer. "Impact of Anchoring Groups on Ballistic Transport: Single Molecule vs Monolayer Junctions." The Journal of Physical Chemistry C 119, no. 36 (2015): 21198-21208.

[4] Zotti, Linda A., Thomas Kirchner, Juan-Carlos Cuevas, Fabian Pauly, Thomas Huhn, Elke Scheer, and Artur Erbe. "Revealing the Role of Anchoring Groups in the Electrical Conduction Through Single-Molecule Junctions." small 6, no. 14 (2010): 1529-1535.

[5] Davidson, Ross, Oday A. Al-Owaedi, David C. Milan, Qiang Zeng, Joanne Tory, František Hartl, Simon J. Higgins, Richard J. Nichols, Colin J. Lambert, and Paul J. Low. "Effects of Electrode–Molecule Binding and Junction Geometry on the Single-Molecule Conductance of bis-2, 2′: 6′, 2 ″-Terpyridine-based Complexes." Inorganic chemistry 55, no. 6 (2016): 2691-2700.

[6] Gantenbein, Markus, Lin Wang, Alaa A. Al-jobory, Ali K. Ismael, Colin J. Lambert, Wenjing Hong, and Martin R. Bryce. "Quantum interference and heteroaromaticity of para-and meta-linked bridged biphenyl units in single molecular conductance measurements." Scientific Reports 7 (2017).

[7] Finch, Christopher M., Skon Sirichantaropass, Steven W. Bailey, Iain M. Grace, Victor M. Garcia-Suarez, and Colin J. Lambert. "Conformation dependence of molecular conductance: chemistry versus geometry." Journal of Physics: Condensed Matter 20, no. 2 (2007): 022203.

[8] Dell, Emma J., Brian Capozzi, Kateri H. DuBay, Timothy C. Berkelbach, Jose Ricardo Moreno, David R. Reichman, Latha Venkataraman, and Luis M. Campos. "Impact of molecular symmetry on single-molecule conductance." *Journal of the American Chemical Society* 135, no. 32 (2013): 11724-11727.

[9] Bailey, Steven, David Visontai, Colin J. Lambert, Martin R. Bryce, Harry Frampton, and David Chappell. "A study of planar anchor groups for graphene-based single-molecule electronics." The Journal of chemical physics 140, no. 5 (2014): 054708.

[10] XH Zheng, GR Zhang, Z Zeng, VM García-Suárez, CJ Lambert. “Effects of antidots on the transport properties of graphene nanoribbons,” Physical Review B 80 (7), (2009): 075413

[11] Sadeghi, Hatef, Sara Sangtarash, and Colin J. Lambert. "Enhanced thermoelectric efficiency of porous silicene nanoribbons." Scientific reports 5 (2015).

[12] García-Suárez, V. M., A. R. Rocha, S. W. Bailey, C. J. Lambert, S. Sanvito, and J. Ferrer. "Single-channel conductance of H 2 molecules attached to platinum or palladium electrodes." Physical Review B 72, no. 4 (2005): 045437.

[13] VI Fal'Ko, CJ Lambert, AF Volkov "Andreev reflections and magnetoresistance in ferromagnet-superconductor mesoscopic structures" Journal of Experimental and Theoretical Physics Letters 69 (7), (1999): 532-538

[14] CJ Lambert, R Raimondi, V Sweeney, AF Volkov, "Boundary conditions for quasiclassical equations in the theory of superconductivity" Physical Review B 55 (9), (1997): 6015

[15] VC Hui, CJ Lambert "Andreev scattering, universal conductance fluctuations and phase periodic transport," Europhysics Letters 23 (3), (1993): 203